Universitetet
i Stavanger

FACULTY OF SCIENCE AND TECHNOLOGY

MASTER'S THESIS

Study programme/specialisation: Structures and materials	Autumn semester, 2019 Open
Author: Fredrik Meidell Knutsen	Fredrik Knutsen (signature of author)
Programme coordinator: Kjell Tore Fosså Supervisor: Kjell Tore Fosså (UIS)	
Title of master's thesis: Workability over time and mechanical properties of ultra-high performance concrete.	
Credits: 30	
Keywords: Concrete UHPC Workability over time Durability mechanical properties	Number of pages: 87 + supplemental material/other: 76 Stavanger, 15.12.2019 date/year

Preface

This master thesis was carried out at the Department of Mechanical and Structural Engineering and Materials science at the University of Stavanger in autumn 2019.

It consists of a material characterization program of ultra-high performance concrete (UHPC). This thesis aimed to map UHPC´s workability over time and study its mechanical properties when the material constituents in the mix design were modified. It also includes a literary study on UHPC.

Concrete technology has been my area of interest during the 5 years spent at the University of Stavanger. My bachelor thesis involved a full scale study in mapping low heat concrete in cooperation with Norcem AS. I have also carried out some volunteer laboratory work on geopolymer concrete during my second year in addition to covering three courses on concrete technology/structural design. I previously had little knowledge about ultra-high performance concrete but feel personally very satisfied by the learning outcome of this thesis.

I would like to express my gratitude to my teaching supervisor Kjell Tore Fosså for his guidance and professional support during this semester. All batching and testing were performed in the concrete laboratory in Ivar Langenes house at the University of Stavanger. I would also like to thank head engineer Jarle Berge for his assistance and guidance in the laboratory.

Fredrik Meidell Knutsen, Stavanger, December 2019

Abstract

Ultra-high performance concrete (UHPC) is characterized by high compressive and tensile strength along with excellent durability due to a densely packed matrix with low porosity. It has a low water-to-binder ratio (w/b) that can be compensated by the supplementation of superplasticizers (SP) to improve its workability. This thesis presents a literary study on UHPC and a laboratory report in which a total of 22 mix designs were batched and tested with respect to their mobility and stability over time. Compressive, tensile, and flexural strength were determined in the concretes hardened state, in addition to the modulus of elasticity, permeability, and porosity. For each new mix design, a material component was altered, either in quality of quantity, to isolate its effect on the material´s properties. A total of five binders, two fillers, four aggregates, two superplasticizers, and a shrinkage-reducing admixture were utilized in the mix designs. The main focus of this thesis was to understand how alterations to the mix design affect the workability over time, mechanical properties, and durability of UHPC. This was achieved though a range of tests performed both in its fresh and hardened states. The results show that UHPC´s have a similar density to that of a normal strength concrete. The mix designs examined exhibited good stability with no sign of water separation, only a tendency for paste separation when larger-sized aggregates were used. Improving the concrete´s mobility over time can lead to a reduction in its mechanical properties. A higher SP dosage increases mobility over time and, in most instances, improves the compressive strength as well. A higher w/b ratio indicates higher mobility but decrease in compressive strength and durability due to a higher capillary pore structure. A higher initial slump flow usually preserves the mobility over longer periods compared to a concrete with a low initial slump flow. The use of smaller particle-sized granular constituents of under 1mm in diameter can on an overall improve the material´s properties both in its fresh and hardened state.

The tensile strengths for the mix designs qualified as UHPC; however, there were unexpected large variations registered in specimens of the same design that had undergone the same curing regime, whether this is a result of uncertainties in the method of measurement, or actual variations in the tensile strength was uncertain.

Water permeability tests were performed and showed that the mix designs had low capillary porosity with a very gradual ingress of water, providing the material with superior resistance to chemical attack such as chlorides.

Contents

List of Figures

List of Tables

Acronyms

- **ACM** Advanced Cementitious Materials.
- **AFGC** The Association Francaise de Génie.
- **C-H-S** Calcium Silicate Hydrate.
- **CH** Calcium Hydroxide.
- **fib** The international Federation for Structural Concrete.
- **ITZ** Inter-facial transition zone.
- **NSC** Normal Strength Concrete.
- **PCE** Polycarboxylate ethers.
- **PDS** Product data sheet.
- **RCP** Reactive Concrete Powder.
- **SF** Silica Fume.
- **SP** Superplasticizer.
- **SRA** Shrinkage reducing admixture.
- **UHPC** Ultra-high-performance concrete.
- **UHPFRC** Ultra-high-performance fiber-reinforced concrete.
- **w/b** Water-Binder ratio.
- **w/c** Water-Cement ratio.

1 Introduction

Ultra-high performance concrete (UHPC) is a material that has been developed over the past three decades and is characterized by its high compressive strength, durability, and ductility with the presence of fiber reinforcement. When utilizing steel fibers, the material is often referred to as ultra-high performance fiber-reinforced concrete (UHPFRC). In this thesis, UHPC will be used as a joint term.

UHPCs have many advantages compared to normal strength concretes (NSCs). An enhancement in their mechanical properties such as compressive and tensile strengths can possibly help reduce the cross sectional areas of members and, thus, the designing of more slender constructions. This may lead to a cost reduction and lower CO_2 emissions, i.e, a more environmentally friendly construction. UHPCs have a high density matrix that contribute to its superior durability. Compared to NSC, UHPCs have increased resistance to abrasion, fire, and chemical attack such as chlorides. These characteristics make this composite material very well suited for a variety of applications.

Currently, there are no standardized codes and regulations in Norway that can be used when utilizing UHPC (Eurocode 2). NS-EN 1991-1-1:2004 only covers strength classes B12 to B95. The development and research into material behavior is a step toward this goal.

1.1 Objective

This thesis aims to map UHPC´s workability over time and attempts to understand its mechanical properties and durability when the material constituents in the mix design are modified.

1.2 Outline

This thesis entails two sections: the first is a literature study on the subject of UHPC with a focus on its workability and mechanical properties. The second section is a material characterization program including the proportioning of 22 mix designs where 16 different materials were used in varying quantities. A range of tests were performed to determine the mechanical properties of each mix design.

2 Literature

2.1 Concepts of UHPC

2.1.1 Definition of Ultra-high performance concrete (UHPC)

UHPC is a new generation of cementitious composites with exceptional mechanical properties and durability. In the reviewed literature, there is no exact definition of UHPC; however, there seems to be a consensus that this is a concrete with compressive strengths that surpass 150 MPa. To ensure a high performing material, other characteristics are also prevalent in the literature. Direct tensile strength should exceed 6 MPa, and the water-to-binder ratio (w/b) should usually be below 0.25. A large binder content reduces the capillary porosity, and steel fibers contribute to an increase in ductility. Without the use of fiber reinforcement, the material may achieve a modulus of elasticity of around 60 GPa, causing a brittle behavior when failing, restricting its applications [10, 3, 11].

2.1.2 History of UHPC

In the early 1950´s, *Otto Graf* developed a concrete with a compressive strength of 70 MPa and, in 1966, *Kurt Walz* showed that by implementing special production methods, this strength could be increased to 140 MPa [10]. Neither of these events attracted much attention from the construction industry. However, in the 1980´s, the discovery of silica fumes effects on concrete and the development of SP paved the way for its possible applications. In the early stages, this high strength concrete was in limited use due to its high cost compared to NSCs [10].

Today, producing a concrete with compressive strengths surpassing 200 MPa in a controlled laboratory environment is not a problem. Uncertainties may arise in large scale production of UHPC and if there is a market for this product. The economical aspect to the material selection process plays an important role besides the product´s mechanical properties and is often a deciding factor in assessing if the cost is worth its higher performance.

France has conducted considerable research on UHPC and published two standards for UHPCs: NF P18-470 that covers the test procedures and NF18-710, which is a national addition to Eurocode 2, that gives guidelines for its use in buildings, bridges, and other constructions.

2.1.3 Pros versus cons

Pros

As mentioned in the introduction, UHPC allows the designing of thinner constructions due to its improved mechanical properties. This has several advantages: first, the price may be reduced if the savings due to use of lesser concrete exceeds the increased price per cubic meter because of more expensive material components. Second, a thinner construction means a smaller self weight, which is often a significant factor in designing constructions such as buildings and bridges. Third, looking at the architectural aspect of making a thinner cross section, more elegant shapes and forms but with the same structural capacity. Figure 2.1 shows a photograph of a museum in Marseille where UHPC has been used as both the structural member and sheathing on a vast scale. In 2013, the International Symposium on Ultra High Performance Fiber Reinforced Concrete was held at this museum. The objective was to gain an overview of the achievements in infrastructure, constructions, and rehabilitations with a focus on design, reliability, and sustainability.

Cons

In Norway, along with most other countries, there are no codes and regulations for testing and designing constructions with UHPC.

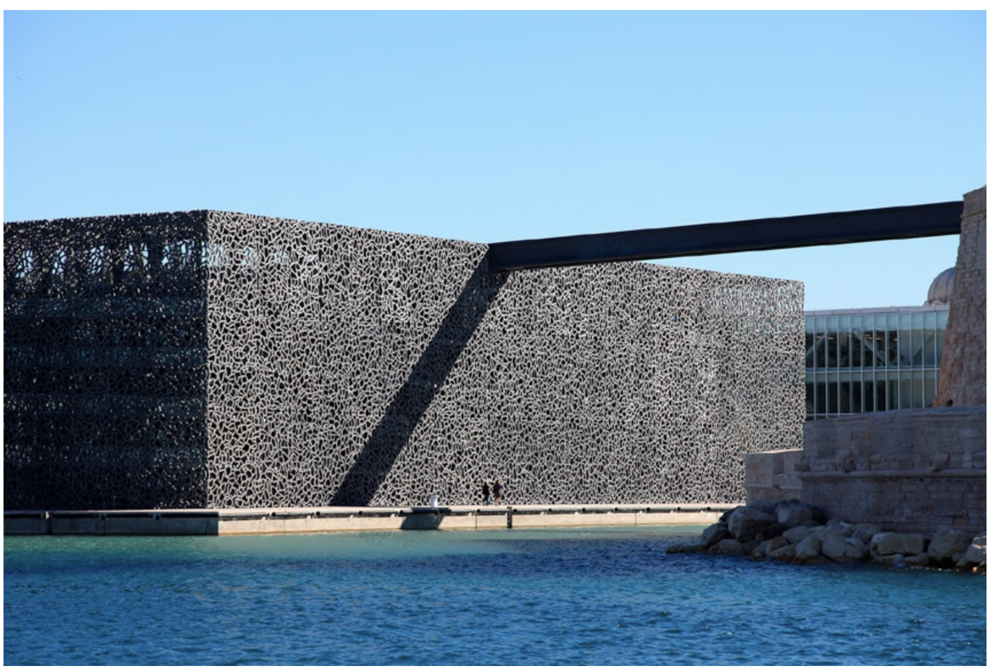

Figure 2.1: Musée des civilisations de l'Europe et de la Méditerranée in Marseille [1]

2.2 Mix design

UHPC has a material composition that is very similar to that of NSC. Its constituents are cement, water, aggregates, additives, admixtures and, often, fibers. The main variation between UHPC and NSC lies in the amount of binder used, aggregate particle size, and the use of fiber reinforcement. Figure 2.2 shows an example of the mix design of a NSC compared to that of UHPC.

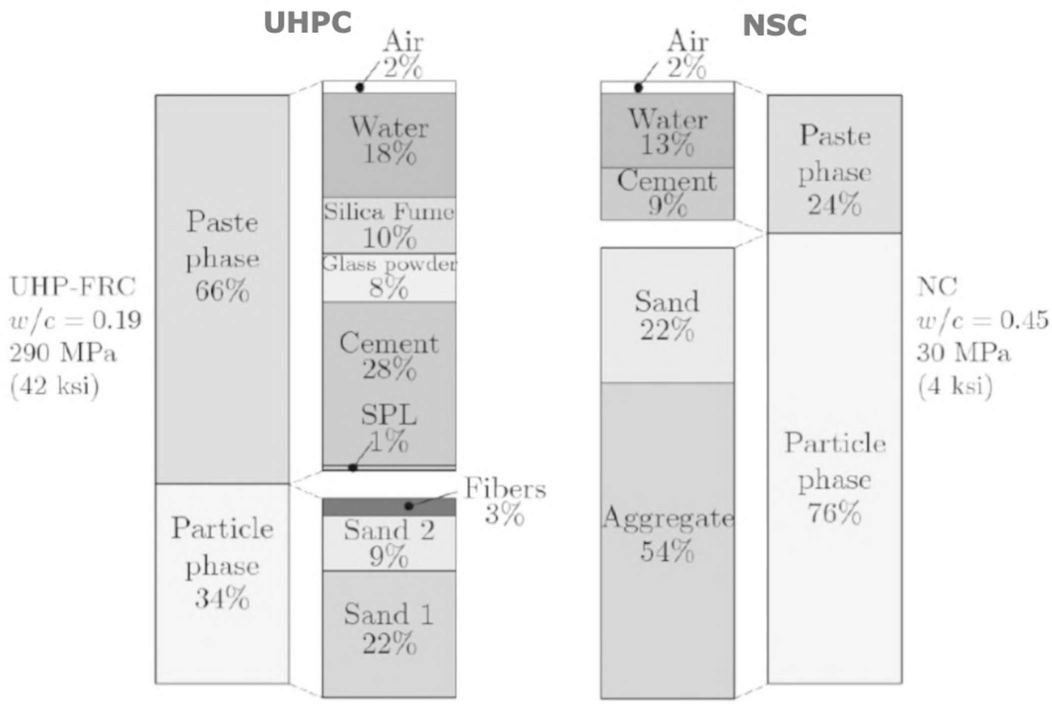

Figure 2.2: Mix proportions by volume comparing UHPC with NSC.[2]

A concrete material´s constituents are divided into the matrix and particle phase. Free water, additives, and all the solid particles with a diameter under 0.125mm are included in the matrix phase. Larger constituents over 0.125mm belong to the particle phase [12]. This shows the matrix phase comprises both chemically reactive and inert materials.

2.2.1 Grading optimization

A densely packed system is beneficial and an essential part of concrete technology. A smaller binder quantity is required in the mixture if a refined optimization of the granular components is carried out, where a densely packed system is the objective. There is however a balancing act when proportioning a concrete mixture. A more densely packed system will exhibit better mechanical properties and durability. However, it may have a negative impact on the rheological aspect. The properties of fresh concrete can be described by the concept of workability [7]. By introducing large amounts of small-sized particles, the void space between the larger particles will fill up, leading to an increase in density. Figure 2.3 shows an illustration of packing density. The use of water reducing additives such as SP can contribute to a better material flow in its fresh state.

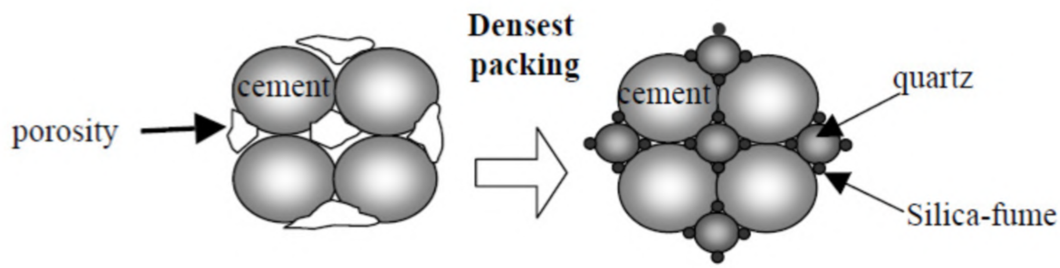

Figure 2.3: Packing density of concrete [3].

2.2.2 Local packing phenomena in concrete

The inter-facial transition zone (ITZ) is a porous and weak layer that occurs due to what is called the packing phenomena in concrete. This takes place in the part of the concrete paste in proximity to larger aggregates. This layer occurs as a consequence of the cement particles inability to be properly packed beside the aggregate grains. In addition to a weaker layer and high porosity, an increase in the formation of ettringite and portlandite (CH) crystals is also documented [13]. The ITZ has several unfavorable effects on concrete. Mechanical properties such as compressive and tensile strength are diminished and the material´s durability reduced due to an increase in sulfate attack and immersion of chlorides.

Lagerblad & Kjellsen in 1999 suggests the following five factors influence the thickness of ITZ layer [14]:

- Particle packing around the aggregates grains,
- Stability of the cement paste and the micro-mortar,
- Volume stability of the concrete,
- Cement composition and
- Fineness and chemical reactions of the aggregates.

By adding a filler with a particle diameter smaller than that of cement, stability and particle packing can be improved, in addition to positively effecting the rheology of the fresh concrete. [14]

2.2.3 Water-to-binder ratio

An essential variable to ensure optimal material properties is the w/b ratio. The binder refers to the chemically active portion of the matrix phase. This includes cement and the sum of all pozzolanic constituents. Figure 2.4 illustrates the strength as a function of w/b for a range of different concrete classes. As displayed, UHPC requires w/b values from 0.16 to 0.25 while a normal concrete lies between 0.4 to 0.7.

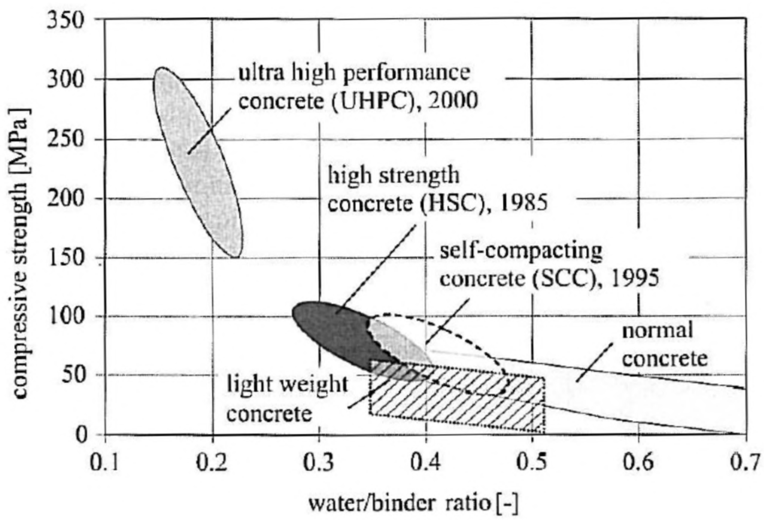

Figure 2.4: Strength as a function of w/b for different concrete types [3].

The ratio is determined by Equation 1.

$$\boxed{w/b = \frac{w}{c + \sum(k \cdot p)}} \tag{1}$$

It is derived on the basis of a k-value in accordance with NS-EN 206-1:2000+NA:2007 and takes into account the hydraulic activity of the supplementary cementitious materials (SCMs) compared to the cement with k = 1. When adding flyash, k-values are dependent on the cement´s strength classification. (k = 0.4 for class 42.5 or higher). The k-value for silica is determined by using table NA.7 and depend on the cement type and exposure class.

2.2.4 Cement

UHPC usually contains about twice the amount of cement as an ordinary concrete. Values between 600 to 1000 kg/m^3 are normal, and the fineness should be between 3000 and 4500 cm^2/kg [3]. Usually a Portland cement with low aluminate (C_3A) is preferred as it reduces the need for water which, in return, reduces the w/b ratio. As a result of large amounts of cement in the matrix, not all the particles come in contact and react with water; the excess cement is chemically inert and positively contributes to the particle packing density.

2.2.5 Pozzolans

There are numerous amounts of chemically reactive constituents that can be added to the concrete mix. They either work alone or in combination with the cement clinker or its hydration products [15]. Chemically inert materials are also widely used and are referred to as fillers; They have many benefits such as improved workability and optimized material density. Figure 2.5 displays a scanning electron micro-graph of two different pozzolans commonly used in concrete, silica fume (SF) and fly ash (FA).

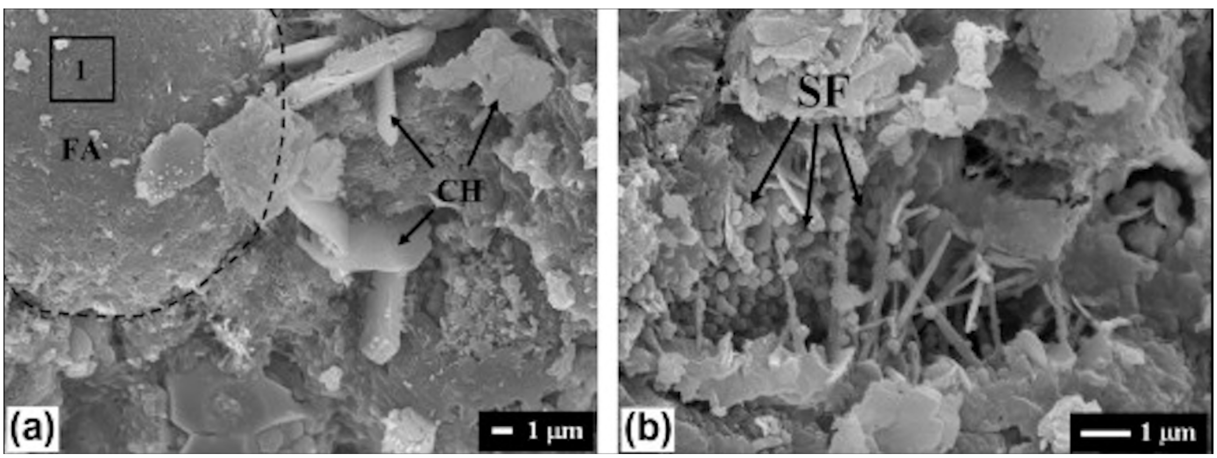

Figure 2.5: SEM of SF and FA [4]

Silica fume
SF is an industrial by-product from the manufacture of silicon metal and ferro-silicon alloys. These particles contain 85-98% SiO_2, they are spherically shaped with an average particle size ranging from 0.1 to 0.2 μm and has an amorphous structure. SF plays an important role in UHPC because it reacts with the hydration product of Portland cement, calcium hydroxide (CH), and generates C-S-H binder, which inhibits higher strength and gives a lower material porosity, especially in the ITZ [15]. It also improves the packing density of all the granular constituents as its particle diameter is approximately 1% to that of cement.

In an ordinary cement paste, a certain level of water is required to fill the void space between the granular constituents to give the desired workability. Using SF in the mix design, a substantial amount of water can be replaced to fill these voids. As a result of the silica fume´s spherical form, a “ball-bearing effect” may exist, improving the mobility in its fresh phase [15].

Fly ash

FA is an industrial by-product obtained from furnace fires with pulverized coal. This pozzolanic material´s composition may vary depending on the coal used, but will include high levels of silicon dioxide SiO_2. FA has a blaine fineness in the range of 300-450 m^2/kg and a density of 2300 kg/m^3 [15].

The high fineness and the reduction of water in the mix design reduce the probability of bleeding in the fresh phase. The concrete´s early age strength may be confined; however, after the hydration reaction between cement and water diminishes, the pozzolanic reaction continues, resulting in a higher final strength, which is noticeable after 28 days.

2.2.6 Admixtures

Superplasticizers (SP)

SP´s are organic polymers and crucial elements when producing UHPC. This admixture maintains an acceptable workability when w/b values are decreased. The main role of SPs are to disperse flocculated cement particles [16]. This is accomplished by reducing the cohesion and internal friction between the different material components by neutralizing surface changes [7]. As stated earlier, the SP dosage should exceed 5 mass % of the cement to maintain its workability. Polycarboxylate ethers (PCE) are third-generation SPs and the only admixture that allows the replacement of the large water amounts required to make a UHPC. Figure 2.6 shows the stabilization effect of polycarboxylate ethers; they have comb-like structures and are absorbed on to the cement particle surface, preventing the cement from coming in close proximity to each other [5].

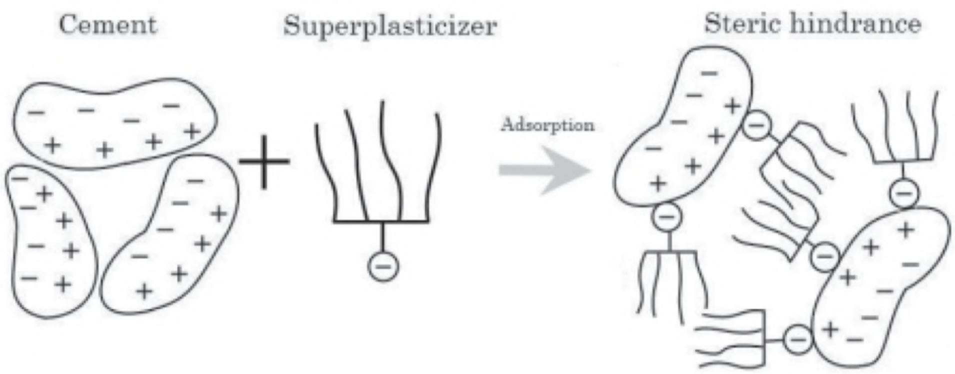

Figure 2.6: Schematic draft showing stabilization by steric hindrance [5]

Shrinkage reducing admixtures (SRA)

UHPC experiences minimal dry shrinkage due to low water volume; however, it undergoes a large autogenous shrinkage due to a high binder volume. Studies have shown that the addition of shrinkage reducing admixtures can diminish this substantially [6]. Figure 2.7 displays the effect of a shrinkage reducing agent provided by German Evonik Industries at dosages 0, 0.5, 1, and 2%.

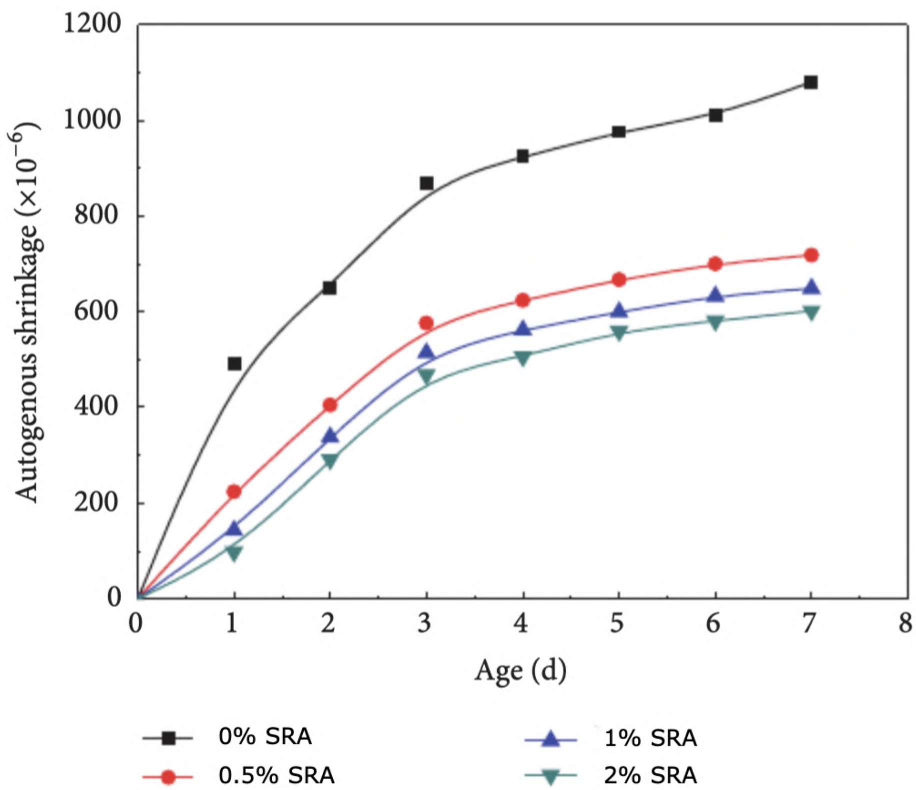

Figure 2.7: Effects of SRA on autogeneous shrinkage of UHPC at different dosages [6].

2.2.7 Aggregates

The aggregates used in UHPC should have a grain size distribution that produces a dense particle packing. Compared to an ordinary concrete, the largest aggregate fraction is usually removed, and the mean particle size often lies below 1 mm. The removal of course aggregates can strengthen the material´s homogeneity. The aggregates should inhibit high mechanical strength to prevent the particle phase from becoming the weakest link in the material. Calcined bauxite, basalt and granite are often utilized in UHPC because of their high strength. When the largest grain size used in the mix design is 0.5 mm, the material can be classified as a reactive powder concrete (RPC) [3]. Addition of courser aggregates may result in a lower autogenous shrinkage; however, the thickness of the constructional element should be sufficiently large compared to the maximum aggregate fraction used [17]. Furthermore, the addition of courser aggregates in the mix design has the potential of reducing the material cost significantly. The strength of a fully compacted concrete with a certain water/binder ratio is for the most part independent of the aggregate grading; however, without adequate workability, the fresh concrete cannot be compacted sufficiently to attain its maximum strength potential [18]. Therefore, the grading of aggregates plays a substantial but indirect part in the mechanical properties.

2.2.8 Fibers

UHPCs exhibit brittle behavior without the use of fiber reinforcement. Fibers are therefore important if the material is to be utilized in construction members. They improve ductility in both tension and compression as well as enhance the flexural and tensile strength significantly [3]. The use of fibers can have a negative impact on the workability depending on the fiber dimensions and volume percent used. Both the geometry of the construction member and stress type can influence the size and shape of a crack opening when its yield limit is reached. The fiber length and diameter can determine which cracks it can handle without ending in brittle failure. The amount of fibers proportioned is measured as percent of the total composite volume termed volume fraction (V_f). The aspect ratio is defined by the fiber length (l) divided by its diameter (d). Steel fibers provide the composite material with a high modulus of elasticity, high ductility, strength, and durability. The high alkaline environment in concrete protects the fibers from corrosion. Closer to the carbonated layer at the surface, corrosion may take place if the moisture level is high enough. However, studies have shown that due to the fiber´s slenderness, corrosion does not build up enough pressure to induce spalling in the material [19]. An ordinary fiber-reinforced concrete usually contains 0.25 to 2 vol-% steel fibers while UHPC can be proportioned with as much as 11 vol-% [3]. A study has established that a volume percentage of around 2.5 with an aspect ratio between 40 to 60 provides a good balance between the fresh and hardened phase properties [19].

2.3 Rheology - Workability

A material´s strength, volume stability and durability is not only influenced by its composition but also how the concrete has performed in its fresh phase. Its ability to become compact and reworkable in addition to maintaining its homogeneity before hardening play an important role in its final performance. UHPCs with fiber reinforcement need high quantities of SP to accomplish an acceptable flow and level of workability. According to some studies, SP should exceed 5 mass-% of cement to attain this [19]. The use of air-entraining agent also has a positive effect on workability as well as frost resistance. Workability can be summed up by three elements: stability, mobility, and compactability [7].

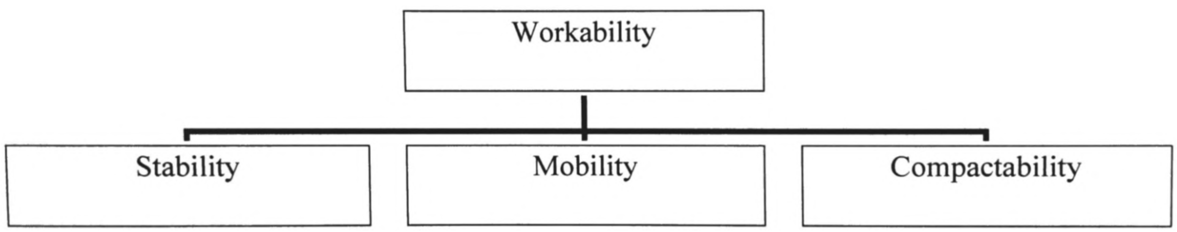

Figure 2.8: The workability concept [7]

2.3.1 Stability

During its fresh phase, concrete is subjected to numerous loads due to transportation, casting, and compacting. Stability refers to concrete´s ability to sustain its homogeneity through these processes as well as at rest. Separation is an example of poor stability and occurs due to the low cohesion and internal friction between the material components compared to the variations in densities. There are different forms of separation; in ordinary strength concretes, the most likely form is water separation. In UHPCs, however, the low water/cement ratio is low, reducing the possibility of water separation. The stable cement paste itself may separate from the other larger granular constituents. This can be avoided by increasing the fine filler fraction with diameter under 0.125mm and limiting the flow of concrete by restricting the quantity of SP in the mix design [7].

2.3.2 Mobility

The term mobility refers to the concrete´s ability to move when subjected to dynamic forces. Factors that influence concrete´s mobility include the friction between particles, internal cohesion to solid surfaces, and the liquid phase´s resistance to internal flow [7]. UHPCs have a large paste volume, creating a larger distance between the aggregate particles, lowering the internal friction, and increasing the mobility. Additives such as

SPs and air-entraining admixtures can also be used to increase the mobility. When proportioning a mix design to have a high flow and be self-compacting, a high level of fine particles and a smooth grading curve are essential, as higher mobility often reduces stability. Figure 2.9 illustrates how the mobility of concrete is affected by altering the material´s components. The vertical axis displays the yield value (g), and the horizontal axis shows the plastic viscosity (h). The arrow directions illustrate increasing values. Take the slump flow test as an example (described in Section 3.2), the concrete will continue to flow if the stress due to gravity is greater than the yield value. The plastic viscosity determines the velocity of movement.

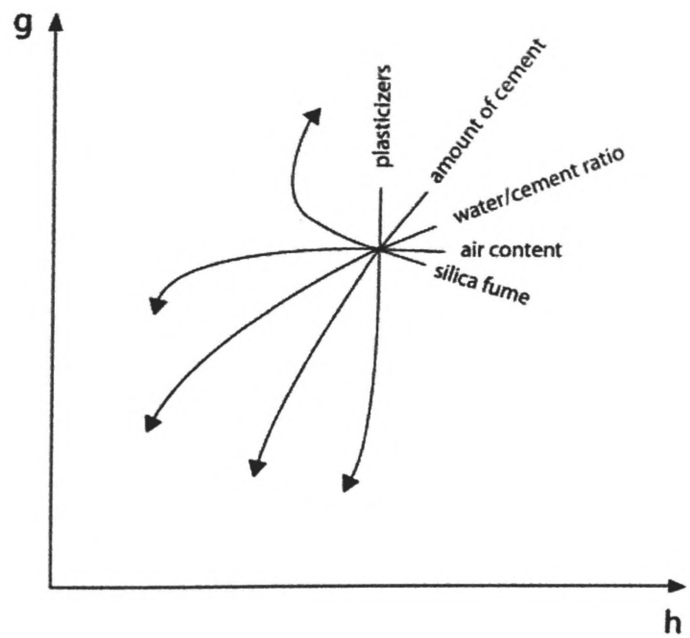

Figure 2.9: Effect of material composition on concrete´s yield value and plastic viscosity [7].

2.3.3 Compactability

Compactability refers to concrete´s ability to be compacted and release encapsulated air pockets during casting. Cohesion, shock absorption, density, air void content, and mobility are factors that effect compactability. A higher mobility gives higher compactability, but reduces stability. Air voids are weak zones in hardened concrete, affecting both strength and permeability. These voids are often course and irregular shaped with a diameter of 1mm or larger.

2.4 Material properties

2.4.1 Compressive strength

Compressive strength is an essential factor when designing a concrete construction, and is the property most often measured. UHPC typically has compressive strengths ranging from 150 to 250 MPa. Fibers do not have a significant influence on the compressive strength; however, they do affect the stress-strain behavior of the material. At failure, UHPC without fibers will act brittle and can be described as an explosion. The presence of fibers has a restraining and confining effect on the concrete and will experience a ductile failure with adequate vol-%.

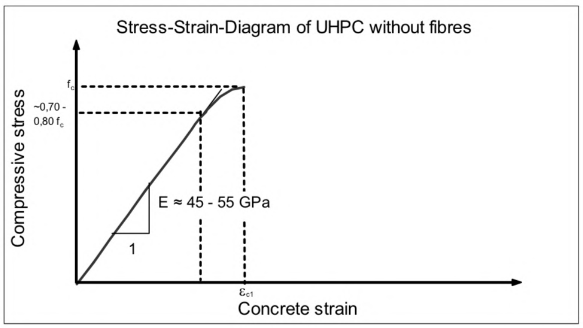

(a) Without Fibers

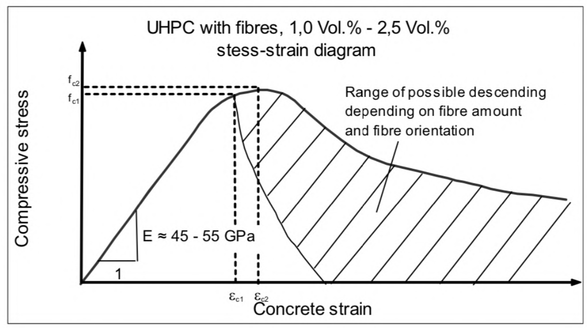

(b) With Fibers

Figure 2.10: Stress-strain curve for UHPC

Figure 2.10 displays a stress-strain curve for an UHPC with and without fiber reinforcement. The slope of the descending branch depends on: [20]

- Fiber content
- Fiber geometry (length, diameter)
- Fiber length in relation to maximum aggregate size
- Fiber stiffness (in case of fiber cocktails)
- Fiber orientation

A study on the compression strength of UHPC and its relationship to the modulus of elasticity was published in 2007 by *Benjamin Graybeal* [21]. This paper included three empirical linear equations, connecting E-modulus and 28-day compressive strength, one for NSC (Equation 2) and two for UHPC (equations 3 and 4). This paper stated that achieving the correct stress-strain response and modulus of elasticity is difficult due to the material´s heterogeneous nature with a variety of possible mix designs.

$$E = 4730\sqrt{f_c}[MPa] \tag{2}$$

$$E = 3320\sqrt{f_c} + 6900[MPa] \tag{3}$$

$$E = 19000\sqrt[3]{\frac{f_c}{10}}[MPa] \tag{4}$$

The maturation speed of compressive strength in concrete depends on the heat regime; a higher temperature environment will accelerate the chemical reaction and may also improve the final micro-structure. Studies have shown that heat curing at 90 degrees Celsius for a duration of 48 hours can result in higher compressive strengths than immersion in water for 28 days [20].

Table 2.1 shows the strength classes up to B95 in NS-EN206-1; as previously stated, the Norwegian standards do not cover UHPC´s strengths.

Table 2.1: NS-EN206-1 table NA2

Specimens	Strength classes										
	B10	B20	B25	B30	B35	B45	B55	B65	B75	B85	B95
Cylinders (150x300mm)	10	20	25	30	35	45	55	65	75	85	95
Cubes (100x100mm)	12	25	30	37	45	55	67	80	90	100	110

2.4.2 Tensile and flexural strength

UHPC subjected to tensile forces can be categorized either as strain softening or strain hardening and define how the material behaves after crack initiation. Figure 2.11 illustrates a typical stress-strain response for UHPC in tension. Here, σ_{cc} is the strength at which crack initiation takes place. Strain softening occurs when the maximum tensile capacity decreases after crack initiation, indicating the fibers do not have a restricting effect on crack propagation. Stain hardening on the other hand occurs when the fibers help stitch the crack together though plastic deformation, allowing the tensile capacity to increase beyond the point of cracking; this illustrated in Figure 2.11 as σ_{pc} (post cracking strength). For this to be possible, it usually requires a fiber volume percentage larger than 2 [8]. As stated above, the residual strength after crack initiation depends on fiber content, geometry, length, stiffness, and orientation. Here, orientation and distribution depend on viscosity and casting methods. Typical tensile strengths of UHPCs lie in the range of 6-20MPa [3, 8].

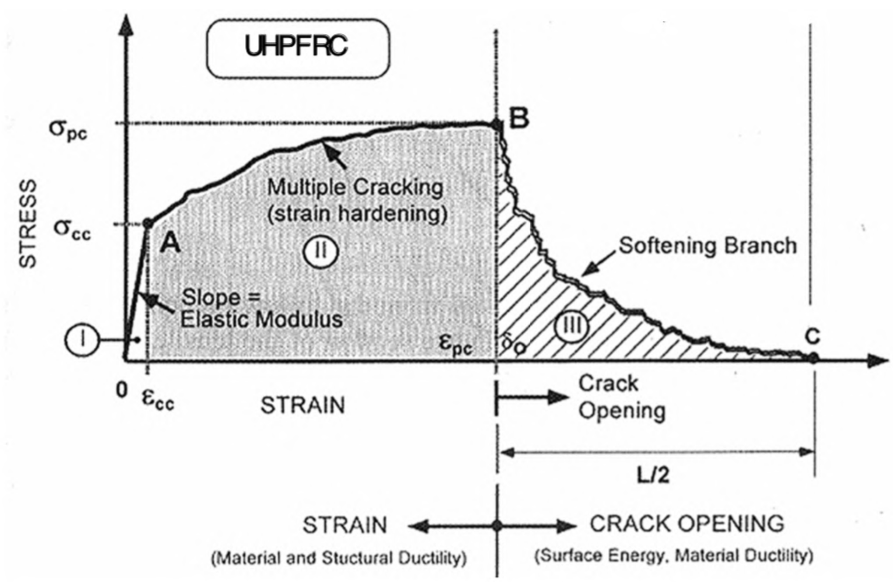

Figure 2.11: Typical stress-strain response of UHPC in tension [8].

2.5 Durability

Concrete´s durability can be defined by its ability to withstand significant deterioration over time, whether it be resistance to weathering action, abrasion, or chemical attack [22].

2.5.1 Porosity

During hydration, the external volume remains approximately constant where the volume change is mostly affected by the storage conditions. Internally, hydration causes significant alterations to the solid volume, affecting the degree of porosity. Here, porosity can be defined by the internal volume that can be filled with water [9]. The largest influence on porosity are by the water-to-cement ratio and the degree of hydration. The low w/c of UHPCs results in low porosities, as can be seen in Figure 2.12.

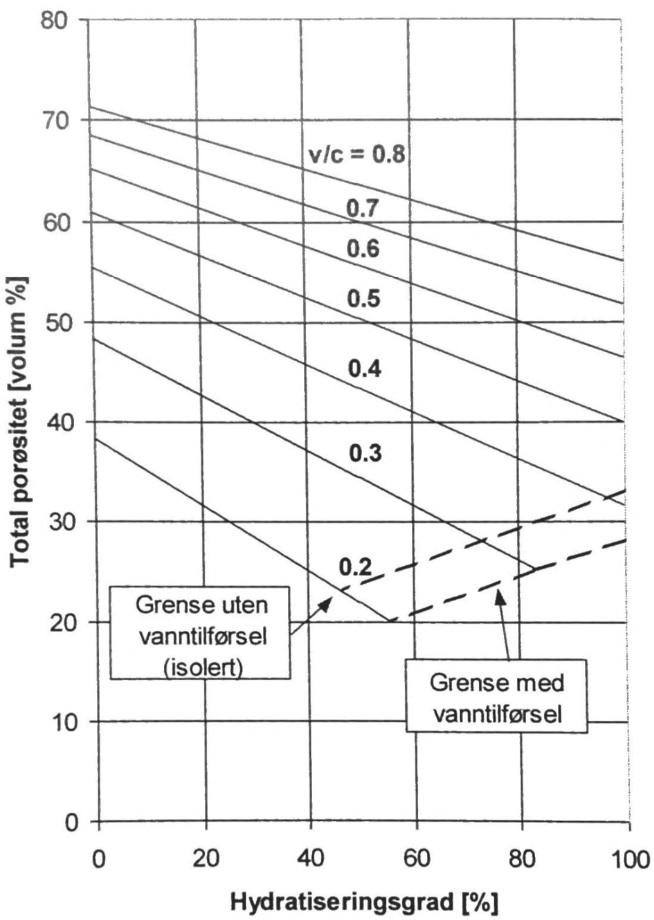

Figure 2.12: Total porosity of cement paste [9].

Concrete is a porous media, with a pore structure consisting of a wide range of sizes and shapes ranging from nanometers to micrometers. The total porosity displayed in Figure 2.12 above can be subdivided into air/macro pores (d<1000nm), gel pores (around 2 nm), and capillary pores (4nm < d < 1000nm). Macro pores are often formed by encapsulated air during casting and compacting. Gel pores occur in the small space between the solid parts of the C-S-H phase formed during hydration. The original water-filled volume between the cement particles that are not filled with the hydration products form the capillary pores. Figure 2.13 illustrates the volumetric composition of the cement paste, neglecting the presence of macro pores. The low w/c of UHPCs means low porosity and a higher level of CH / C-H-S and unhydrated cement particles.

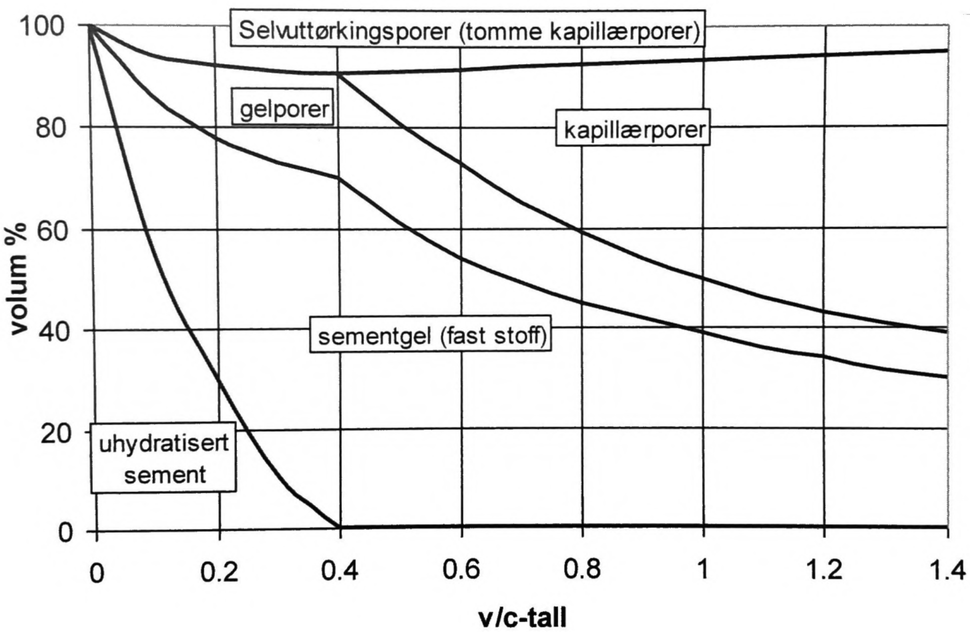

Figure 2.13: Volumetric composition of cement paste [9].

2.5.2 Permeability

Permeability is the transport of mass though a substance and, for concrete, an important factor that is either directly or indirectly responsible for most of the deterioration mechanisms. The low porosity of UHPC mitigates the intrusion of chloride ions and other aggressors, improving its durability over time.

2.5.3 Elephant skin

UHPCs have a tendency to form a thin surface skin after mixing, which is colloquially known as elephant skin. This layer is only a few micrometers thick and consists of enriched sodium and potassium, originating from the accumulation of SP. This thin layer hinders the out-gassing of entrapped air during compaction, resulting in a higher macro porosity.

2.5.4 Autogenous shrinkage

All UHPC mix designs are proportioned after a low w/b, which is one of the main contributing factors to its high strength. However, UHPCs display large autogenous shrinkage, which can lead to early age cracking in the concrete structure. The hydration reaction between the cement particles and water produce hydration products. These products have a smaller volume than the reactants. A larger dosage of cement in the mix design can also lead to a larger volume reduction. It is estimated that the volume is reduced by 0.06 cm^3 per gram cement that hydrates. With w/b as 0.4, a reduction of 8 vol-% is normal [23].

3 Methods of measurement

This section describes the test procedures carried out before and after batching and on the specimens in their hardened state.

3.1 Moisture in aggregates

The amount of water added to the concrete mixture is adjusted based on the moisture already present in the aggregate to attain the desired w/b ratio. This can be done by using the speedy moisture tester that measures the gas pressure generated by a reaction between the available moisture within the aggregate sample and a pulverized calcium carbide reagent. A 20g sample of the aggregate is measured and placed in the vacuum container and then two scoops of reagent added in the container´s inverted cap, keeping the sample and reagent separate as to not start the reaction prematurely. The cap is placed on the container in a horizontal position, then sealing it air tight. It is shaken with a rotating motion and turned 180 degrees for 20 seconds, rested, and then shaken for another 20 seconds. A gauge underneath the container displays the moisture percentage by wet weight and needs to be converted into percentage by dry weight using Equation 5 given:

$$\boxed{\%moisture_{(dry)} = \frac{\%moisture_{(wet)} \cdot 100}{100 - \%moisture_{(wet)}}} \tag{5}$$

3.2 Workability of fresh concrete

The workability of fresh concrete can be measured with the slump flow test which indicates the concrete´s filling ability and some insight into the its resistance to segregation. This test is governed by NS-EN 12350 part 8[10]. The base plate and inside of a truncated cone-shaped mold, with dimensions 200mm at base, 100mm at top, and 300mm height are moistened. The cone is placed centrally on the level base board and held down firmly. Concrete is poured in the mold, and any surplus concrete outside the cone is removed. The mold is raised vertically in a controlled manner, allowing the concrete to flow freely. The diameter is recorded in two places perpendicular to each other and the average slump flow value calculated.

A miniature variant of this test is used to measure workability over time; although this variant is not standardized in any code, it can give an indication of how the concrete´s workability degrades over time after mixing. Several base boards are created by laminating A3 papers with circular distance markings. The molds are made by cutting a plastic pipe with an inner diameter of 7.2 cm into 10cm pieces. Figure 3.1 illustrates this slump flow setup.

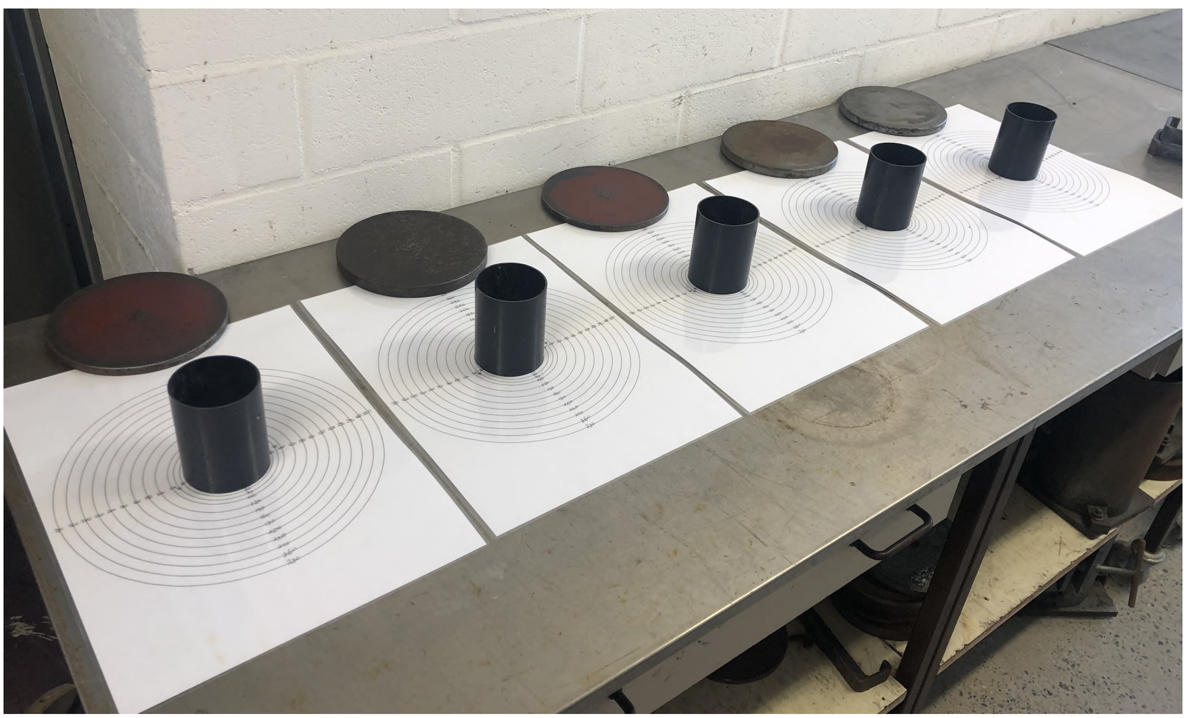

Figure 3.1: Miniature slump flow to measure workability over time

3.3 Hardened density

The density of hardened concrete can be determined by first measuring the mass (m) of a specimen. A container filled with water is placed on a weight scale and the specimen is submerged in water while hanging in an apparatus to ensure it does not touch the container walls. The weight displayed on the scale represents the volume (V) as water has a density of 1 kg/m^3. The concrete´s density is then determined by Equation 6.

$$\boxed{\rho = \frac{m}{V}} \tag{6}$$

3.4 Compressive strength

Compressive strength is measured in accordance with NS-EN 12390-3 [13]. Concrete cubes, 100x100mm, are placed and aligned centrally in a compression testing machine shown in Figure 3.2. A compressive load of 0.8 N/mm^2s is applied until fracture. The failure load is divided by the cross sectional area resisting the load and measured in units newton per millimeters or mega-pascals.

$$\boxed{f_c = \frac{F}{A_c}} \tag{7}$$

Figure 3.2: Photograph of specimen undergoing compressive testing

3.5 Splitting tensile strength

The splitting tensile strength is determined in accordance with NS-EN 12390-6 [14]. This is an indirect method for testing the tensile strength of concrete and is a simpler method compared to a uniaxial tensile test. The sample size of the concrete specimen is a cylinder with 150mm diameter (d) and 300mm length (L). Diametrical lines are drawn on the two ends of the specimen to ensure the force is exerted on the same axial place. The specimen is placed in a compression testing machine in a jig, as illustrated in Figure 3.3. A continuous load is applied to the specimen until fracture. The failure load (F) is noted and used in Equation 8 to determine the splitting tensile strength:

$$\boxed{f_{ct} = \frac{2 \cdot F}{\pi \cdot d \cdot L}} \tag{8}$$

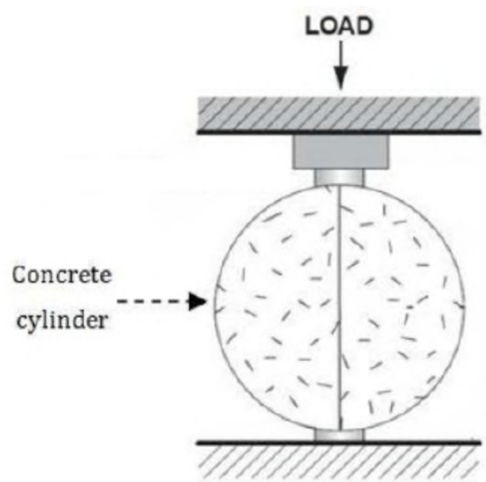

Figure 3.3: Illustration of splitting tensile testing.

3.6 Modulus of elasticity

The modulus of elasticity is governed by NS-EN 12390-13 [15]. Method A is described in this section. A cylinder with 150mm diameter (d) and 300mm length (L) is placed in a compression testing machine. The deformation of the specimen is recorded at different load variations by fitting the specimen with a strain measuring instrument. First, three preloads are carried out to check for wiring stability and specimen positioning, followed by three load cycles, where stress and strain values are registered. This is illustrated in Figure 3.4 below. The load rates are set to 0.6 ± 0.2 MPa/s and the upper/lower stresses are held at 20 second period per cycle.

The stabilized modulus of elasticity can be determined by Equation 9.

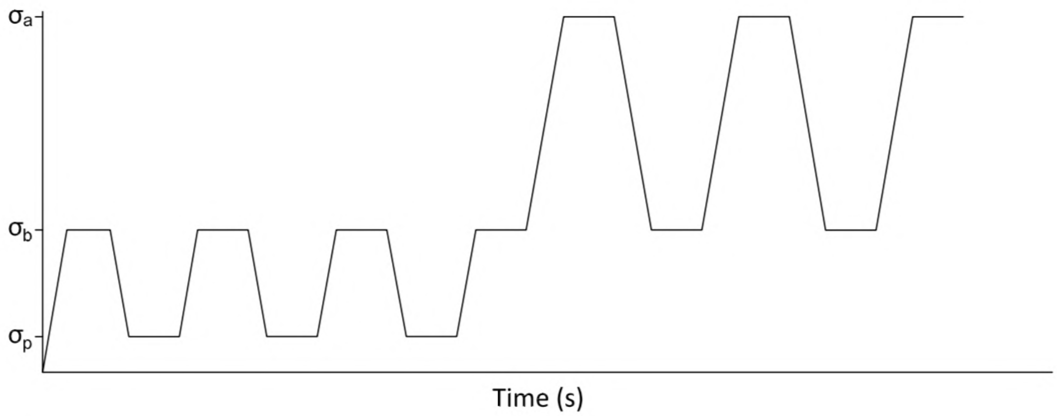

Figure 3.4: Miniature slump flow to measure workability over time.

$$\boxed{E_{c,s} = \frac{\sigma_a^m - \sigma_b^m}{\epsilon_{a,3} - \epsilon_{b,2}}} \tag{9}$$

where,

- σ_a^m is the measured upper stress and can be calculated by the equation,

$$\boxed{\frac{f_c}{3}} \tag{10}$$

where f_c is the cylinder´s compressive strength. In the case where compressive strengths have been measured on 100x100mm cubes, a conversion factor can usually be applied based on its strength class according to NS-EN 206-1 (Table 1). However, as this standard does not account for UHPCs, the conversion factor of 0.86 corresponding to B95 is chosen, keeping in mind this may lead to a small source of error.

- σ_b^m is the measured lower stress and lies within the following interval:

$$\boxed{0.10 \cdot f_c \leq \sigma_b \leq 0.15 \cdot f_c} \tag{11}$$

- $\epsilon_{a,3}$ is the average strain measured at the third upper stress cycle,
- $\epsilon_{a,3}$ is the average strain measured at the second upper stress cycle, and
- σ_p is the preload stress and lies between 0.5MPa and σ_b^m.

3.7 Flexural strength

The flexural strength test is standardized in NS-EN 12390 part 5 [16]. A beam with dimensions 100x100x500mm is supported at each end with steel rollers with a diameter of 20 mm. This is illustrated in Figure 3.5 below. The beam is subjected to a central point loading F that is gradually increased by 0.05 MPa/s until failure occurs. The failure load is used in Equation 12 to determine its flexural strength.

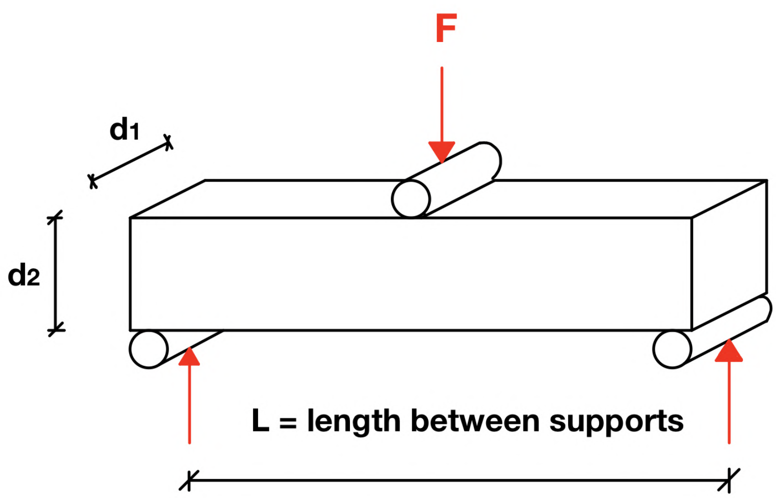

Figure 3.5: Illustrative drawing of flexural strength test.

$$\boxed{f_{ct} = \frac{F \cdot L}{d_1 \cdot d_2^2}} \tag{12}$$

3.8 Sorptivity and Porosity

The method for testing sorptivity and porosity in hardened concrete is standardized in publication 426 (PF method) at The Norwegian Public Roads Administration. This method derives various water porosities by exposing dried concrete specimens to water, both with and without pressure [9].

Method

- Concrete cubes/cylinders are cut into 20 ± 1 mm thick specimens; the concrete can either be casted or core drilled from an existing construction.
- Specimen thickness is control measured.
- The specimens are air dried at 105 °C for 7 days followed by a minimum 2 hours of cooling in room temperature sealed in plastic foil.
- The specimens are weighed (m_1).
- Specimens are placed in a tub where the cut surface is exposed to a water front, with the water level not surpassing 1-2mm up the sides. This is illustrated in Figure 3.6. The specimens are weighed after 10 and 30 minutes and 1,2,3,4,6, 24, 48, 72, and 96 hours. (96 hour weight = m_5)
- When weighing the specimens, they are removed from the tub, making sure the water does not drip onto the other specimens. The surface water is removed by using a damp cloth, weighted and placed back in the tub.
- The specimens are now submerged in water for 72 hours and weighed in air (m_2). The volume (V) is determined by weighing the specimen under water.
- The specimens are submerged in a pressure tank at 50 atm for minimum 24 hours before being removed and immediately weighed (m_3).

Figure 3.6 illustrates the specimens while undergoing capillary sorption from one side.

Figure 3.6: Photograph of specimens undergoing capillary sorption

Calculations

- Bulk Dry Density (g/cm^3):

$$\boxed{\rho_{BD} = \frac{m_1}{V}} \tag{13}$$

- Saturated Surface Dry Density (g/cm^3):

$$\boxed{\rho_{SSD} = \frac{m_2}{V}} \tag{14}$$

- Solid Density (g/cm^3)

$$\boxed{\rho_S = \frac{\rho_{BD}}{1 - \epsilon_{tot}}} \tag{15}$$

- Air porosity Vol-%

$$\boxed{\epsilon_{air} = \frac{m_3 - m_2}{V}} \tag{16}$$

- Saturated by suction porosity Vol-%

$$\boxed{\epsilon_{suc} = \frac{m_2 - m_1}{V}} \tag{17}$$

- Pressure saturated porosity Vol-%

$$\boxed{\epsilon_{tot} = \frac{m_3 - m_1}{V}} \tag{18}$$

- Pore Protection Factor

$$\boxed{PF\% = \frac{\epsilon_{air}}{\epsilon_{tot}}} \tag{19}$$

For a concrete to be classified as frost resistant, the pore protection factor defined as the air content as a percentage of the total porosity, should be greater than 25% [9]. The air porosity (ϵ_{air}) entails macro/air pores that are too large to produce capillary tension in the water; pressure is required to determine the air porosity, i.e, the m_3 weight needs to be calculated. The ϵ_{suc} contains smaller gel/capillary pores that can suck water through the material.

The rate of capillary suction depends on the concrete´s quality; however, it is almost linear when presented in a graph with the square root of time as an axis. UHPCs with a higher density matrix have a more gradual slope than NSC. When the capillary pores have been filled with water, the slope evens out horizontally and the gradual incline represents the small portion of the macro pores being filled. Figure 3.7 illustrates this effect.

Capillary number (k) is derived by Equation 21 and is an empirical value that represents the slope of the first linear section; it can be used to characterize the permeability of concrete. UHPCs with a high density matrix and lower porous micro-structure have a lower capillary number than NSCs.

Resistance number (m) derived by equation 22 shows the water front´s suction velocity into the concrete specimen, indicating to the capillary pore size. This is due to the fact that capillary tension in water is inversely proportional to the water´s meniscus radius, i.e, pore size.

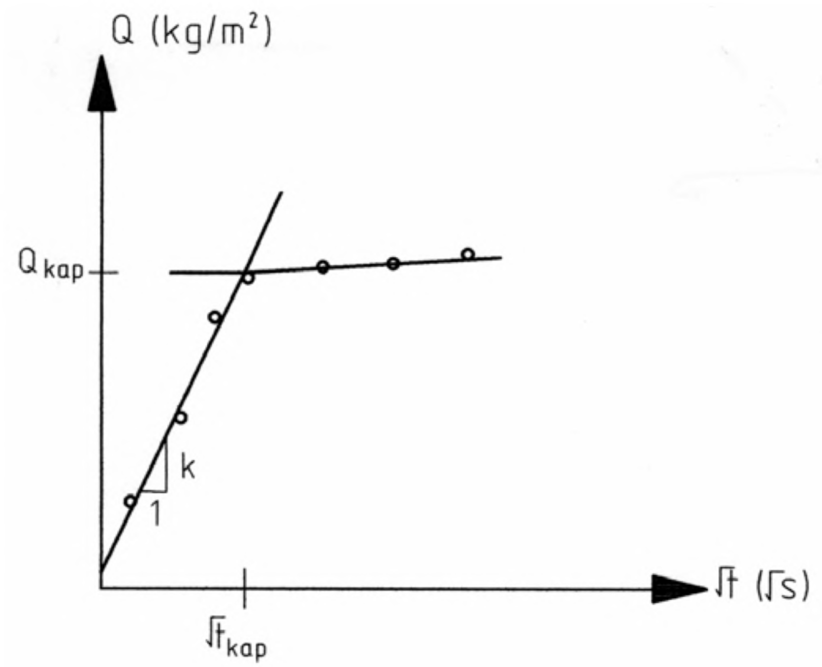

Figure 3.7: Capillary sorption over square root of time

$$\boxed{k = \frac{Q_{cap}}{\sqrt{t_{cap}}}} \tag{20}$$

$$\boxed{m = \frac{t_{cap}}{z^2}} \tag{21}$$

where,

- Q_{cap} represents the point of capillary capacity.
- t_{cap} is the time where capillary capacity is reached.
- z is the specimen thickness.

4 Research plan

The stated goal of this thesis is the mapping of UHPC´s workability over time and attempt to understand its mechanical properties and durability, when the material constituents in the mix design are modified. The curing treatment applied to concrete is especially crucial when working with UHPC. The specimens researched underwent two different curing treatments; either immersed in water or air tempering. These curing regimes will be described in more detail later.

This section describes the test matrix, specimen nomenclature, mix designs, and procedures undertaken when batching, casting, and curing. Individual test programs were performed when investigating specific aspects of UHPC.

4.1 Batch and Specimen nomenclature

The test matrix includes over 200 separate concrete specimens; so a naming schedule is devised to correctly identify each of them. Most of these specimens were a part of a standardized program to identify the hardened state behavior of UHPC when the mix design and curing condition varied. The remaining specimens were part of an extraneous program to determine specific properties, such as durability and flexural strength when the workability and compressive strengths were within favorable parameters.

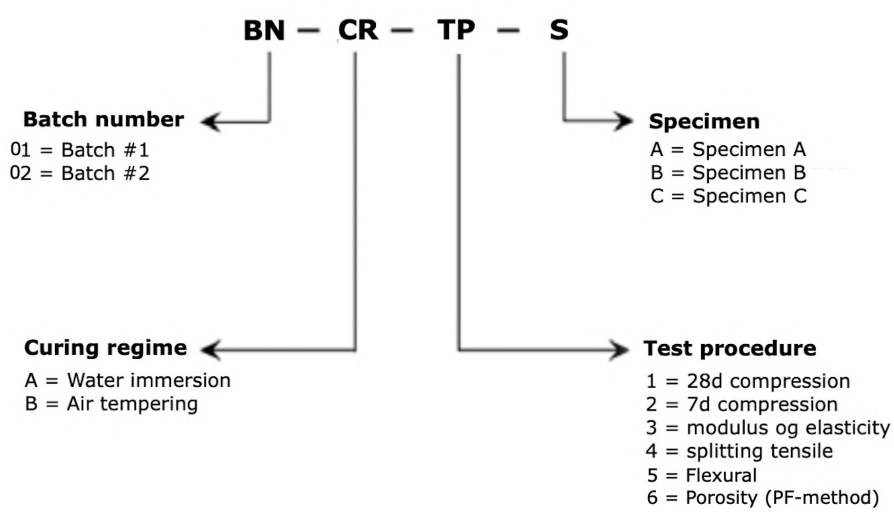

Figure 4.1: Specimen naming schedule

The nomenclature used was a five digit alphanumeric identifier, where the first two digits were numerical, displaying the batch number. The third digit disclosed the curing treatment the specimen underwent, where A represents immersion in a water bath at 20 degrees Celsius. B represents an air tempering program where the specimen is after unmolding sealed in plastic and placed in 90 °C for 48 hours followed by 20 °C for the remaining period. The fourth digit is numerical and identifies the test procedure to be undertaken. Figure 4.1 shows which test corresponds to which number. The fifth digit is a letter A,B, or C, separating specimens from the same batch that have undergone the same curing and tests. An example is 01B2A, indicating the specimen is from batch 1, has been air-tempered, compression-tested 7 days post mixing, and is the first of three specimens.

4.2 Test matrix

The test matrix prepared for this program focuses on the material´s characteristics in both fresh and hardened states. The tests to be performed focused on determining workability over time, mechanical strengths, and durability. Two different mixers were used, an Eirich R09t with a capacity of 150 liters or 240 kg and an Eirich intensive mixer R02/Vac with a capacity of 3-5L or max 8kg. The amount and type of concrete specimens to be casted for each batch depend on the type of mixer used as the volume capacity varies between them. A total of 22 different mix designs were batched and are described in detail in the next subsection. Each batch underwent a mapping of its workability over time, independent of the mixer used. This was done by using a miniature version of a flow board test and is described in Section 6.2. Measurements were carried out at 0,5,10,15, and 30 minutes. The 7-day compressive strength were also determined after undergoing curing regime B for all 22 mix designs. When using the larger mixer the 7-day and 28-day compressive strengths, modulus of elasticity, and tensile splitting tests were also determined for specimens that underwent curing regime A. Table 4.1 gives an overview of the test matrix for the standardized test program depending on the type of mixer.

Table 4.1: Matrix for standardized test program (batches 1-22)

Type of test	Mixer	Specimens cast	Curing regime
Flow board	R02/Vac and R09t	5	-
7d compressive strength	R02/Vac and R09t	3 100x100mm cubes	B
7d compressive strength	R09t	3 100x100mm cubes	A
28d compressive strength	R09t	3 100x100mm cubes	A
Modulus of elasticity	R09t	2 150x300mm cylinder	A
Tensile splitting strength	R09t	2 150x300mm cylinder	A

where A = water immersion at 20 °C, B = air tempering at 90 °C, R09t = 150L Eirich mixer, and R02/Vac = 5L Eirich intensive mixer.

The three batches that result in the most promising workability over a 30-minute period and also possess a compressive strength of over 150 MPa after 28 days with curing regime A, were re-batched with modifications made to the amount of SP. Trying to achieve a similar initial slump flow value so that the workability over time can be analyzed more accurately. Results were compared to that of batches 1 through 19. The four best mix designs were re-batched in an 85 liter batch in the R09t mixer. Workability measurements were now registered up to one hour after mixing (0, 5, 10, 15, 20, 30, 40, 50, and 60 min); a larger test program was undertaken for these batches. This includes compressive strengths after 7 and 28 days, modulus of elasticity, both splitting tensile and flexural strength, and permeability tests using the PF-method. This is displayed in Table 4.2 below.

Table 4.2: Matrix for extraneous test program (Batches 23-26)

Type of test	**Mixer**	**Specimens cast**	**Curing regime**
Flow board	R09t	10	-
7d compressive strength	R09t	3 100x100mm cubes	B
7d compressive strength	R09t	3 100x100mm cubes	A
28d compressive strength	R09t	3 100x100mm cubes	A
Modulus of elasticity	R09t	2 150x300mm cylinder	A
Tensile splitting strength	R09t	2 150x300mm cylinder	A
Flexural strength	R09t	3 100x500mm beams	A
Porosity (PM method)	R09t	3 100x100mm cubes	B

where A = water immersion at 20 °C, B = air tempering at 90 °C, and R09t = 150L Eirich mixer.

4.3 Proportioning the mix designs

A total of five binder materials, two fillers, four aggregates, two superplasticizers and a shrinkage reducing admixture were used in varying degrees for the mix designs. The components and their properties are displayed below. Material data sheets for all the materials used can be found in Appendix I.

Binder
CEM II/A-V 42,5 N
(Norcem Anleggsement FA)
Density: 3020 kg/m^3
Blain: 390 m^2/kg

Binder
CEM I 52,5 R
(Norcem Industrisement)
Density: 3130 kg/m^3
Blaine: 550 m^2/kg

Binder
CEM III/A 52,5 R
(Dyckerhoff Variodur 40)

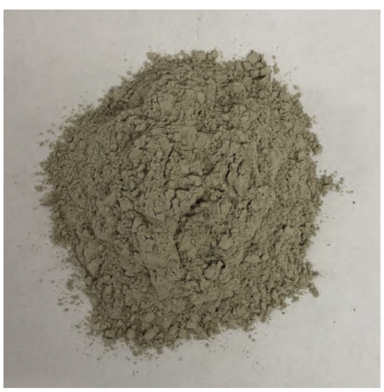

Binder
Slag (Merit 5000)
Density: 2920 kg/m^3
Blaine: 500 m^2/kg

Binder
Silica fume
(Elkem microsilika 940U)
Density: 2650 kg/m^3

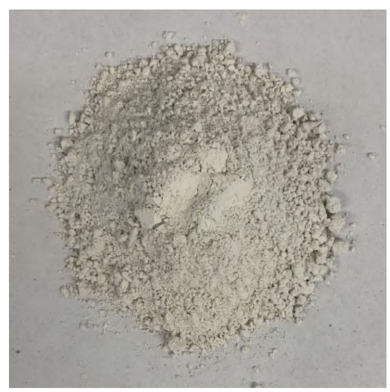

Filler
Millisil W12
Density 2650 kg/m^3
Silica powder

Filler
Betofill VK50
Density: 2720 kg/m^3
Limestone powder

Aggregate
Hostrup quartz sand
Particle diameter 0-1mm
Density: 2640 kg/m^3

Aggregate
Quarzwerke H33
Particle diameter $<$ 0.5mm
Density 2650 kg/m^3

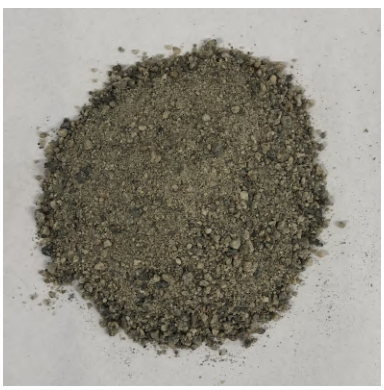

Aggregate
Gneiss-granite
Particle diameter 0-4mm
Density: 2660 kg/m^3

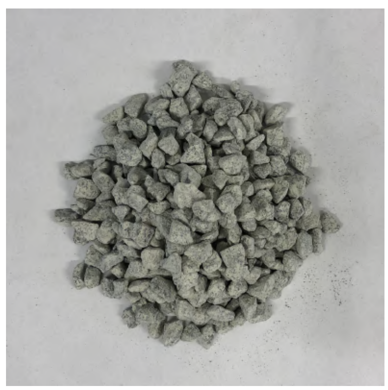

Aggregate
Quartz-diorite
Particle diameter 5-8mm
Density: 2770 kg/m^3

Steel fiber (Weidacon)
Length: 9 mm
Diameter: 0.15 mm
Aspect ratio: 60

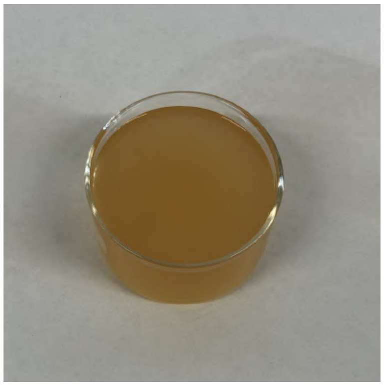

Superplasticizer
Mapei Dynamon SX-N
Density: 1.06 kg/L
Solid content≈ 18.5%

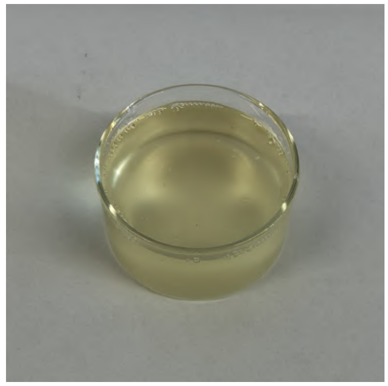

Superplasticizer
Sika Visco-Crete UHPC-2
Density: 1.08 kg/L
Solid content≈ 40.0 %

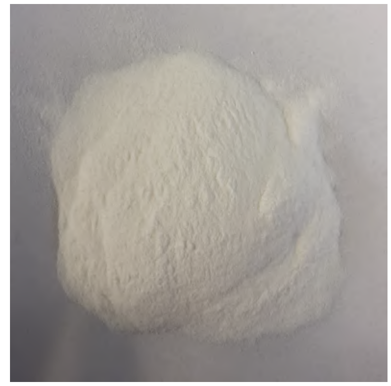

Shrinkage reducing
admixture
SAPs BASF

4.3.1 Standardized test program

First series

A mix design was taken from a UHPC bachelor thesis previously written at the University of Stavanger [24]. This mixture was fine grained with a maximum grain size of 0.5mm. As binder material, a CEM III/A 52,5 N ENCI was used however in this thesis CEM II/A-V 42,5N was used (Norcem Anleggsement FA) in addition to microsilica as these are most accessible for concrete suppliers in Norway. The chemically inert constituents included quartz sand H33 with a grain size ranging from 0.1-0.5mm and a German filler (Millisil W12). The steel fibers had a length/diameter of 9/0.15mm respectively, utilizing the SP Mapei Dynamon SX-N. This is a reference mixture in this thesis and shown as batch number 1 in Table 4.3 below. The first test series consists of 7 batches with different mix designs. One material constituent is replaced one at a time in order to isolate the effect it has on both the fresh and hardened phase properties. This first series focuses on modifying the fillers, aggregates, and SPs, keeping the quantity and type of binder, water, and fiber constant.

Table 4.3: Mix design - Series 1 - Batches 1-7 (kg/m^3)

Batch number	1	2	3	4	5	6	7
CEM II/A-V 42,5 N (Anl-FA)	740	740	740	740	740	740	740
CEM III/A 52,5 R (Variodur 40)	-	-	-	-	-	-	-
CEM I 52,5 R (Industri)	-	-	-	-	-	-	-
Merit 5000 (slag)	-	-	-	-	-	-	-
Elkem microsilica 940 U	146	146	146	146	146	146	146
Millisil W12	198	198	198	198	-	-	198
Betofill VK50	-	-	-	-	215	215	-
Danish quartz sand 0-1mm	-	-	934	-	-	-	-
German quartz H33	938	938	-	-	-	-	-
Gneiss-granite 0-4mm	-	-	-	942	942	659	659
Quartz-diorite 5-8mm	-	-	-	-	-	293	293
Weidacon 0,15/9mm	146	146	146	146	146	146	146
SAPs BASF	-	-	-	-	-	-	-
Mapei Dynamon SX-N	30	-	-	-	-	-	-
Sika Visco-Crete UHPC-2	-	10	10	10	10	10	10
Free water	210	210	210	210	210	210	210
Total	2408	2391	2384	2392	2409	2419	2402
w/b	0.224	0.210	0.210	0.210	0.210	0.210	0.210
EIRICH R09t	✓	✓	✓	-	-	✓	✓
EIRICH R02/Vac	-	-	-	✓	✓	-	-

Batch number 2 replaces Mapei Dynamon SX-N with another SP (UHPC-2), especially developed for use in UHPC. This SP is more effective so the dose was adjusted to 10 kg/m^3. Batch number 3 replaces the German quartz H33 with a Danish quartz sand 0-1mm. The volume of the granular constituents is constant when substituting a material; so the weight per cubic meter is adjusted based on its density. Batch 4 uses a gneiss-granite sand (0-4mm). Batch 5 changes the filler from Millisil W12 to Betofill VK50, which is a less expensive product. The aim here was to investigate whether the use of a cheaper filler has an impact on the material´s properties. Batch 6 replaces 30 % of the gneiss-granite with quartz-diorite, 5-8mm; 30% is chosen as it gives an even particle size distribution curve (Appendix H, Figure H.4). Batch 7 utilizes Millisil W12 as a filler while also using the larger fraction quartz-diorite, 5-8mm.

The water-binder ratio is derived by using a k-value of 2 for silica in accordance with NS-EN 206-1:2000+NA:2007 and assuming that the SP contain on average 70 % water.

Second series

The second series tests the use of a shrinkage reducing admixture SAPs BASF. This mix design was proportioned by a faculty member and is a part of an external research project undertaken at the University of Stavanger. Whether the SRA has an effect on minimizing the autogenous shrinkage was not examined in this thesis. The focus here was to understand its effect on workability over time and mechanical properties. Table 4.4 shows the mix design for this series, batches 8 and 9.

Table 4.4: Mix design - Series 2 - Batches 8-9 (kg/m^3)

Batch number	8	9
CEM II/A-V 42,5N (Anl-FA)	-	-
CEM III/A 52,5 R (Variodur 40)	778	778
CEM I 52,5 R (Industri)	-	-
Merit 5000 (Slag)	-	-
Elkem Microsilica 940 U	154	154
Millisil W12	-	-
Betofill VK50	186	186
Danish quartz sand 0-1mm	-	-
German quartz H33	-	-
Gneiss-granite 0-4mm	402	402
Quartz-diorite 5-8mm	649	649
SAPs BASF	-	2.34
Mapei Dynamon SX-N	-	-
Sika Visco-Crete UHPC-2	8.56	9.34
Free water	186	249
Total	2364	2430
w/b	0.177	0.239
EIRICH R09t	✓	✓
EIRICH R02/Vac	-	-

Batch number 8 is a reference batch, while the ninth batch contains a SRA at a dose of 0.3 wt% of cement. The water content has been increased by 63 kg/m^3.

Third series

In the third series, modifications were made to the binder, SP, and water while the filler, aggregate, and fiber remained constant. Table 4.5 displays the mix designs for series 3, batches 10 through 19.

Table 4.5: Mix design - Series 3 - Batches 10-19 (kg/m^3)

Batch number	10	11	12	13	14	15	16	17	18	19
CEM II/A-V 42,5 N (Anl-FA)	740	740	740	740	740	518	-	-	740	-
CEM III/A 52,5 R (Variodur 40)	-	-	-	-	-	-	-	-	-	740
CEM I 52,5 R (Industri)	-	-	-	-	-	-	766	766	-	-
Merit 5000 (Slag)	-	-	-	-	-	215	-	-	-	-
Elkem microsilica 940 U	146	146	146	146	146	146	146	146	146	146
Millisil W12	198	198	198	198	198	198	198	198	198	198
Betofill VK50	-	-	-	-	-	-	-	-	-	-
Danish quartz sand 0-1mm	-	-	-	-	-	-	-	-	-	-
German quartz H33	938	938	938	938	938	938	938	938	938	938
Gneiss-granite 0-4mm	-	-	-	-	-	-	-	-	-	-
Quartz-diorite 5-8mm	-	-	-	-	-	-	-	-	-	-
Weidacon 0.15/9mm	146	146	146	146	146	146	146	146	146	146
SAPs BASF	-	-	-	-	-	-	-	-	-	-
Mapei Dynamon SX-N	-	-	-	-	-	-	-	-	-	-
Sika Visco-Crete UHPC-2	12.69	12.69	12.69	15	15	15	15	17.5	17.5	15
Free water	195	180	180	180	170	180	230	230	170	180
Total	2376	2361	2361	2363	2353	2356	2439	2441.5	2355.5	2363
w/b	0.198	0.183	0.183	0.185	0.175	0.186	0.227	0.229	0.177	0.185
EIRICH R09t	✓	✓	-	-	-	-	-	-	-	-
EIRICH R02/Vac	-	-	✓	✓	✓	✓	✓	✓	✓	✓

Batch number 10 replicates batch number 2 with a reduction in free water to 195 kg/m^3. Batch 11 reduces the free water additionally to 180 kg/m^3. Batch 12 has the same mix design as batch 11, but the R02/Vac mixer is used to check its effect on the concrete´s properties. Batch 13 increases the SP dosage from 12.69 to 15 kg/m^3. Batch 14 reduces the free water to 170 kg/m^3 while keeping the SP dosage at 15 kg/m^3. Batch 15 replaces 30 % of the cement (CEM II/A-V 42,5N) with slag (Merit 5000). Batch 16 uses a CEM 1 52,5 R cement (Norcem Industrisement) because of an increase in the cement´s blaine value; the free water is increased to 230 kg/m^3 to achieve a similar initial slump flow reading. Batch 17 increases the SP dosage of batch 16 to 17.5 kg/m^3. Batch 18 increases the SP dosage to 17.5 kg/m^3 from batch 14. Batch replicates batch 13 but replaces the CEM II/A-V 42,5 N with a CEM III/A 52,5 R (Variodur 40).

4.3.2 Extraneous test program

As described in the test matrix, the four mix designs with the best workability over a 30-minute window after mixture were re-batched with the exact same mix design, only in a larger volume as more specimens would be casted.

4.4 Batching, casting and curing

All material components were weighed up and placed in separate containers; the moisture content in the aggregates were measured with the speedy test as described in Section 6.1. Corrections were made to the amount of free water to account for this moisture percentage; these calculations are displayed in appendix A. The mixing procedure depends on the mixer used as the Eirich R02/Vac intensive mixer is more effective than the R09t; this has been described in Table 4.6.

Table 4.6: Mix procedure depending on type of mixer

Eirich R09t	**Eirich R02/Vac**
Add all dry components	Add binder, filler and 25% of aggregates*
Mix for 1 minutes	mix for 1 minute
Add water and superplasticizer	Add water and superplasticizer
Mix for 4 minutes	Mix until kW value peaks*
Add steel fibers	Add the remainder of aggregates
Mix for 4 minutes	Mix for 2 minutes
	Add steel fibers
	Mix for 2 minutes

* The R02/Vac can display the real time kW value being used; the mixer is sensitive to a sudden increase in the kW level due to a build up of dry material between the tool and mixing pan. seventy five percent of the aggregates were added after the mixture had achieved a level of plasticity, which can be indicated by a peak drop in kW.

After mixing, the miniature slump flow test was carried out, in addition to a regular sized slump flow test if the R09t mixer is used. As UHPCs have a more viscous behavior than ordinary concrete, the material requires more time before it can come to a rest because of its reduced flow ability. Measurements of the diameter were therefore consistently taken 20 seconds after lifting the mold to get comparable results. Visual observations of the concrete´s stability or other factors were noted. The amount of cubes, cylinders, and beams were cast in accordance with the test matrix described in Section 4.2. Twenty four hours after casting, the concrete specimens were de-molded and placed in their respective curing environments. Material testing commenced 7 and 28 days after casting in accordance with the test matrix; the procedures for this are described in Section 3.

5 Results

This section presents the results from the tests performed where a thorough analysis of these can be found in Section 6. The results from the standardized test program (batches 1-22) are presented first followed by the extraneous program (batches 23-26). Appendix A presents the material components as weight in kilograms per batch, measurements of surface moisture in the aggregates, and adjustments to the free water content to compensate for this effect to ensure an accurate w/b ratio. Figure 5.1 shows the specimens that were cast from batch 24.

Figure 5.1: Photograph of the specimens cast from batch 24.

5.1 Standardized program (Batches 1-22)

5.1.1 Workability

Table 5.1 displays results from the miniature slump flow test for batches 1-19. These values are visually presented in Figure 5.2. Images of every slump flow test can be found in Appendix G. The initial slump flow measured at 0 min varies from 150mm for batch 16 to 295mm for batch 3.

Table 5.1: Slump flow values for batches 1-19.

Batch number	**Miniature slump flow (mm)**				
	0 min	**5 min**	**10 min**	**15 min**	**30 min**
1	170	146	135	120	110
2	280	280	263	253	238
3	295	290	270	248	238
4	250	218	190	188	155
5	230	200	185	178	153
6	250	245	205	195	185
7	270	245	225	210	170
8	280	248	238	220	195
9	215	170	165	145	115
10	225	218	213	193	190
11	195	165	160	150	140
12	215	195	170	168	143
13	230	215	190	185	180
14	225	185	173	170	145
15	240	215	205	190	185
16	150	145	140	135	113
17	153	145	140	135	130
18	213	185	180	168	155
19	260	253	248	235	233

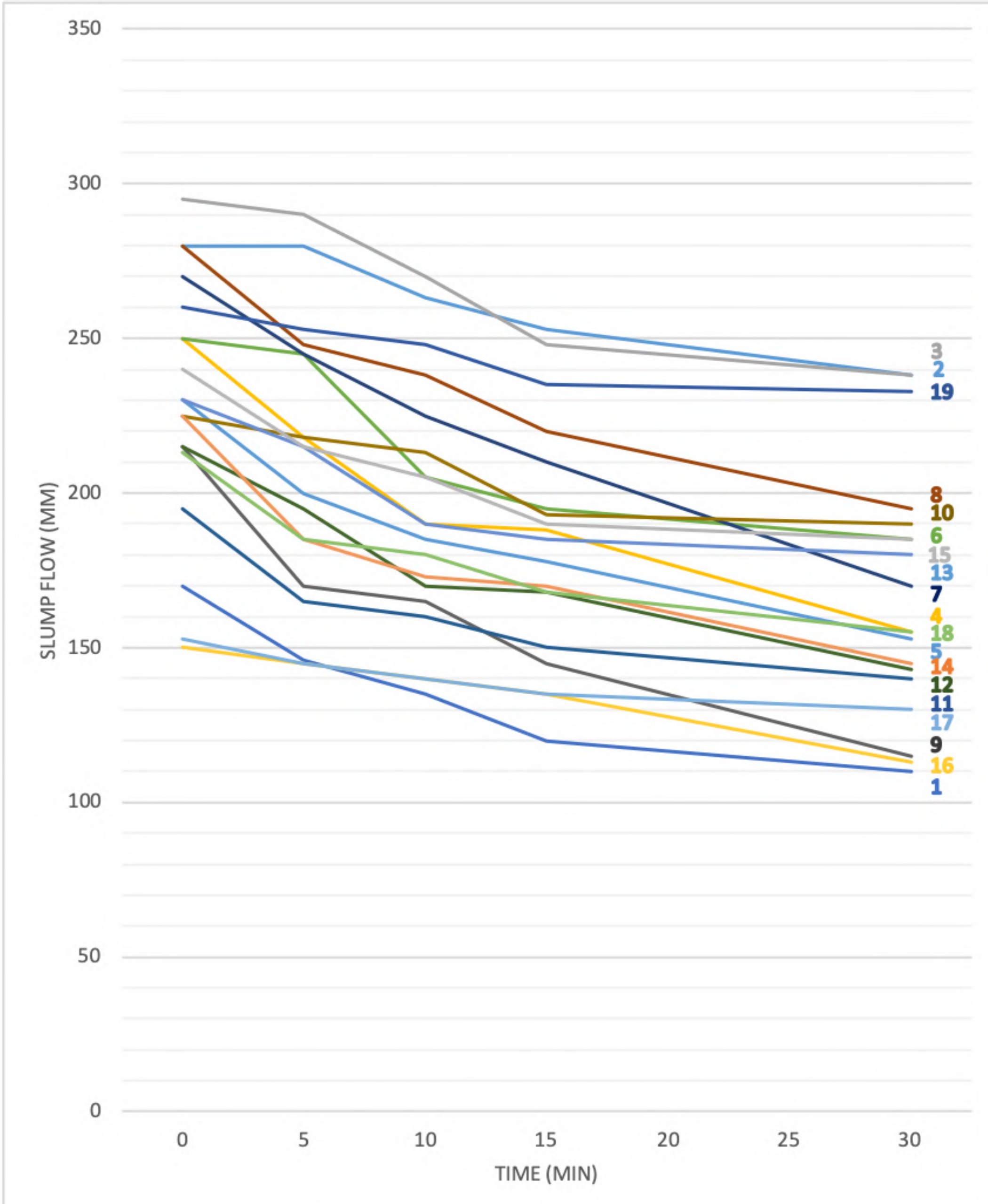

Figure 5.2: Slump flow (mm) for batches 1-19.

To get a better image of how the workability decreases over time, Table 5.2 shows the slump flows as a percentage reduction from the initial value at 0 min. These are also illustrated in Figure 5.3. Batch 19 containing CEM III/A 52.5R (Variodur 40) had the lowest reduction while batch 9 containing the shrinkage reducing admixture had the highest reduction during the first 30 minutes after mixing.

Table 5.2: Slump reduction as a percentage of the initial slump value (batches 1-19).

Batch	Percent reduction from initial slump flow (%)			
	5 min	10 min	15 min	30 min
1	85.9	79.4	70.6	64.7
2	100	93.9	90.4	85.0
3	98.3	91.5	84.1	80.7
4	87.2	76.0	75.2	62.0
5	87.0	80.4	77.4	66.5
6	98.0	82.0	78.0	74.0
7	90.7	83.3	77.8	62.9
8	88.6	85.0	78.6	69.6
9	79.1	76.7	67.4	53.5
10	96.9	94.7	85.8	84.4
11	84.6	82.1	76.9	71.8
12	90.7	79.1	78.1	66.5
13	93.5	82.6	80.4	78.3
14	82.2	76.9	75.6	64.4
15	89.6	85.4	79.2	77.1
16	96.6	93.3	90.0	75.3
17	94.8	91.5	88.2	85.0
18	86.9	84.5	78.9	72.8
19	97.3	95.4	90.4	89.6

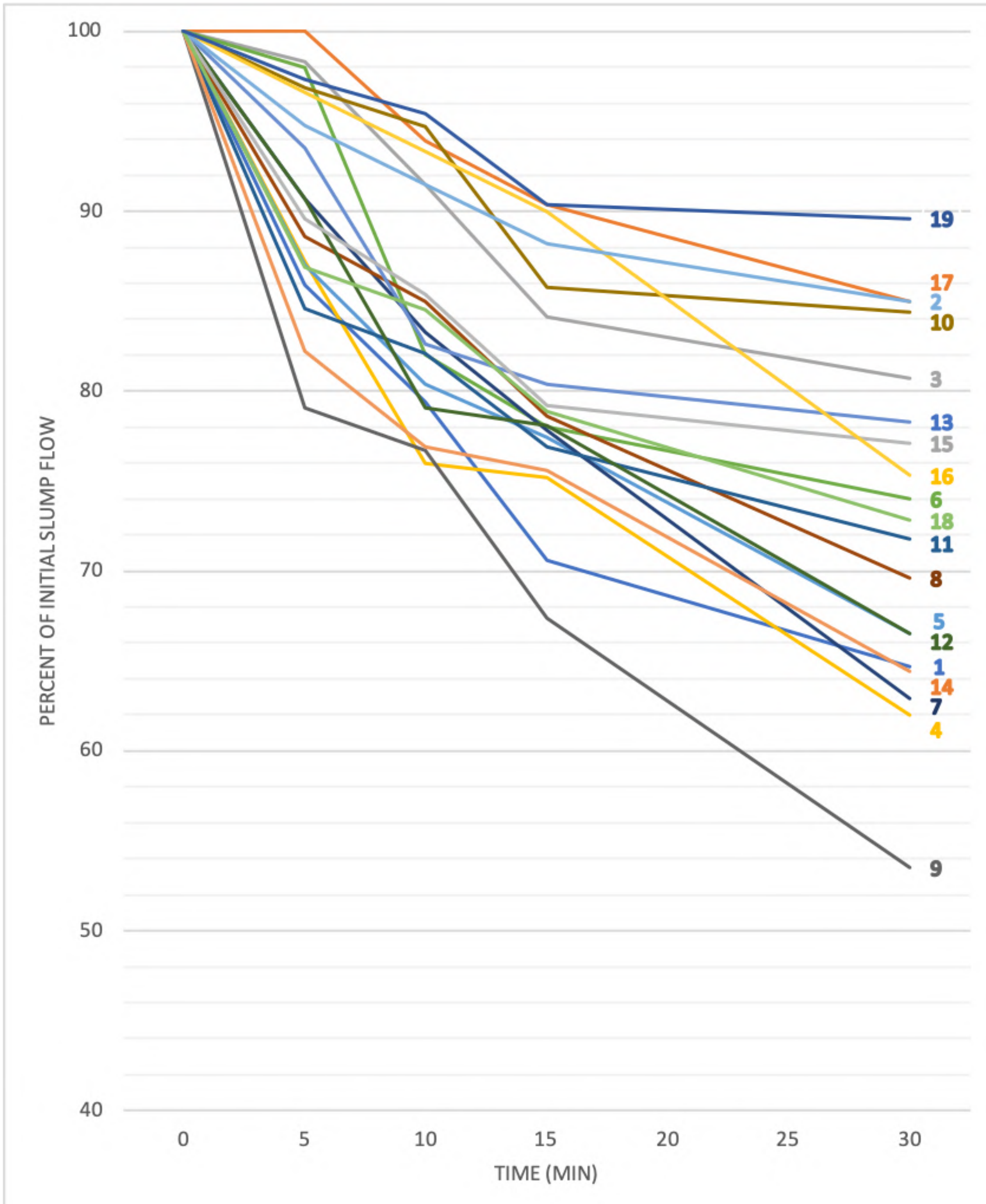

Figure 5.3: Slump reduction as a percentage of the initial slump value (batches 1-19)

Observations

Batch 1 became very stiff 30 minutes after mixing and was very adhesive towards the plastic mold. It took approximately 10 seconds before the concrete sample completely slipped out of the mold with a low plastic viscosity.

Batch 2 was the first mix design containing the SP Sika Visco-Crete UHPC-2 and, during the mixing process, 2.7 kg/m^3 was added as the SP dosage seemed to be insufficient compared to the previous batch. Batch 1 took approximately 1 minute to achieve a level of plastic viscosity in the mixer while the batches with UHPC-2 took approximately 30 seconds longer to reach the same degree.

Batch 3 had the largest initial slump flow reading of all 19 mix designs. There was no indication of flocculated steel fibers, and they seemed to be evenly spread out along the slump flow´s circumference. This was also the case for batches 1 and 2.

Batch 4 was designed with the larger granular gneiss-granite (0-4mm). Here, a minor paste separation was observed, as shown in Figure 5.4. This occurs when the amount of cement paste is too large compared to the sand, or the sand lacks the finer fractions. No expelling of water was observed. The particle size distribution curve for the gneiss-granite produced by the supplier shows a smooth almost linear curve, as shown in Appendix H.

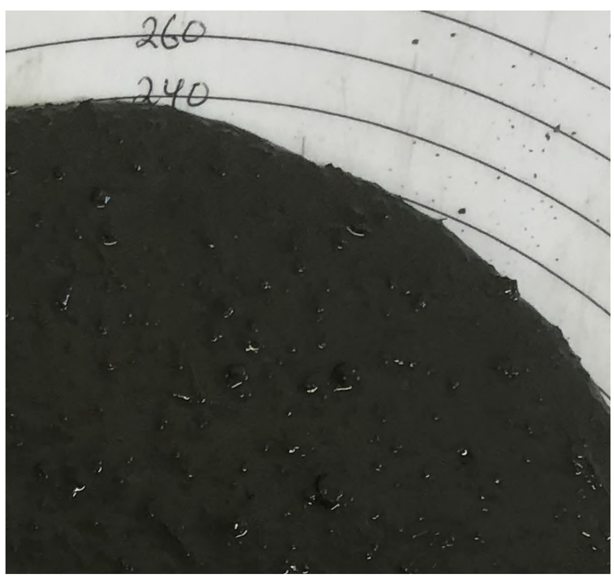

Figure 5.4: Magnified view of the slump flow for batch 4 showing a slight paste separation

Batch 5 was similar to batch 4 with regard to stability. The distribution of the fibers for batches 4 and 5 seemed even from visual observation.

Batch 6 contained the largest granular fraction 5-8mm, of quartz-diorite. Figure 5.5a shows how this granular fraction is not evenly distributed in the fresh concrete.

Batch 7 containing the same granular components as batch 6 also show gathering of the larger fraction in some areas; the fibers seemed to accumulate at the same places (illustrated in Figure 5.5b).

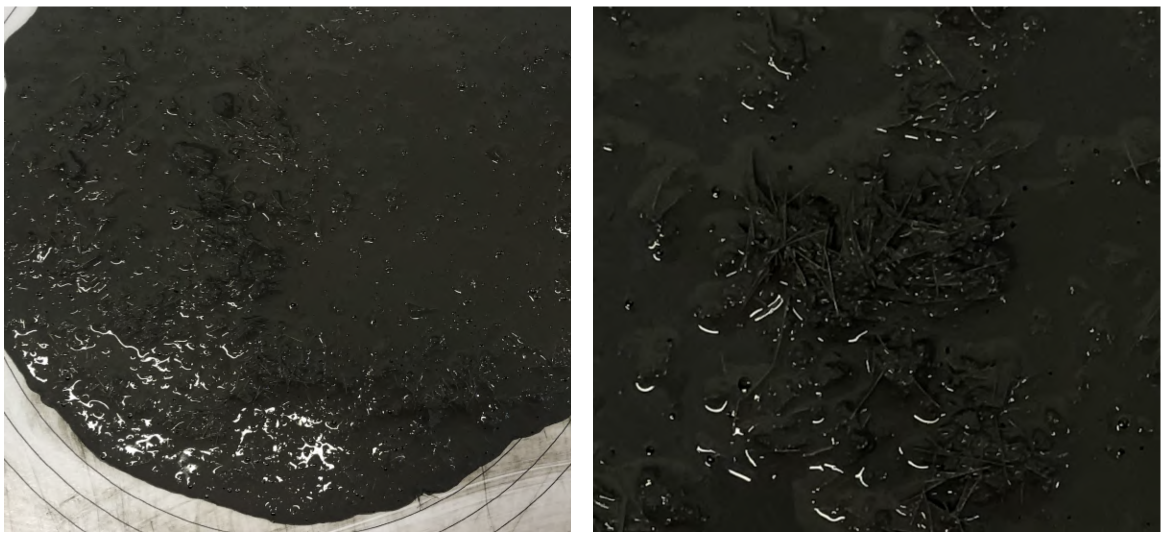

(a) Batch 6 (b) Batch 7

Figure 5.5: Magnified view of the slump flows showing paste separation.

Batch 8 also contained the larger sized aggregate fraction; however, they were more evenly distributed, and the stability was found to be better than that for batches 6 and 7.

Batch 9 showed the same level of stability as batch 8, but experienced the largest drop in mobility after mixing, were mobility refers to the flow-ability and velocity of movement as described in Section 2.3.2. This mix design contained a shrinkage reducing admixture and a larger dose of both water and SP, but still had a smaller slump flow and drop in mobility over time. As mentioned earlier, the mix design for batches 8 and 9 were proportioned independent of this thesis, so there were several differences in both the quantity and material choices compared to the other batches.

Batch 10 had an even fiber distribution with a similar loss of mobility over time as batch 2 with almost the same design. A slight elephant skin was observed on the surface of the sample, forming approximately five minutes after lifting the slump flow cylinder.

Batches 11, 12, and 13 also formed a layer of elephant skin; the stability seemed good with no visual signs of separation. With a water dosage of 180 kg/m^3, the last slump flow measurment after 30 minutes took longer time to release from the cylindrical mold.

Batch 14 had the lowest w/b ratio of all the 19 mix designs, and the formation of elephant skin was found to be very rapid compared to the other batches. The same issue arose for the last slump flow measurement as for the previous three.

Batch 15 showed good stability with a slight formation of elephant skin.

Batches 16 and 17 contained the CEM I 52,5R (Norcem Industri) and, even with larger w/b ratios (≈ 0.228), they still had a small slump flow.

Batch 18 had similar characteristics as batch 14 with a quick formation of elephant skin.

Batch 19 had the lowest loss of workability over time. Large air pores rose to the surface creating a more uneven surface; this was also the case when filling the cubic forms.

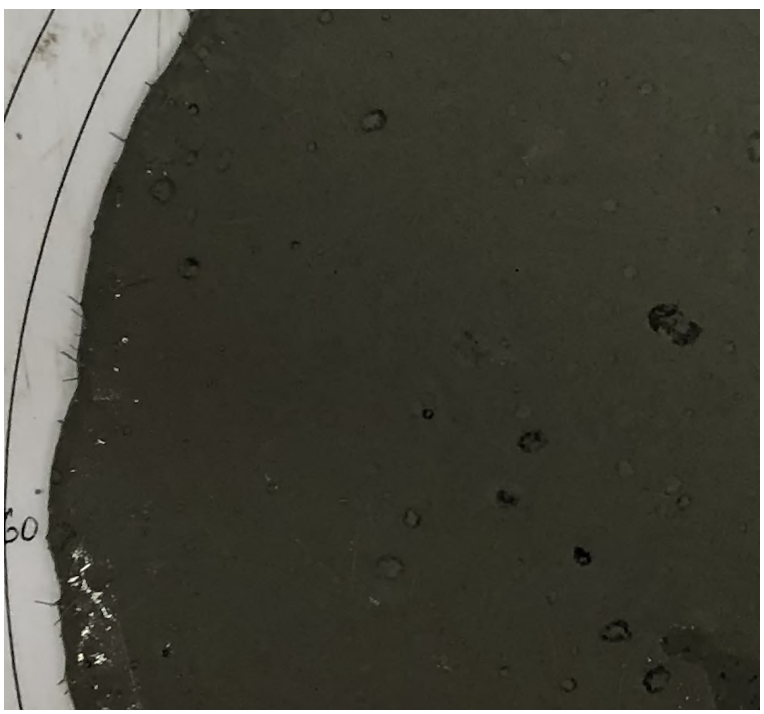

Figure 5.6: Magnified view of the slump flow for batch 19

Batches 2,10,17, and 19 displayed the lowest loss of workability over a time period of 30 minutes after mixing. Batch 17 did not classify as UHPC when only considering compressive strength, as can be seen in the next section. Small modifications to the SP dosage were made to batches 2,10, and 19 with a goal of producing approximately the same high initial slump value so that the workability over time could be better analyzed. For batch 19, the SP dosage was reduced to 12.69 instead of $15kg/m^3$, displayed as batch 20 in Table 5.3. Since batch 2 had the largest initial slump flow value, the SP dosage was adjusted to 10 kg/m^3 (now batch 21). The SP was increased for batch 10 from 12.69 to 15 kg/m^3 (now batch 22).

Table 5.3: Mix design - Series 4 - Batches 20-22 (kg/m^3)

Batch number	20 (19)	21 (2)	22 (10)
CEM II/A-V 42,5N (Anl-FA)	-	740	740
CEM III/A 52,5R (Variodur 40)	740	-	-
CEM I 52,5R (Industri)	-	-	-
Merit 5000 (Slag)	-	-	-
Elkem Microsilica 940 U	146	146	146
Millisil W12	198	198	198
Betofill VK50	-	-	-
Danish quartz sand 0-1mm	-	-	-
German quartz H33	938	938	938
Gneiss-granite 0-4mm	-	-	-
Quartz-diorite 5-8mm	-	-	-
Weidacon 0.15/9mm	146	146	146
SAPs BASF	-	-	-
Sika UHPC-2	12.69	10	15
Free water	180	210	195
Total	2360.7	2388	2378
w/b	0.177	0.210	0.199
EIRICH R09t	-	-	-
EIRICH R02/Vac	✓	✓	✓

Table 5.4 displays the results from the miniature slump flow test for batches 20-22; these values are visually presented in Figure 5.8 in red compared to batches 1-19 in gray.

Table 5.4: Slump flow values for batches 20-22

Batch number	**Miniature slump flow (mm)**				
	0 min	**5 min**	**10 min**	**15 min**	**30 min**
20	255	248	238	233	228
21	250	235	218	213	195
22	233	223	213	205	190

Figure 5.7: Workability testing

Observations

Batch 20 showed the same formation of air crater at the surface. It had a good fiber distribution on all sides and a minimal loss of workability over the first 30 minutes.

Batches 21 and 22 exhibited good visual stability and a gradual drop in workability.

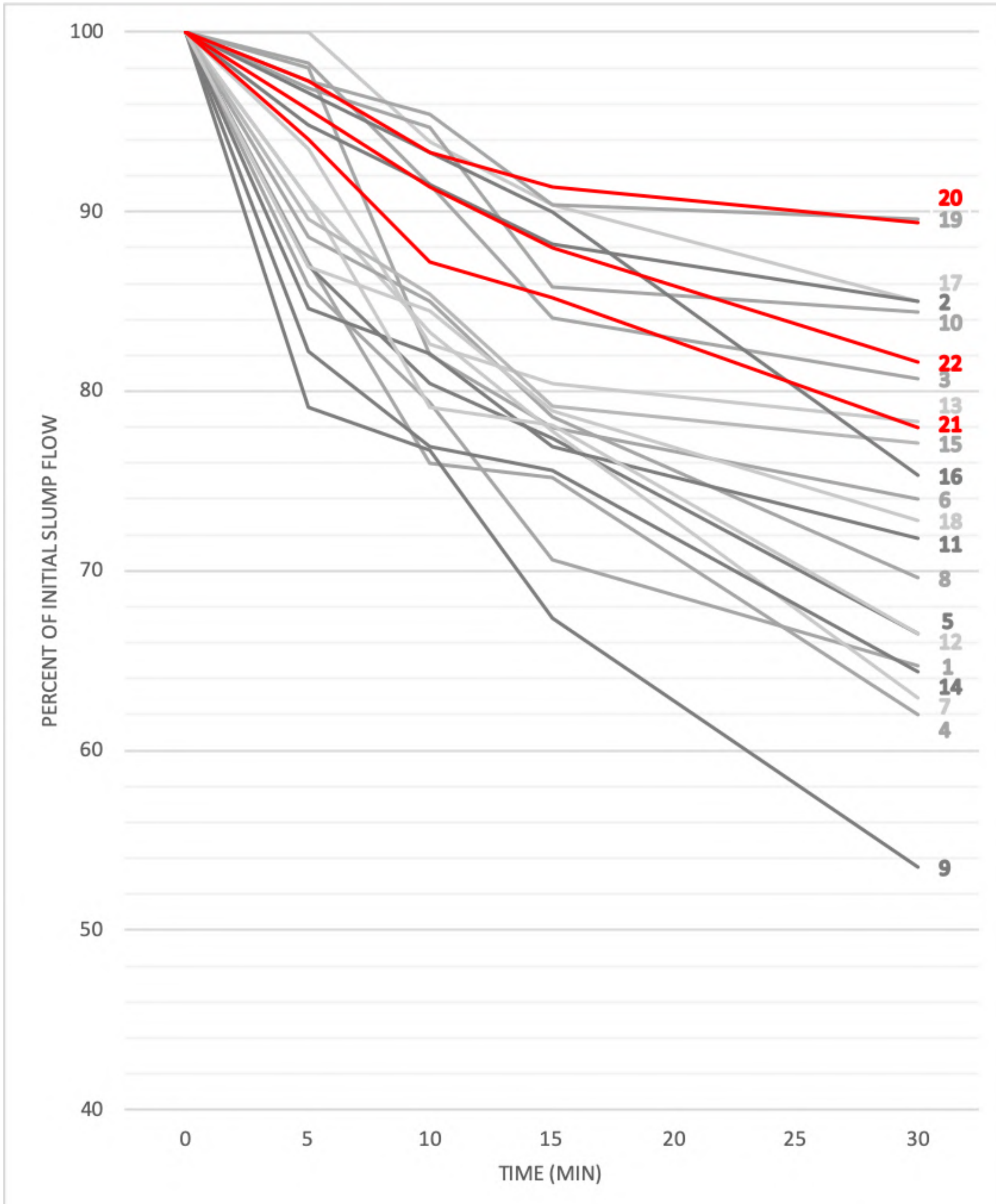

Figure 5.8: Slump reduction as a percentage of the initial slump value for batches 20-22.

5.1.2 Compressive strength and hardened density

Tables 5.5 to 5.8 show the densities and compressive strengths for all cubic specimens from batches 1-22. The average compressive strength for each batch and curing regime is displayed in the column to the right.

Table 5.5: Compressive strengths and densities for batches 1-4

Batch	**Curing regime**	**Specimen**	$\rho (kg/m^3)$	σ **(MPa)**	$\overline{\sigma}$ **(MPa)**
1	7d. A (20°C)	01A2A	2386	90.3	92.5
		01A2B	2390	90.5	
		01A2C	2394	93.8	
	28d. A (20°C)	01A1A	2384	134.2	132.2
		01A1B	2389	130.8	
		01A1C	2381	131.5	
	7d. B (90°C)	01B2A	2354	168.3	167.3
		01B2B	2350	169.7	
		01B2C	2356	163.9	
2	7d. A (20°C)	02A2A	2423	113.0	112.8
		02A2B	2425	112.0	
		02A2C	2430	113.4	
	28d. A (20°C)	02A1A	2427	152.3	154.6
		02A1B	2418	154.2	
		02A1C	2415	157.3	
	7d. B (90°C)	02B2A	2401	182.0	183.9
		02B2B	2397	186.3	
		02B2C	2396	183.4	
3	7d. A (20°C)	03A2A	2426	105.0	105.8
		03A2B	2428	106.4	
		03A2C	2422	106.1	
	28d. A (20°C)	03A1A	2418	151.9	151.2
		03A1B	2413	150.0	
		03A1C	2416	151.6	
	7d. B (90°C)	03B2A	2399	177.1	176.5
		03B2B	2392	177.3	
		03B2C	2388	175.1	
4	7d. B (90°C)	04B2A	2376	166.8	163.1
		04B2B	2376	164.0	
		04B2C	2391	158.6	

Table 5.6: Compressive strengths and densities for batch 5-8

Batch	**Curing regime**	**Specimen**	$\rho(kg/m^3)$	σ **(MPa)**	$\overline{\sigma}$ **(MPa)**
5	7d. B (90°C)	05B2A	2388	155.9	154.5
		05B2B	2386	152.1	
		05B2C	2390	155.4	
6	7d. A (20°C)	06A2A	2445	103.6	103.1
		06A2B	2439	103.7	
		06A2C	2439	102.1	
	28d. A (20°C)	06A1A	2448	137.4	139.5
		06A1B	2458	137.9	
		06A1C	2451	143.1	
	7d. B (90°C)	06B2A	2405	161.4	159.0
		06B2B	2404	155.2	
		06B2C	2401	160.2	
7	07d. A (20°C)	07A2A	2454	106.9	107.9
		07A2B	2455	109.4	
		07A2C	2443	107.6	
	28d. A (20°C)	07A1A	2461	150.4	147.7
		07A1B	2461	149.9	
		07A1C	2453	142.8	
	7d. B (90°C)	07B2A	2404	171.7	171.0
		07B2B	2374	168.4	
		07B2C	2400	172.9	
8	7d. A (20°C)	08A2A	2406	125.5	123.6
		08A2B	2408	123.7	
		08A2C	2417	121.7	
	28d. A (20°C)	08A1A	2389	135.8	138.3
		08A1B	2400	135.5	
		08A1C	2415	143.7	
	7d. B (90°C)	08B2A	2384	158.6	157.2
		08B2B	2371	154.2	
		08B2C	2369	158.8	

Table 5.7: Compressive strengths and densities for batch 9-14

Batch	**Curing regime**	**Specimen**	$\rho(kg/m^3)$	σ **(MPa)**	$\overline{\sigma}$ **(MPa)**
9	28d. A (20°C)	09A1A	2309	125.8	124.4
		09A1B	2300	117.6	
		09A1C	2312	129.8	
	7d. B (90°C)	09B2A	2282	131.6	131.6
10	07d. A (20°C)	10A2A	2415	113.5	114.6
		10A2B	2426	114.7	
		10A2C	2435	115.5	
	28d. A (20°C)	10A1A	2430	148.7	151.4
		10A1B	2429	149.5	
		10A1C	2429	156.0	
	7d. B (90°C)	10B2A	2396	182.5	188.5
		10B2B	2399	194.5	
		10B2C	2397	188.4	
11	07d. A (20°C)	11A2A	2414	114.7	116.0
		11A2B	2416	118.3	
		11A2C	2416	115.0	
	28d. A (20°C)	11A1A	2423	156.9	155.5
		11A1B	2438	159.0	
		11A1C	2424	150.6	
	7d. B (90°C)	11B2A	2384	192.9	193.3
		11B2B	2395	197.2	
		11B2C	2387	189.7	
12	7d. B (90°C)	12B2A	2386	194.9	194.8
		12B2B	2386	194.8	
		12B2C	2407	194.5	
13	7d. B (90°C)	13B2A	2382	190.3	187.6
		13B2B	2377	183.2	
		13B2C	2391	189.3	
14	7d. B (90°C)	14B2A	2398	190.6	191.7
		14B2B	2387	192.7	
		14B2C	2415	191.7	

Table 5.8: Compressive strengths and densities for batch 15-22

Batch	**Curing regime**	**Specimen**	$\rho(kg/m^3)$	σ **(MPa)**	$\overline{\sigma}$ **(MPa)**
15	07d. B (90°C)	15B2A	2385	181.0	177.9
		15B2B	2363	175.5	
		15B2C	2399	177.2	
16	7d. B (90°C)	16B2A	2333	166.7	153.6
		16B2B	2332	147.0	
		16B2C	2342	147.0	
17	7d. B (90°C)	17B2A	2329	163.7	161.3
		17B2B	2338	165.8	
		17B2C	2332	154.5	
18	7d. B (90°C)	18B2A	2392	189.0	183.2
		18B2B	2383	178.5	
		18B2C	2411	182.3	
19	7d. B (90°C)	19B2A	2418	208.3	203.1
		19B2B	2432	197.7	
		19B2C	2440	203.3	
20	7d. B (90°C)	20B2A	2424	205.2	205.4
		20B2B	2408	200.8	
		20B2C	2393	210.1	
21	7d. B (90°C)	21B2A	2339	171.1	171.4
		21B2B	2346	173.8	
		21B2C	2341	169.2	
22	7d. B (90°C)	22B2A	2347	176.3	176.6
		22B2B	2347	176.3	
		22B2C	2352	177.3	

Observations

When the specimens were cured at 90°C for 48 hours, starting 24 hours after casting, they were seen to posses a higher compressive strength than specimens cured in water at 20°C. Cubes from the same batch that had undergone the same curing regime exhibited small differences in compressive strengths and densities. The values are calculated with equations 6 and 7 in Section 3.

5.1.3 Tensile Strength

Table 5.9 displays the failure load in kN from the tensile splitting tests performed on the specimens that were mixed using the larger Eirich R09t mixer. These were converted into tensile strength using Equation 8; the average value of the two specimens is displayed in the last column.

Table 5.9: Tensile Strengths f_{ct} (MPa)

Batch	**Curing regime**	**Specimen**	**Failure load (kN)**	f_{ct} **(MPa)**	$\overline{f_{ct}}$ **(MPa)**
01	28d. A (20°C)	01A4A	1104.0	15.6	11.6
		01A4B	529.7	7.5	
02	28d. A (20°C)	02A4A	632.0	8.9	8.9
		02A4B	631.5	8.9	
03	28d. A (20°C)	03A4A	436.7	6.2	7.9
		03A4B	676.5	9.6	
06	28d. A (20°C)	06A4A	450.0	6.4	8.0
		06A4B	684.9	9.7	
07	28d. A (20°C)	07A4A	716.9	10.1	10.4
		07A4B	758.1	10.7	
10	28d. A (20°C)	10A4A	964.5	13.6	11.6
		10A4B	677.0	9.6	
11	28d. A (20°C)	11A4A	694.1	9.8	14.1
		11A4B	1299.1	18.4	

Observations

There are large variations in the tensile strength between the two specimens that have been cast from the same batch. Specimen 11A4A (9.82 MPa) is almost half the strength as 11A4B (18.38 MPa). All the values are between 6-20 MPa which, according to the literature, is a common conception of where the tensile strength of a UHPC should be.

5.1.4 Modulus of elasticity

Table 5.10 shows the modulus of elasticity for the batches mixed in the larger mixer. The lowest value of 35.1 GPa was measured for batch 9 with the SRA. The highest average value of 49.3 GPa was obtained for batch 2.

Table 5.10: Modulus of elasticity $E_{c,s}$ (MPa)

Batch	**Curing regime**	**Specimen**	$E_{c,s}$ **(MPa)**	$\overline{E_{c,s}}$ **(MPa)**
01	28d. A (20°C)	01A3A	43325	44275
		01A3B	45224	
02	28d. A (20°C)	02A3A	47815	49322
		02A3B	50828	
03	28d. A (20°C)	03A3A	46784	49045
		03A3B	51305	
06	28d. A (20°C)	06A3A	42666	43644
		06A3B	44621	
07	28d. A (20°C)	07A3A	42837	42617
		07A3B	42396	
08	28d. A (20°C)	08A3A	41871	41871
09	28d. A (20°C)	09A3A	35106	35106
10	28d. A (20°C)	10A3A	46376	48838
		10A3B	51299	
11	28d. A (20°C)	11A3A	50157	49254
		11A3B	48351	

5.2 Extraneous program (Batches 23-26)

The following results are from the extraneous test program described in Section 4.2, where the four best mix designs were re-batched in a larger volume in order to perform a greater range of tests.

5.2.1 Workability

The batches that had a measured or estimated 28-day compressive strength of over 150 MPa and produced good workability over time are 20, 19, 2, 10, 22, 3, and 13. As some of these mix designs contained materials that were in short supply at the university (Danish quartz sand and Variodur 40), batches 19,20, and 3 were disregarded for the last extraneous test program where 4x85L mixtures were produced. The mix designs 2,10,22, and 13 were re-batched in a larger volume, and renamed as 23,24,25, and 26, respectively.

Table 5.11: Mix design - Series 4 - Batches 23-26 (kg/m^3)

Batch number	23 (2)	24 (10)	25 (22)	26 (13)
CEM II/A-V 42,5N (Anl-FA)	740	740	740	740
CEM III/A 52,5R (Variodur 40)	-	-	-	-
CEM I 52,5R (Industri)	-	-	-	-
Merit 5000 (Slag)	-	-	-	-
Elkem Microsilica 940 U	146	146	146	146
Millisil W12	198	198	198	198
Betofill VK50	-	-	-	-
Danish quartz sand 0-1mm	-	-	-	-
German quartz H33	938	938	938	938
Gneiss-granite 0-4mm	-	-	-	-
Quartz-diorite 5-8mm	-	-	-	-
Weidacon 0.15/9mm	146	146	146	146
SAPs BASF	-	-	-	-
Sika UHPC-2	12.69	12.69	15	15
Free water	210	195	195	180
Total	2394	2376	2378	2363
w/b	0.210	0.198	0.199	0.185
EIRICH R09t	✓	✓	✓	✓
EIRICH R02/Vac	-	-	-	-

Table 5.12 shows the results from the miniature slump flow tests for batches 23-26 during the first hour after mixing.

Table 5.12: Slump flow values for batches 23-26

Batch	**Miniature slump flow (mm)**								
	0 min	**5 min**	**10 min**	**15 min**	**20 min**	**30 min**	**40 min**	**50 min**	**60 min**
23	270	260	260	258	240	225	210	208	200
24	225	218	210	193	185	170	140	135	130
25	253	235	220	218	210	200	185	180	168
26	228	208	190	180	180	168	155	140	130

The results were visualized against those of the previous batches with the same mix design to determine if large variations had occurred. Figure 5.9 shows the results in millimeters, and Figure 5.10 displays them as a percentage reduction of the initial value. The batches with the same mix design had the same color and were seen to follow the same pattern as a whole; however, some singular measurements at specific times were seen to vary more than others. For instance, at 30 minutes batch 10 leveled off while batch 24 experienced a continuous drop. The exact cause of this variation is hard to pin point; one theory may be the presence of residual concrete on the A3 laminated sheet causing a larger friction and thus restricting its flow.

Observations

All the slump flows performed for batches 23-26 had almost identical mix designs with the exception of water and SP volumes. All the slump flows had what looked like an even distribution of fibers at the edges and good stability. The mobility was seen to decline for every measurement in time, and batches 24 and 26 took a long time to release from the cylinder mold. The formation of elephant skin occurred on all 4 batches and faster for batches 24 and 26.

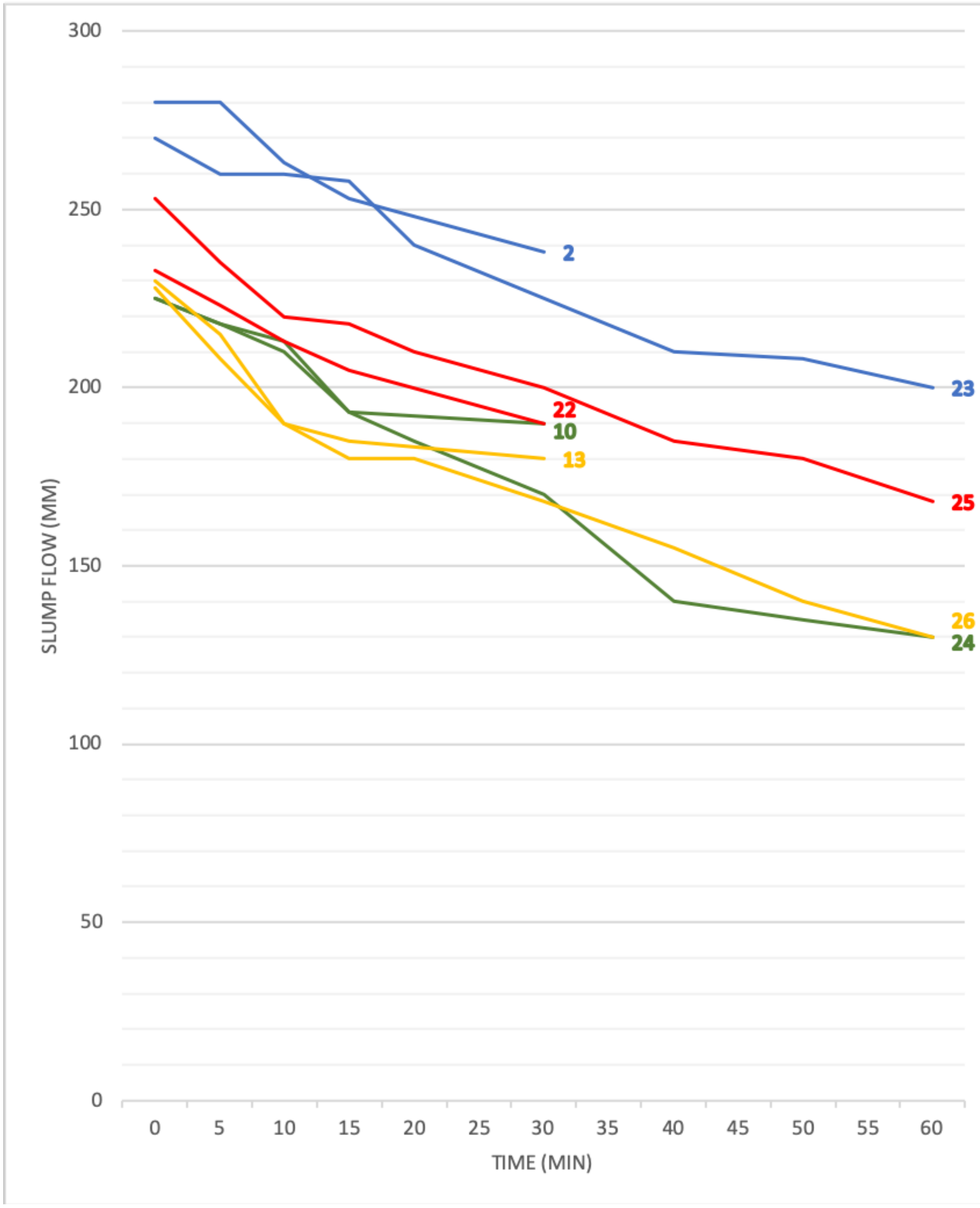

Figure 5.9: Slump flow (mm) for batches 23,24,25, and 26 compared to batches 2,10,22, and 13.

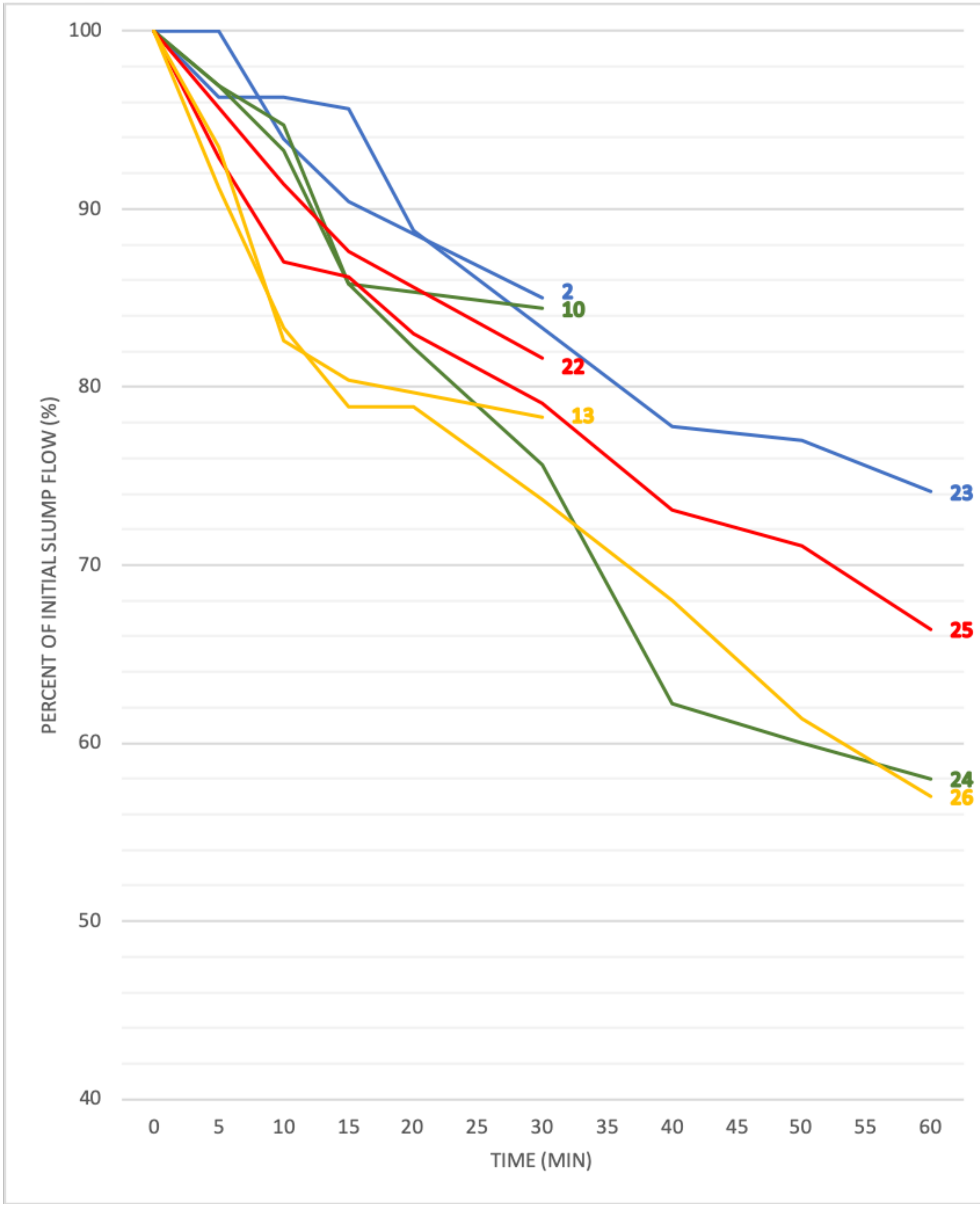

Figure 5.10: Slump reduction as a percentage of the initial slump value for batches 23,24,25, and 26 compared those of batches 2,10,22 and 13.

5.2.2 Compressive strengths and hardened densities

Table 5.13 presents the compressive strengths and hardened densities for batches 23-26. Specimen 24A2A shows a substantially lower strength than 24A2B/C. This specimen had an uneven side due to overfilling the mold and cannot be considered a reliable result.

Table 5.13: Compressive strengths and densities for batches 23-26

Batch	**Curing regime**	**Specimen**	$\rho(kg/m^3)$	σ **(MPa)**	$\overline{\sigma}$ **(MPa)**
23	7d. A (20°C)	23A2A	2459	109.6	106.3
		23A2B	2425	104.8	
		23A2C	2423	104.4	
	28d. A (20°C)	23A1A	2423	159.2	155.4
		23A1B	2426	151.1	
		23A1C	2434	156.0	
	07d. B (90°C)	23B2A	2385	185.7	186.5
		23B2B	2379	187.6	
		23B2C	2416	186.3	
24	7d. A (20°C)	24A2A	2394	87.6	99.4
		24A2B	2396	104.2	
		24A2C	2394	106.4	
	28d. A (20°C)	24A1A	2392	142.9	141.6
		24A1B	2397	145.6	
		24A1C	2400	136.2	
	7d. B (90°C)	24B2A	2367	179.4	182.3
		24B2B	2379	184.4	
		24B2C	2270	183.1	
25	7d. A (20°C)	25A2A	2412	110.5	109.2
		25A2B	2401	107.7	
		25A2C	2434	109.4	
	28d. A (20°C)	25A1A	2416	142.7	145.9
		25A1B	2424	152.6	
		25A1C	2435	142.5	
	7d. B (90°C)	25B2A	2399	192.0	188.5
		25B2B	2366	190.0	
		25B2C	2371	183.4	
26	7d. A (20°C)	26A2A	2427	113.5	111.0
		26A2B	2410	108.4	
		26A2C	2423	111.0	
	28d. A (20°C)	26A1A	2403	146.1	153.2
		26A1B	2409	155.0	
		26A1C	2402	158.5	
	7d. B (90°C)	26B2A	2361	183.6	182.7
		26B2B	2374	183.9	
		26B2C	2372	180.6	

5.2.3 Tensile strengths

Table 5.14 shows the failure load and tensile strength for batches 23-26.

Table 5.14: Tensile Strengths f_{ct} (MPa).

Batch	**Curing regime**	**Specimen**	**Failure load (kN)**	f_{ct} **(MPa)**	$\overline{f_{ct}}$ **(MPa)**
23	28d. A (20°C)	23A4A	641.4	9.1	8.7
		23A4B	582.6	8.2	
24	28d. A (20°C)	24A4A	610.4	8.6	8.4
		24A4B	576.6	8.2	
25	28d. A (20°C)	25A4A	512.3	7.3	8.4
		25A4B	669.1	9.5	
26	28d. A (20°C)	26A4A	887.9	12.4	10.9
		26A4B	656.7	9.3	

5.2.4 Modulus of elasticity

Table 5.15 presents the modulus of elasticity for batches 23-26.

Table 5.15: Modulus of elasticity $E_{c,s}$ (MPa).

Batch	**Curing regime**	**Specimen**	$E_{c,s}$ **(MPa)**	$\overline{E_{c,s}}$ **(MPa)**
23	28d. A (20°C)	23A3A	48265	47737
		23A3B	47208	
24	28d. A (20°C)	24A3A	44610	45398
		24A3B	46186	
25	28d. A (20°C)	25A4A	46729	46796
		25A4B	46862	
26	28d. A (20°C)	26A4A	46156	46626
		26A4B	47096	

5.2.5 Flexural strength

Table 5.16 displays the failure load and flexural strength for batches 23-26. The tests were performed as described in the methods of measurement in Section 3.7. The load rate was set to 0,05 MPa/s and the length between the supports set to 460mm. The flexural strength for the batches varied from 14 to 20 MPa. Only two specimens were casted and tested for batch 26, the reason being a shortage of molds as all four batches had been mixed on the same day. Figure 5.11 shows specimen 24A5C after failure.

Table 5.16: Flexural strength f_{ct} (MPa)

Batch	**Curing regime**	**Specimen**	**Failure load F_f (kN)**	$\overline{F_f}$ **(kN)**	**Flexural strength f_{ct} (MPa)**
23	28d. A (20°C)	23A5A	33.0	31.3	14.4
		23A5B	31.8		
		23A5C	29.1		
24	28d. A (20°C)	24A5A	36.7	38.2	17.6
		24A5B	42.8		
		24A5C	35.0		
25	28d. A (20°C)	25A5A	31.1	30.7	14.1
		25A5B	33.4		
		25A5C	27.6		
26	28d. A (20°C)	26A5A	45.8	42.3	19.5
		26A5B	38.7		

Figure 5.11: Photograph of specimen 24A5C that underwent flexural testing.

5.2.6 Permeability - Porosity

The weights measured at the different stages of the PF method, in addition to the calculated capillary absorption, can be found in appendices E and F. The densities, porosities, and pore protection factor are derived by equations 13-19 and shown in Table 5.18. The unidirectional capillary suction was carried out on dried specimens, and the amount of water absorbed (kg/m^2) over time ($\sqrt{s}$) for each specimen is presented in Figure 5.15. The procedure for this is described in Section 3.8. The capillary number (slope of linear section) is shown in table 5.18.

Observations

The capillary porosity lies on an average between 3-4 vol-% and a macro porosity of under 1 vol-% for batches 23-26. Batch 23 had the highest total porosity followed by batches 24,25, and 26 respectively. Figure 5.12 shows the cross section of a specimen from batch 26. The large macro pores are clearly visible, as well as the distribution of their steel fibers and the randomness of their orientation.

Figure 5.12: Cross sectional view of the specimen from batch 26.

During the 96 hours with unidirectional capillary suction, the water front did not reach the top of the specimens due to its low capillary porosity, i.e, a dry top surface. The graphs in figures 5.13 and 5.15, therefore, only display the first near linear section of the curve, meaning the resistance number (m) could not be determined. Figure 5.13 shows the average capillary suction over time and that batch 23 has the highest water absorption capacity followed by batches 25,24, and 26, respectively. It should be noted that the differences between them were found to be minimal. Figure 5.15 shows the capillary absorption for every specimen; there are minimal variations in absorption for specimens from the same batch. The results from the capillary suction are also presented in tabular form in Appendix F. Table 5.18 shows the capillary number (k) derived in Equation 20, the water absorbed at 96 hours was used as Q_{cap}, causing some source of error. In comparison, a B45 MF40 NSC exhibited a capillary capacity of approximately 2 kg/m^2 after a period of 24 hours, giving a capillary number of 8E-2 [25].

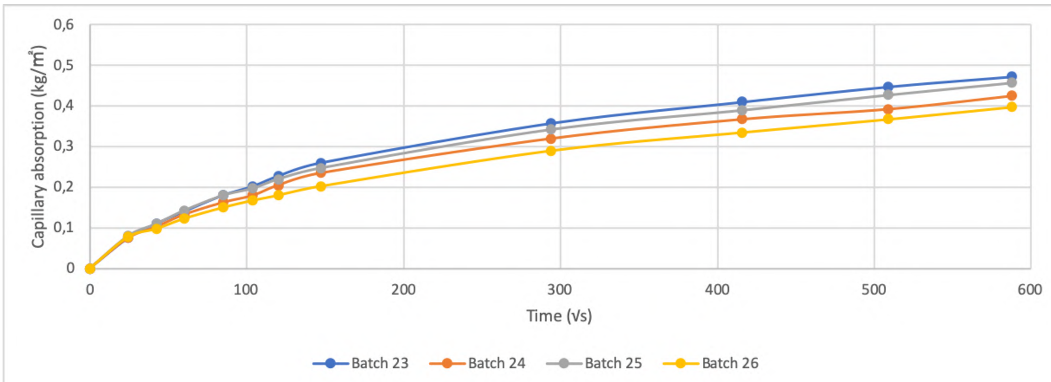

Figure 5.13: Average capillary suction in kg/m^2 over $\sqrt{time}$ for batches 23-26.

Table 5.17: Capillary number

Batch	Q_{cap}	$\sqrt{t_{cap}}$	Capillary number (k)
23	0.4725	588	8.037E-4
24	0.425	588	7.23E-4
25	0.4575	588	7.78E-4
26	0.3975	588	6.76E-4

Figure 5.14 shows a picture of the pressure tank setup used to saturate the largest macro pores to determine the total porosity. The container only had a capacity for 8 specimens; therefore, only A and B for each batch were tested. Some of the entries in Table 5.18 are, therefore, missing.

Figure 5.14: Pressure tank used to determine the pressure saturated porosity.

Table 5.18: Densities and porosities for batches 23-26

Set of samples	**Density (g/cm^3)**			**Porosity (volume percent)**			**PF %**
	Bulk Dry Density (ρ_{BD})	**Saturated Surface Dry Density (ρ_{SSD})**	**Solid Density (ρ_S)**	**Pressure saturated (ϵ_{tot})**	**Saturated by suction only (ϵ_{suc})**	**Air (ϵ_{air})**	
23B6A	2.355	2.396	2.478	4.98	4.17	0.81	16.3
23B6B	2.350	2.389	2.465	4.67	3.99	0.67	14.3
23B6C	2.347	2.387	-	-	4.00	-	-
23B6D	2.349	2.387	-	-	3.78	-	-
Average	**2.350**	**2.390**	**2.472**	**4.83**	**3.99**	**0.74**	**15.3**
24B6A	2.336	2.369	2.430	3.88	3.30	0.57	14.7
24B6B	2.345	2.379	2.432	3.61	3.41	0.19	5.3
24B6C	2.346	2.379	-	-	3.33	-	-
24B6D	2.348	2.380	-	-	3.25	-	-
Average	**2.344**	**2.377**	**2.431**	**3.75**	**3.32**	**0.38**	**10.0**
25B6A	2.344	2.378	2.433	3.65	3.36	0.28	8.3
25B6B	2.381	2.417	2.470	3.61	3.46	0.14	3.9
25B6C	2.353	2.384	-	-	3.13	-	-
25B6D	2.341	2.374	-	-	3.32	-	-
Average	**2.355**	**2.388**	**2.452**	**3.63**	**3.31**	**0.21**	**6.1**
26B6A	2.383	2.415	2.478	3.84	3.01	0.83	21.6
26B6B	2.375	2.404	2.453	3.17	2.89	0.28	8.8
26B6C	2.362	2.393	-	-	3.10	-	-
26B6D	2.353	2.384	-	-	3.04	-	-
Average	**2.368**	**2.399**	**2.466**	**3.51**	**3.01**	**0.56**	**15.2**

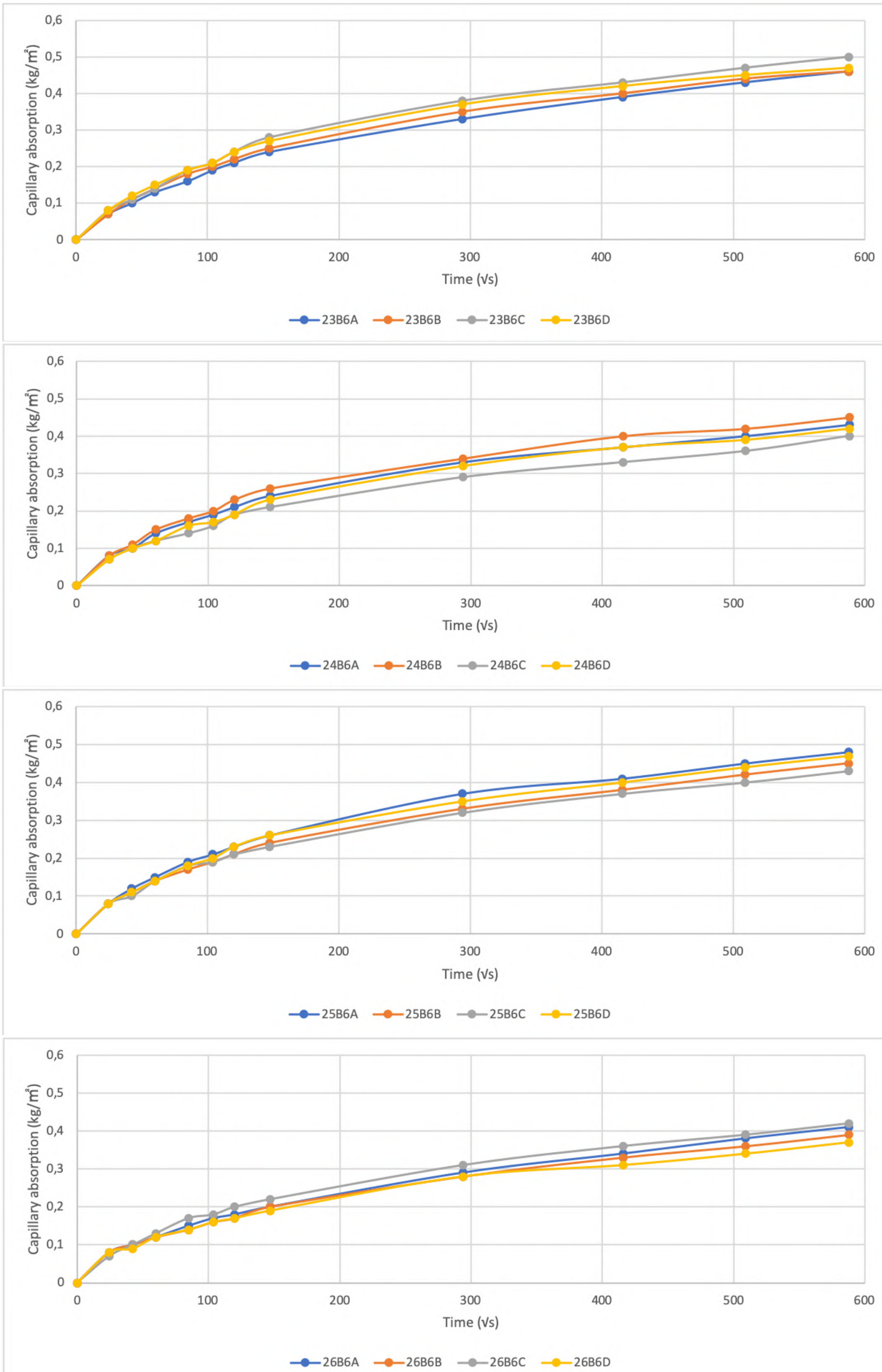

Figure 5.15: Capillary suction in kg/m^2 over $\sqrt{time}$ for all specimens in batches 23-26

6 Analysis

Each mix design was proportioned by replacing or modifying one component at a time, isolating the effect it had on the concrete´s properties. In the following subsections, relevant batches have been discussed for each material category.

6.1 Superplasticizer - quality and quantity

Figure 6.1 shows the slump flow values for batches 1 and 2. Batch 1 was dosed with 30 kg/m^3 Mapei Dynamon SX-N while batch 2 with 12.69 kg/m^3 Sika Visco-Crete UHPC-2. Every other component in the mix designs were identical, with the same mixing and casting procedure. The mobility of batch 1 was reduced to 64 % within the first 30 minutes after mixing, where the largest drop was seen to have occurred during the first 15 minutes, while batch 2 only experienced a total drop to 85 % with a more gradual decline. The slump flow measurements for batch 2 were almost twice as large than those for batch 1, even with a dosage of approximately 1/3 volume of SP. This shows the effectiveness of Sika Visco-Crete UHPC-2. A disadvantage of this is achieving the desired workability may prove harder when a small error in dosage has such a large effect. The Sika Visco-Crete UHPC-2 produced compressive strengths that were 10-20 % larger than the Dynamon SX-N depending on the curing regime. This is illustrated in Figure 6.2. Batch 2 also exhibited on average 50 kg/m^3 higher density than batch 1; a more densely packed matrix normally results in a higher compressive strength, as is the case here.

A more effective SP or higher dosage may result in a more effective dispersion of flocculated cement particles, promoting a larger percentage of hydration to take place, thus increasing its compressive strength. Batch 16 had a compressive strength of 153 MPa and batch 17 with an increase of 2.5 kg/m^3 was measured at 161 MPa. The densities for both the batches were found to be very similar, between 2330 and 2340 kg/m^3. The same was seen between batches 24 (182 MPa) and 25 (188 MPa) with 2.31 kg/m^3 more SP. There was an instance where this was not the case; batch 13 had a slightly lower compressive strength (188 MPa) compared to batch 12 (195 MPa), despite a slightly higher SP dose (increase of 2.31 kg/m^3). The differences in densities were negligible in this case. For all the three cases where UHPC-2 was used, (12 vs 13, 16 vs 17, and 24 vs 25) a higher SP dosage resulted in higher slump flow readings and a lower reduction in mobility over the first 30 minutes after mixing.

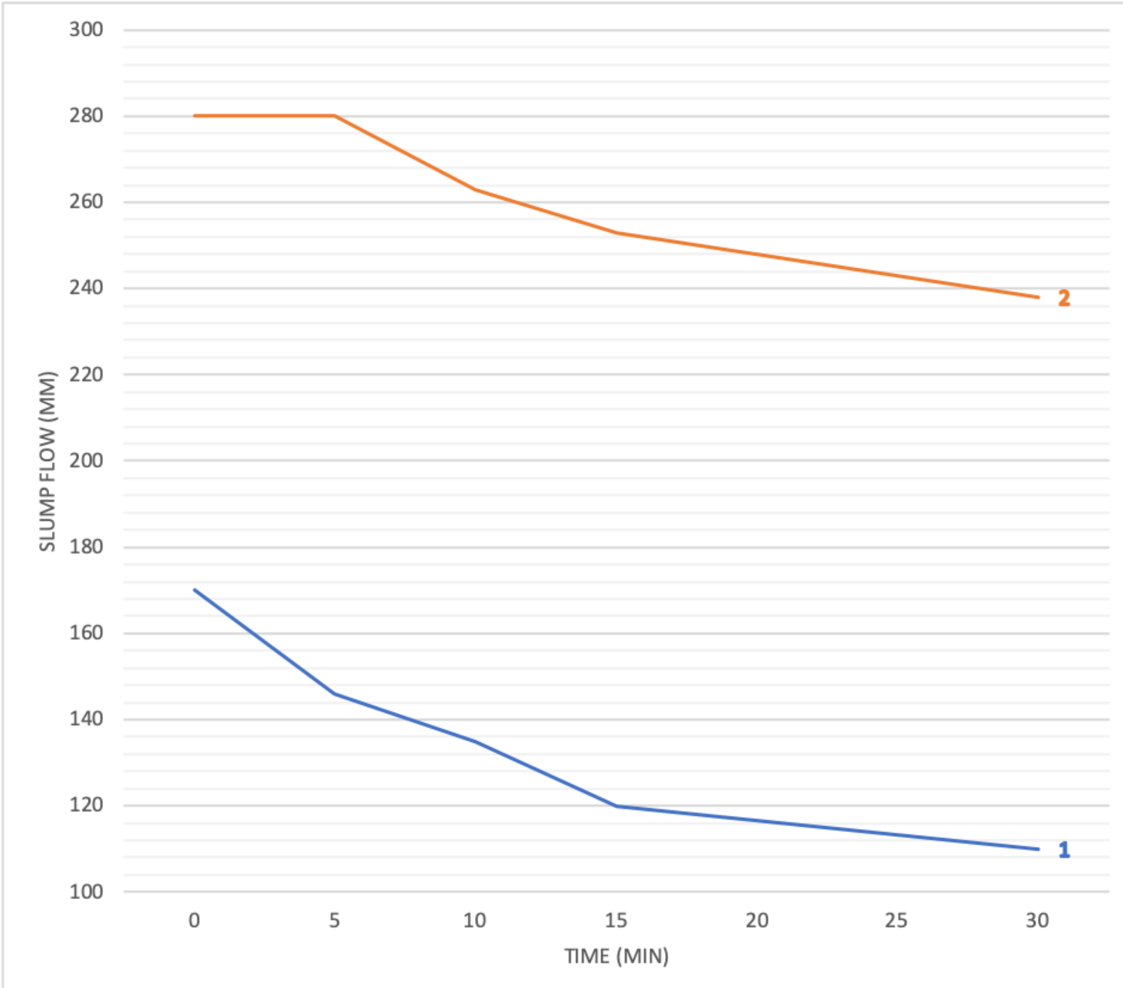

Figure 6.1: Workability for batches 1 and 2.

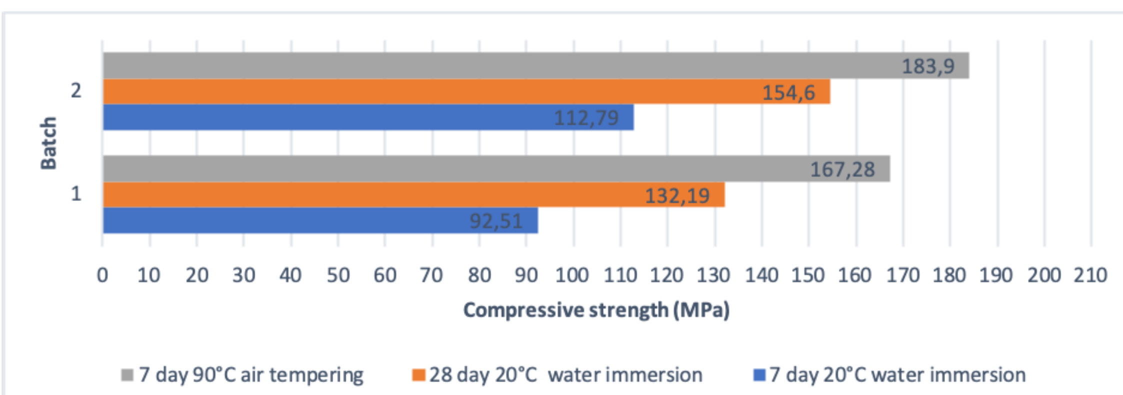

Figure 6.2: Compressive strengths for batches 1 and 2.

6.2 Modifications to water-binder ratio

The slump flow results from batches 2, 10, and 11 are displayed in figure 6.3, where the only variation between the mix designs is water quantity. Batch 2 contains 210 kg/m^3 (w/b = 0.224), batch 10 has 195 kg/m^3 (w/b = 0.198), and batch 11 has 180 kg/m^3 (w/b = 0.183). Reducing the water content by 15 kg/m^3 gives a slump flow reduction of an average of 50mm. The major difference can be seen in the first 5 minutes where batch 2 loses none of its workability, while batch 11 experiences a large drop. After 30 minutes, the mobility of batches 2, 10, and 11 are reduced to 85.0, 84.5, and 71.8 respectively. Batch 13 (180 kg/m^3, w/b = 0.185) and 15 (170kg/m^3, w/b = 0.175) are also comparable as they only vary in water quantity. These are displayed in figure 6.4. Both these batches experience the same large drop in workability during the first five minutes as batch 11 did. Their total loss of workability after 30 min were 78.3 and 77.1, respectively.

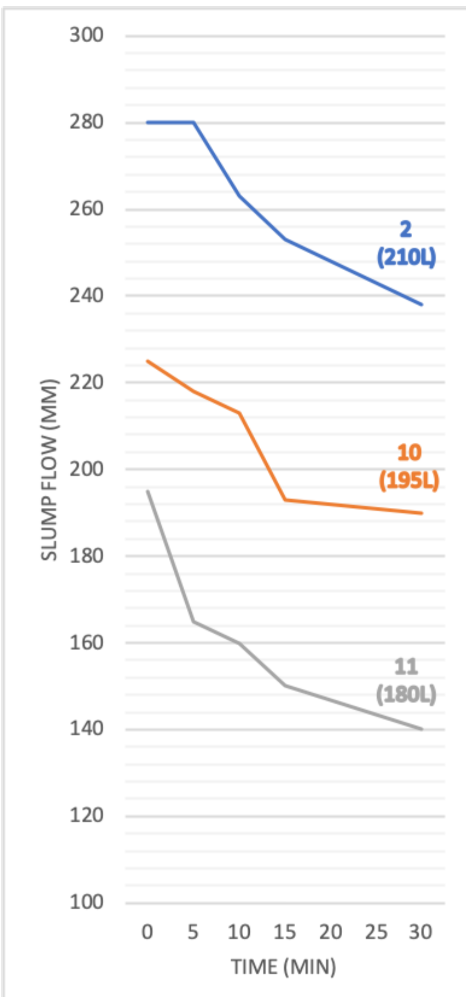

Figure 6.3: Batches 2, 10, and 11

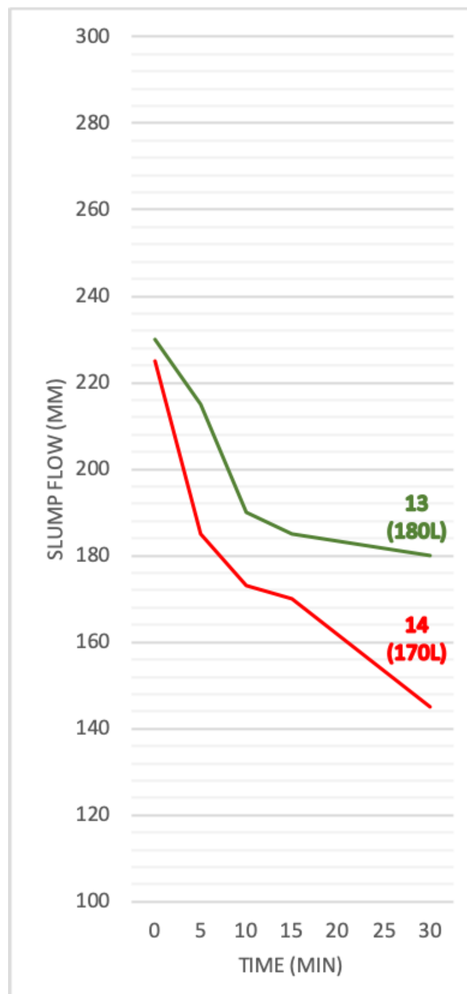

Figure 6.4: Batches 13 and 14

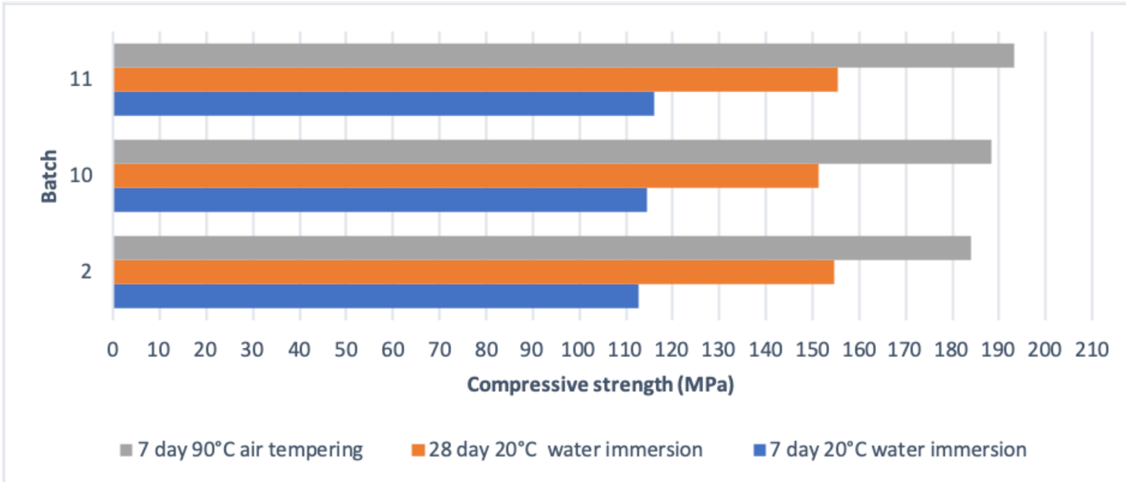

Figure 6.5: Compressive strengths for batches 2, 10, and 11.

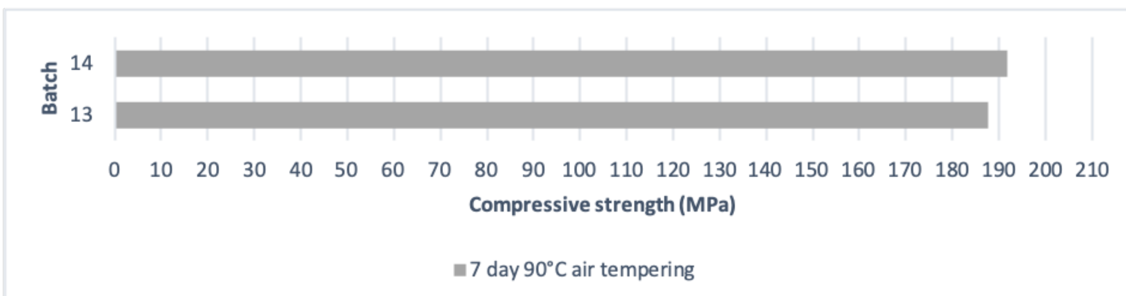

Figure 6.6: Compressive strengths for batches 13 and 14

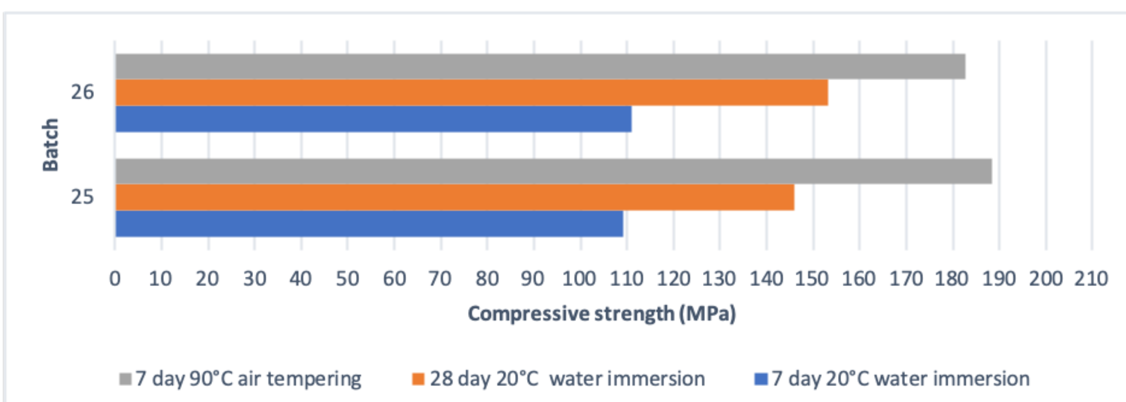

Figure 6.7: Compressive strengths for batches 25 and 26

Figure 2.4 illustrated that a lower w/b ratio should cause a higher compressive strength. Figure 6.5, 6.6, and 6.7 compares the compressive strengths for batches with different w/b ratios, and the results for these batches are in agreement with this theory, with the exception of the specimens from batch 25 (7-day air tempering regime) and batch 10 (28-day water immersion), which had an opposite effect. There was a case where a lower w/b ratio decreased the average compressive strength for all specimens; this is shown in Figure 6.8 below, where batch 23 (210L water, w/b = 0.210) is compared with batch 24 (195L water, w/b = 0.198).

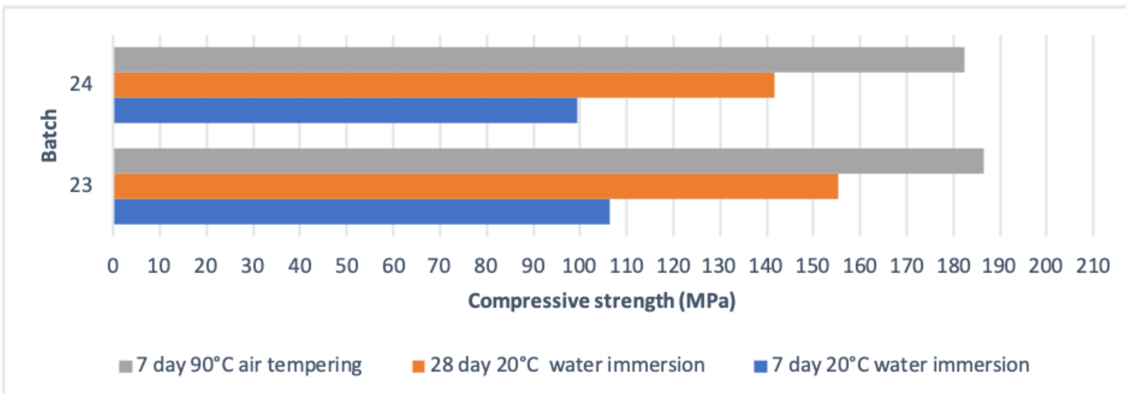

Figure 6.8: Compressive strengths for batches 23 and 24

These results indicate that a higher w/b ratio minimizes the loss of workability over time and that a drastic drop occurs within the first five minutes when the w/b ratio descends below 0.2. In other words, the workability over time and compressive strength most often have an inverse relationship when only the w/b ratio is considered, causing a balancing act between the fresh phase properties and the hardened state performance. A lower w/b ratio also caused a smaller volume percent of capillary pores in the concrete; this was the case for batches 23-26 as shown in Table 5.17. A smaller capillary porosity slows down the rate of mass transport through the material (lower capillary number k) providing more protection against chemical attack such as chlorides. The total porosity also declines when the w/b ratio is lowered, this indicates that a degrease in porosity causes an increase in compressive strength, and is supported by the results found in this thesis. There seems to be a correlation between the size of the initial slump flow and the loss of mobility over time. A cement with a high initial slump flow seems to have the ability to retain its workability over longer periods. This is the case for all the batches 23-26 in the extraneous program as can be seen by comparing figures 5.9 and 5.10.

In the extraneous test program, the flexural strength was increased when the w/b ratio decreased. Reducing the w/b ratio from 0.210 to 0.198 (batch 23 and 24) caused an increase in flexural strength of 3 MPa, and the same was observed for batches 25 and 26, with an increased strength of 5 MPa.

6.3 Fillers - Millisil W12 vs Betofill VK50

Millisil W12 is a silica-based filler (batch 4 and 7) while Betofill VK 50 is a limestone filler (batch 5 and 6), and both of these are chemically inert materials. A comparison of the mobility of batch 4 versus 5 and batch 6 versus 7 indicate that the two batches with Millisil W12 had, on average, a larger slump flow value; however, the Betofill VK50 preserves its mobility slightly better over time when compared to Millisil W12 with 5-10 % larger drop after 30 minutes. The slump flow results for these four batches are shown in Figure 5.6. The mix designs were proportioned on a volumetric basis when substituting a material component, compensating for the higher density of Betofill VK50 (2720 kg/m^3) when compared to Millisil W12 (2650 kg/m^3). Pin pointing an exact reason as to why Betofill VK50 retains a higher mobility over time is difficult with only these results and would need to be studied further. According to the product data sheets in Appendix I, the particle size distribution for both fillers were nominally alike. The specific surface area (m^2/kg) could have an influence on the initial slump flow with regards to the amount of water required to produce the same flow-ability. This may explain why Millisil W12 produced an on-average higher slump flow. This value was not present in the PDSs and neither was it determined as a part of this thesis. A study on the effects of limestone and silica powder on early age performance determined that the calcite in limestone contains Ca^{+2} and $CO3^{-2}$, which contributes to a neutral particle surface, and function as an inter-particle electrostatic repulse towards hydroxyl groups in an aqueous solution [26]. This may be a contributing factor in how Betofill VK50 sustains its mobility over longer periods, as this electrostatic repulse on a molecular level acts similarly as the polycarboxylate-based superplasticizers. These are theories that may support the results obtained here; however, they have not been proven as a part of this thesis. While considering only the workability of concrete, the question arises whether it is more advantageous during casting to increase the slump flow, providing better compactability in the first minutes or to preserve a slightly lower slump flow over a longer time period. On the subject of mechanical strength, Millisil W12 provides a 5-8 percent increase in compressive strength when compared to Betofill VK50. This can be observed in figures 6.8 and 6.9. The question arises whether or not the increase in performance is worth the higher material costs that come with using Millisil W12 as a filler. From an economical point of view, limestone fillers are very advantageous because of their low production costs. A higher specific surface area (blaine value), would require more water to achieve the same slump flow, the blaine value was not available in the PDSs; however, if Betofill VK50 has a higher specific surface area to that of Millisil W12, this could cause a reduction in initial slump flow; meaning less water is available for the hydration of cement, causing a reduction in reduction in compressive strength. This would support the results presented in figures 6.9 and 6.10.

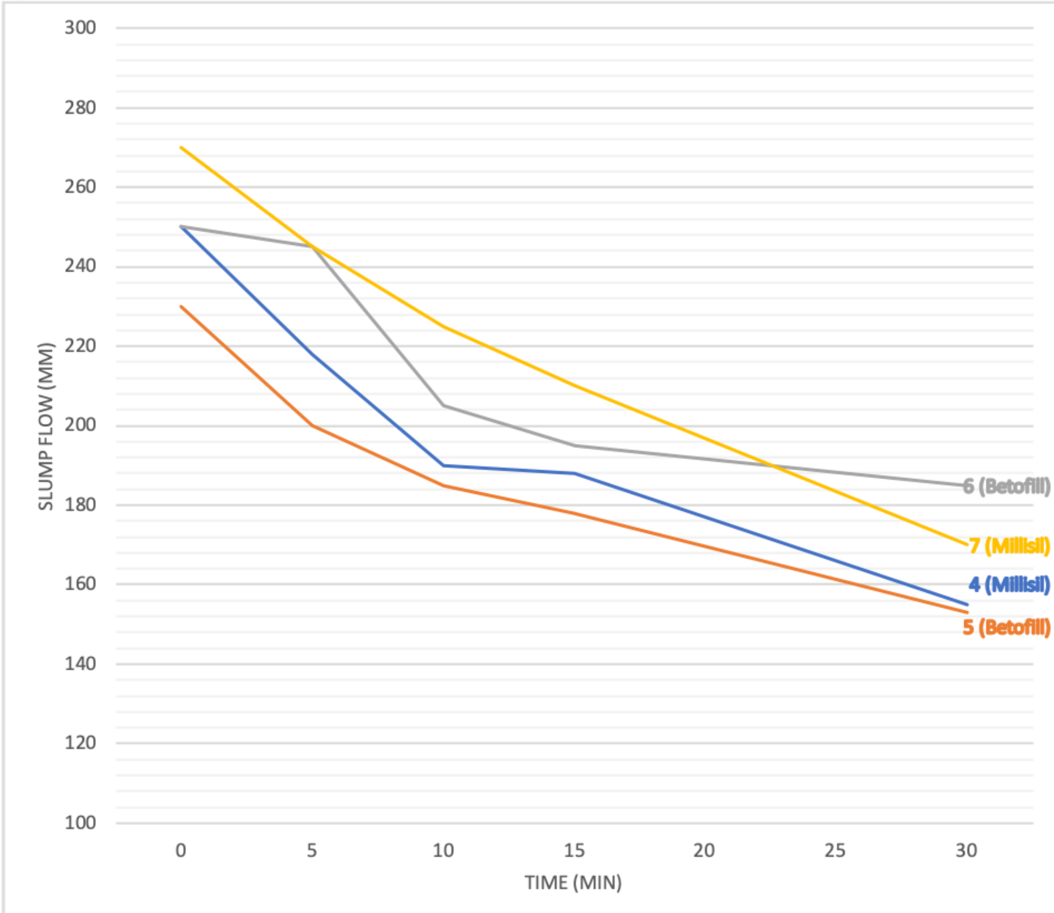

Figure 6.9: Batches 4,5,6, and 7

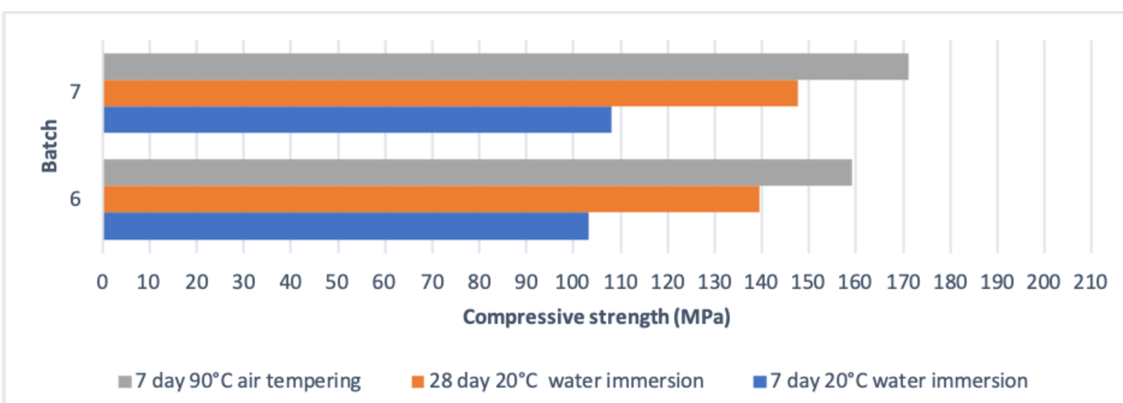

Figure 6.10: Compressive strengths for batches 6 and 7

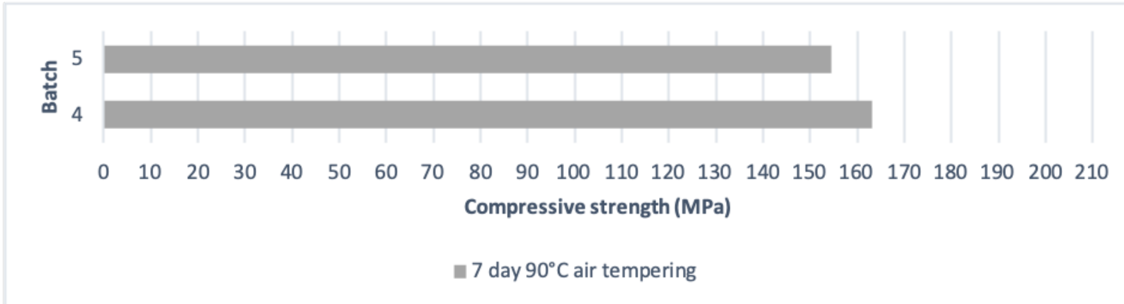

Figure 6.11: Compressive strengths for batches 4 and 5

6.4 Effect of changing the aggregate

The differences between batches 2,3,4, and 7 is the granular component; batch 2 consists of the German quartz sand H33 (d<0.5mm), batch 3 has the Danish quartz sand (0mm < d < 1mm), batch 4 has gneiss-granite (0mm < d < 4mm), batch 7 has both gneiss-granite and quartz-diorite (5mm < d < 8mm) with a volume fraction of 70/30 respectively. It should be noted that batch 4 was mixed in a different mixer than the other 3 batches. The slump flows for these four batches are displayed in Figure 5.7. Batches 2 and 3 with the smallest particle size produce the larges slump flow in addition to a more gradual slope, indicating a better mobility over the first 30 minutes after mixing. The particle phase with a diameter over 0.125mm is, according to the literary study, the largest influencer on fresh phase properties. The particle-size distribution curves for these four batches are presented in Appendix H. The German quartz H33 and Danish quartz are more spherically shaped, creating a "ball bearing" effect when compared to the larger gneiss-granite and quartz-diorite with more angular dimensions. More work is required to overcome the internal friction between angular shaped particles, which will reduce the mobility. The aggregates porosity also has an effect; a higher porosity means a larger absorption of free water, leaving less to provide workability. Porosity tests of the aggregates were not performed during this thesis, and neither is it displayed in the PDSs. Figure 6.11 compares the compressive strengths of these four batches. The smaller particle size also produces higher values. There can be several reasons for this; some theories are that the smaller aggregates lead to a more homogeneous material with less local defects and that the weaker ITZ is more often greater due to the presence of larger aggregates, reducing its strength. Batch 4 and 7 showed a small tendency of paste separation, and as mentioned in the literature, a lower stability increases the thickness of the ITZ, resulting in a diminished strength, as is the case when comparing batches 4 and 7 with 2 and 3.

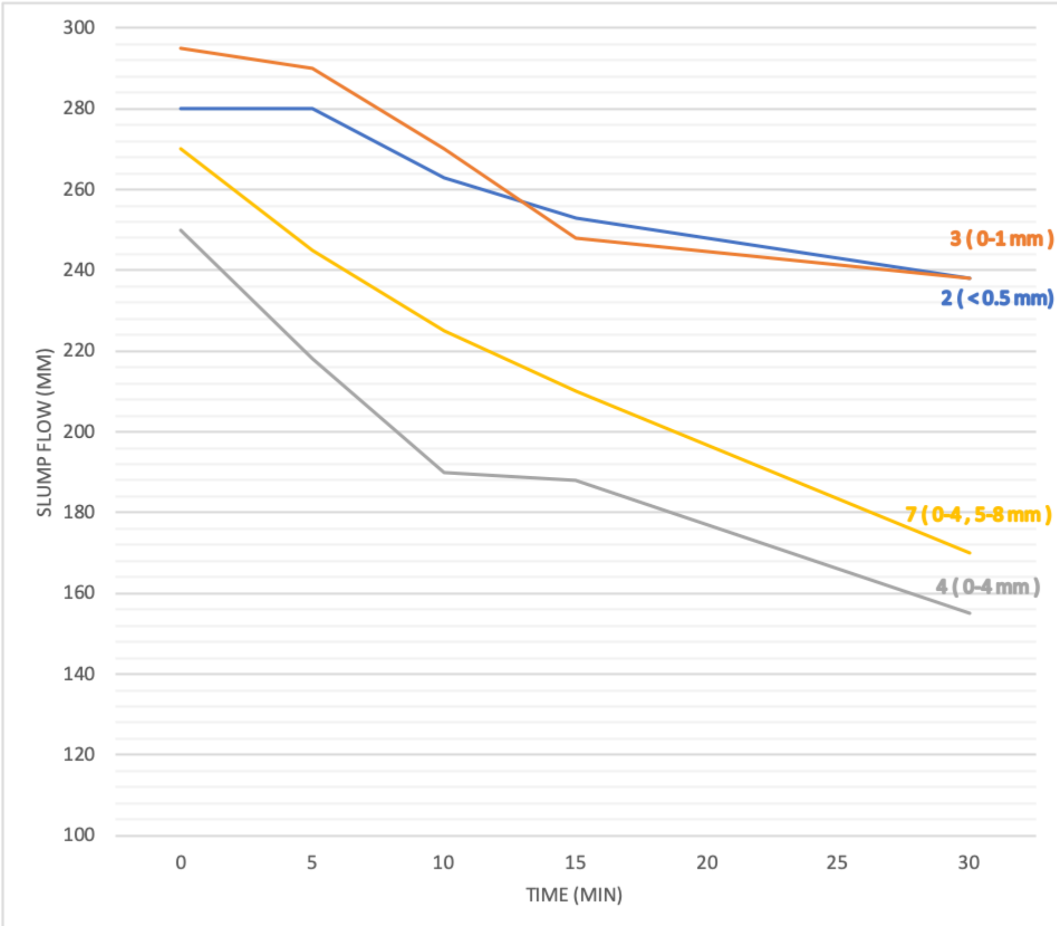

Figure 6.12: Batches 2, 3, 4, and 7

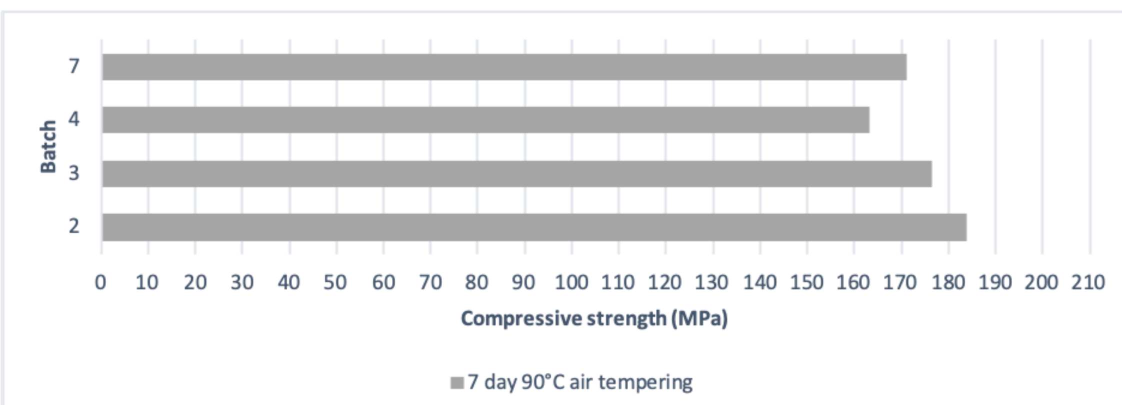

Figure 6.13: Compressive strengths for batches 2, 3, 4, and 7

6.5 Effect of changing the mixer

Batches 11 and 12 have identical mix designs; however, batch 11 was mixed using the larger Eirich R09t mixer while batch 12 was mixed in the smaller, more intensive Eirich R02/Vac mixer. The results for these two batches have been isolated in Figure 5.8 below. In this case, the R02/Vac produces a larger slump flow for all 5 time intervals (0-30min) which could be attributed to higher mixing energy (KJ/kg) in the smaller mixer. The slope of the two curves look very similar. The smaller mixer produced a 4 % drop in mobility over the first 30 minutes and compared to the larger mixer, this drop was very small and may not be significant enough to draw any conclusions. Only one test was performed with the intent of determining the effect of different mixers. Batch 11 had a compressive strength of 193.3 MPa while batch 12 was measured at 194.8 MPa, meaning the strength was not affected greatly by changing the mixer.

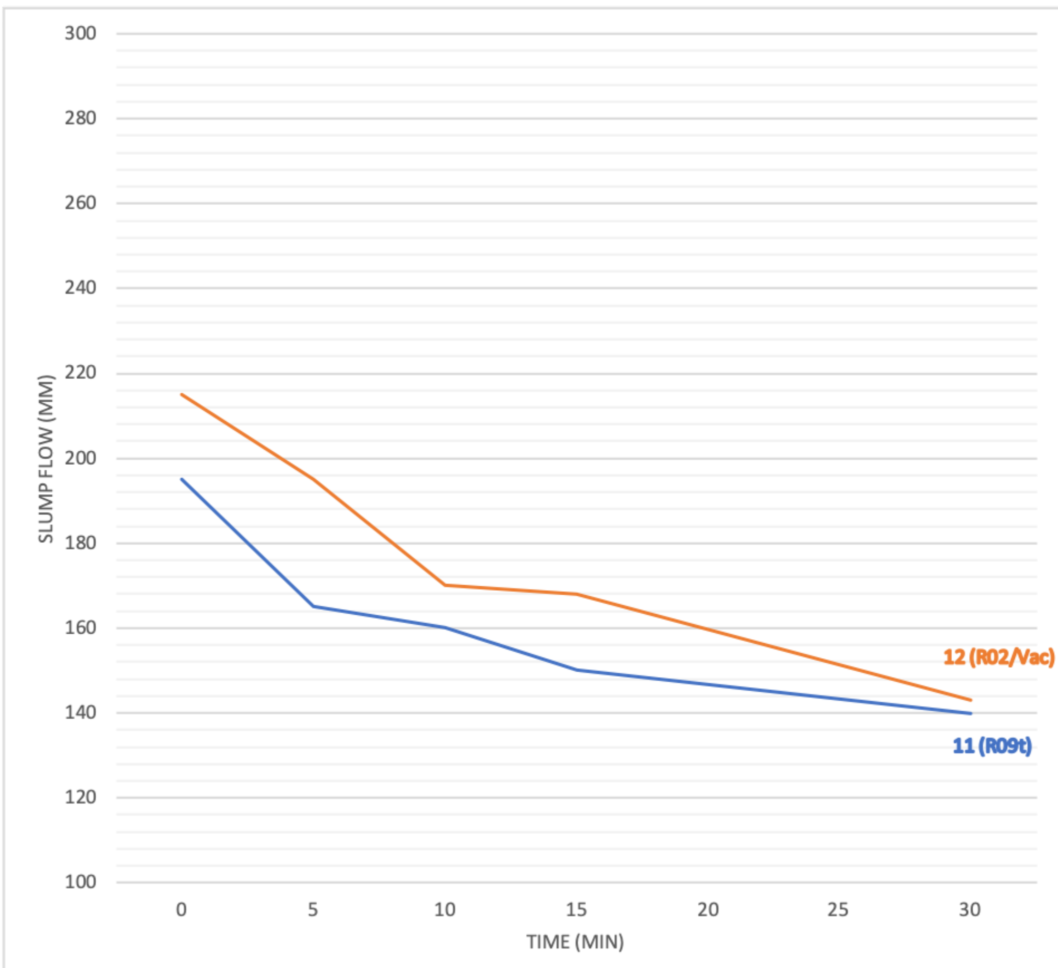

Figure 6.14: Batches 11 and 12

6.6 Effect or changing the binders

Batches 13, 15, 16, and 19 consist of different binders,and the rest of the mix design is identical apart from batch 16, which contains an additional 50 kg/m^3 water to compensate for the higher blaine value of the CEM I 52,5R. Figure 5.9 below shows the slump flow results of these four batches.

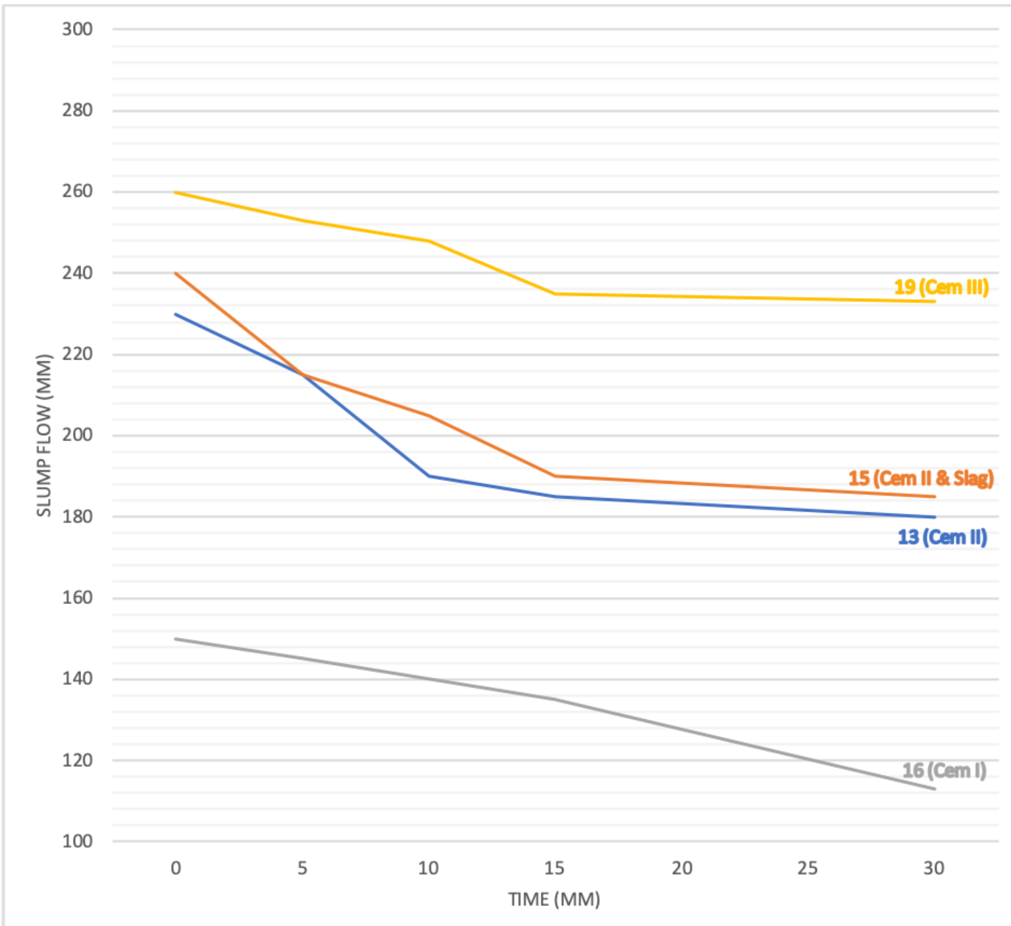

Figure 6.15: Batches 13,15,16, and 19

Batch 19 containing CEM III/A 52,5 R (Variodur 40) and has a much larger slump flow than the others, with only a 10 % drop in mobility over the first 30 minutes, while the three other binders showed a reduction of 25%. The compressive strengths are compared in Figure 6.14, and shows large variations between them. Variodur 40 provides the best compressive strength and workability; however, this product is not as commercially accessible in Norway when compared to the other binders tested from the manufacturer Norcem. Batch 15 replaced 30 vol-% of the CEM II with Slag, which increased the slump flow slightly; however, there was minimal effect on the mobility over time. The slag caused the average compressive strength to drop 10 MPa when considering the specimens that had undergone 48-hour air tempering at 90 degrees

Celsius. A cement with a higher specific surface area (blaine value) will usually require a larger amount of water to preserve the same level of workability. The CEM I 52,5 R (Norcem Industrisement) had a blaine value of 550 kg/m^3, which was much higher when compared to CEM II/A-V 42,5 N (Norcem Anleggsement FA) with 390 kg/m^3. During the proportioning process, an attempt was made to compensate for this by increasing the water content to 230 kg/m^3; this was not sufficient to produce the same initial slump flow, as can be seen in Figure 6.13. The Variodur 40 is an especially developed cement from Dycherhoff marketed for use in UHPC. The blaine value for this cement was not present in the researched literature, so a comparison could not be made from the aspect of cement fineness.

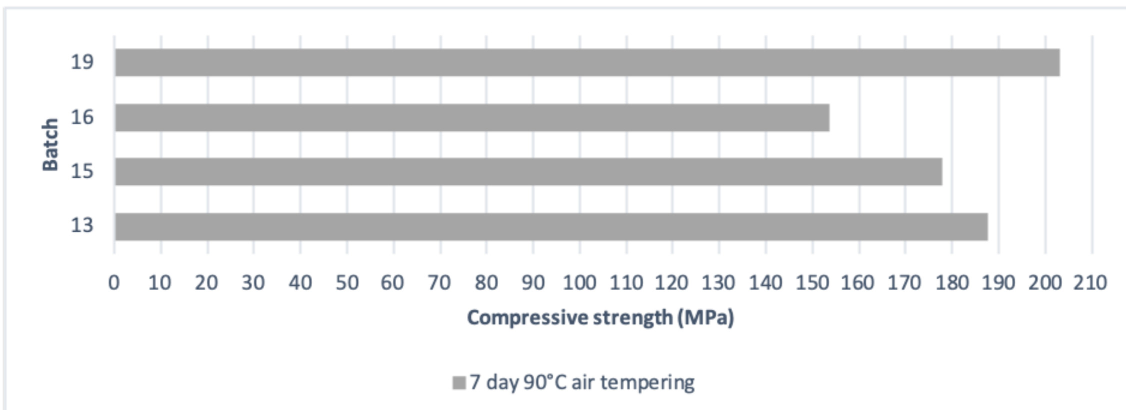

Figure 6.16: Compressive strengths for batches 13,15,16, and 19

All of the specimens that were tensile tested contained the same quantity of Norcem Anleggsement FA, so no analysis is carried out in this thesis on tensile strength with respect to alterations in the quality and quantity of cement.

6.7 UHPCs modulus of elasticity

As stated earlier in the literary study, *Graybeal* established empirical linear equations connecting the modulus of elasticity and 28-day compressive strength for UHPCs. The results determined by material testing in the laboratory are compared to the results calculated by these linear equations, and its deviation in percent are presented in Table 6.1. It can be seen that the linear equations have increasing discrepancies when used on concretes with compressive strengths under the UHPC limit of 150 MPa. For batches 2,3,10,11, and 23, which had strengths of 150-160 MPa, there was only a deviation of ±5%. The output value of the two equations did not vary much between them, and according to the results attained in this thesis, one equation is not more accurate than the other. Batches 8 and 9 were not reinforced with steel fibers, which is a contributing factor to the low modulus of elasticity. These experienced a very brittle failure during the compression testing of the cubic specimens, which could be described as an explosive failure.

Table 6.1: Theoretical vs actual modulus of elasticity for UHPC

Batch	**Avg. comp. strength (MPa) (28 d 20°C water immersion)**	**Measured modulus of elasticity (GPa)**	$E = 3320\sqrt{f_c} + 6900$		$E = 19000\sqrt[3]{\frac{f_c}{10}}$	
			E-modulus (GPa)	**Deviation (%)**	**E-modulus (GPa)**	**Deviation (%)**
1	132.2	44.3	45.1	+1.8	44.9	+1.4
2	154.6	49.3	48.2	-2.2	47.3	-4.1
3	151.2	49.0	47.8	-2.5	46.9	-4.3
6	139.5	43.6	46.1	+5.7	45.7	+4.8
7	147.7	42.6	47.3	+11.0	46.6	+9.4
8	138.3	41.9	45.9	+9.5	45.6	+8.8
9	124.4	35.1	43.9	+25.1	44.0	+25.4
10	151.4	48.8	47.8	-2.0	47.0	-3.7
11	155.5	49.3	48.3	-2.0	47.4	-3.9
23	155.4	47.7	48.3	+1.2	47.4	-0.6
24	141.6	45.4	46.4	+2.2	46.0	+1.3
25	145.9	46.8	47.0	+0.4	46.4	-0.9
26	153.2	46.6	48.0	+3.0	47.2	+1.3

The modulus of elasticity is an essential factor for estimating the deformation of the material, and is most often expressed in terms of compressive strength; however, determining an accurate empirical linear relationship between the two is difficult, as concrete is a heterogeneous material in nature. The results show in general that an increase in 28-day compressive strength, leads to an increase in the concretes modulus of elasticity. Some observations made from the Table 6.1 shows that batches 2, 3, 10, 11, 23 with similar compressive strengths, also produced similar high modulus of elasticities around 48-49 GPa. These batches had the smaller granular fractions, the same binder. When introducing the larger granular fraction in batches 6 and 7, the E-modulus drops to 42-43 GPa. Batch 9 with the SRA and without fiber reinforcement produced the lowest E-modulus. The specimens that underwent modulus of elasticity testing were only curing submerged in 20 degrees Celsius water for 28 days. With heat treatment, this number should be increased above 50; however, this was not tested in this thesis.

6.8 Sources of error

During the laboratory portion of this thesis, some sources of error did arise. There were some instances in the miniature slump flow test where the surface of the laminated base board was not cleaned thoroughly enough after removing the excess concrete after filling the cylindrical mold. This caused a higher friction between the base board and concrete, decreasing the flow velocity in some places, resulting in a lower slump flow. This was the case for some of the first batches. Only one specimen from batch 9 underwent an air tempering curing regime. This was due to not enough material left over, while the other batches had three specimens to calculate the average value. This was also the case for batch 8 and 9 when determining the modulus of elasticity where only one cylinder was tested for each of these batches.

The PF-method was performed on UHPCs where the capillary suction was very retarded when compared to a NSC with higher porosity. This test should have been extended to longer time intervals to identify the moment of capillary capacity when the water front reaches the topside of the specimen, indicating that all the capillary pores are saturated. This may have caused some discrepancies when calculating the capillary number (k).

7 Conclusion

This thesis attempted to understand how the workability over time, mechanical properties, and durability are affected by making alterations to the mix design. By changing one material component at a time, either in quality or quantity, and performing a range of tests made it possible to achieve this. The results attained in this thesis show that the densities for the UHPCs that were tested were in the range of 2350-2450 kg/m^3 with low variations between specimens with the same mix design and curing regime, indicating good homogeneity and high stability. Normal strength concretes usually have a density of around 2400 kg/m^3, so these UHPCs did not vary much from NSCs with respect to density. When using the larger aggregate fraction, there was a tendency for paste separation. There was little variations in the stability over time for the mix designs that were evaluated, but the mobility was reduced depending on the material composition. The factors that had the highest influence on mobility over time was the type and quantity of SP, w/b ratio, initial slump flow, aggregate size, and type of binder. To preserve the fresh-phase properties over a longer period, the concrete should be proportioned with a high SP dose, high w/b ratio, both causing a large initial slump, small aggregate fraction, and a binder like Variodur 40. However, some of these factors will have a negative effect on the mechanical properties. Increasing the w/b value will, in most cases, reduce the compressive and flexural strength with some exceptions; this will increase the permeability due to a higher vol-% of capillary pores, reducing its durability. Increasing the SP usually increases the compressive strength; however, this is not always the case, as was seen in one of four instances in the laboratory program. The reduction of aggregate grain size causes a positive effect on both the workability and mechanical properties.

When disregarding the affects on workability, to produce a UHPC with high compressive strength, the w/b ratio should be reduced, utilizing a binder such as Variodur 40 and a filler based on silica powder, in addition to keeping the largest particle size under 1mm.

The tensile strength of all the mix designs evaluated were in the range of 6-20MPa and was in accordance with the literary study on UHPC; however, there were unexpected large variations in strength between specimens that had the same mix design and curing condition. This is most likely a result of different fiber orientations in relationship to the stress direction. These results were determined by performing the splitting tensile test and converted into tensile strength, which could show some deviations when compared to a uniaxial test.

The elastic modulus for the batches that qualified as a UHPC with regards to the compressive strength were in the range of 45-50 GPa. UHPCs have a high density matrix with a low capillary porosity. This reduces the rate of water intrusion into the material from the surface, improving its resistance to chemical attack. This was verified by performing the PF-method on batches 23-26.

8 Suggestions for further work

In this thesis, the amount of silica and fibers have remained constant throughout all mix designs. How the volume percent and aspect ratio of fiber reinforcement will affect the mobility over time was not determined in this thesis and merits more research.

The autogenous shrinkage was not determined for these mix designs and it would be interesting to see how the large binder content could cause cracking, i.e, reduce the overall material performance and if autogenous shrinkage has an inverse relationship with workability over time or not. Testing the tensile strength of UHPCs by utilizing a uniaxial tensile test is also an interesting next step, although this test is more time consuming and difficult to implement than a conversion though the splitting tensile test. This could be done by 3D printing dog-bone shaped molds with slops to place 8mm re-bars on either end so that they are axially aligned when testing. Initially, the plan was to attempt this test as a part of this thesis to examine the differences between splitting tensile tests and uni-axial tensile tests. However, this was not done but rather considered as a suggestion for further work. Figure 8.1 below shows a drawing done in Autocad for mold designs.

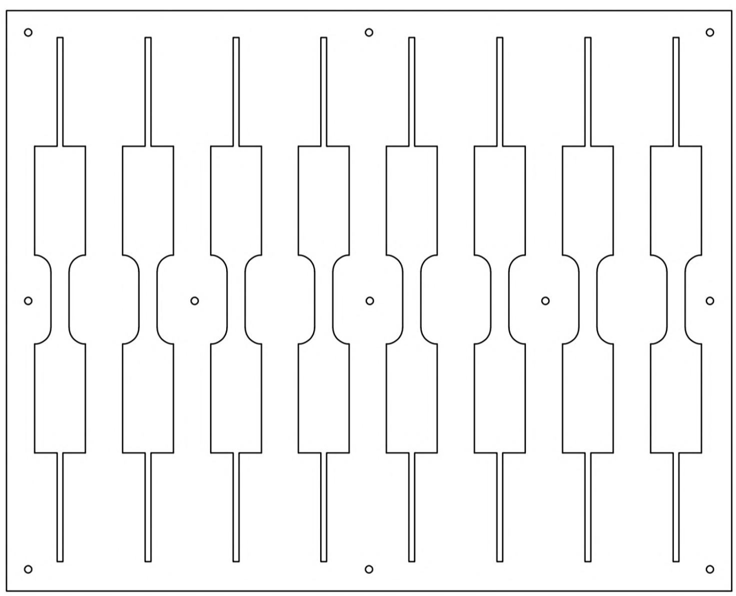

Figure 8.1: Molds for specimens for uni-axial tensile test drawn in Autocad, with the intension of 3D printing or laser-cutting plexiglas for assembly

The binder CEM III/A 52,5 R (Variodur 40) showed the most promising results, both when it came to workability over time and compressive strength. However, due to the short supply of this binder at the university during the time the laboratory part of this thesis was undertaken, this mix design could not be investigated with respect to prolonged mobility tests up to 60 minutes after mixing, flexural strength, and permeability. The tensile strength was not determined in batches where variations were made to the binders and was therefore not investigated in this thesis.

How does different placing techniques affect the fiber orientation and can this help reduce the large variations in tensile strength between two specimens with the same mix design and curing regime? UHPCs large binder content may produce a lot of heat due to the exo-thermal process of hydration. How does this material perform when used in larger constructions with thicker cross sections? The accuracy of the PF methods for use on UHPCs would also be examined further, How often do these specimens need to undergo capillary suction before the capacity is reached? These questions have not been examined in this thesis, but are presented here as suggestions for further work on the subject of UHPC.

References

[1] L. Ricciotti, "Mucem museum, marseille." https://www.inexhibit.com/mymuseum/mucem-museum-marseille/, 11 2019. Accessed: 2019-11-10.

[2] A. E. Naaman and K. Wille, "The path to ultra-high performance fiber reinforced concrete (uhp-frc): five decades of progress," *Proceedings of Hipermat 2012 - 3rd International Symposium on UHPC and Nanotechnology for Construction Materials*, 2012.

[3] M. B. Eide and J.-M. Hisdal, "Ultra high performance fibre reinforced concrete (uhpfrc)–state of the art: Fa 2 competitive constructions: Sp 2.2 ductile high strength concrete," *SINTEF Building and Infrastructure*, no. 44, pp. 11–21, 2012.

[4] W. W. Thanongsak Nochaiya, "Utilization of fly ash with silica fume and properties of portland cement–fly ash–silica fume concrete," *Fuel*, vol. 89, pp. 768–774, 3 2010.

[5] S. Kubens, *Interaction of cement and admixtures and its influence on rheological properties*. PhD thesis, Bauhaus University, Weimar, 6 2010. Page 40-42.

[6] S. Anshuang, L. Qin, Z. Shoujie, Z. Jiayang, and L. Zhaoyu, "Effects of shrinkage reducing agent and expansive admixture on the volume deformation of ultrahigh performance concrete," *Advances in Materials Science and Engineering*, vol. 2017, pp. 1–7, 07 2017.

[7] S. Smeplass, "Frech concrete - workability," in *Concrete Technology* (J. H. M. Stefan Jacobsen, ed.), ch. 3, pp. 1–25, Trondheim: NTNU, 2016. ISBN 82-7482-098-3.

[8] K. Habel, *Structural behaviour of elements combining ultra-high performance fibre reinforced concretes (UHPFRC) and reinforced concrete*. PhD thesis, Federal Institute of Technology in Lausanne, Lausanne, Switzerland, 7 2004. doi: 10.5075/epfl-thesis-3036.

[9] E. J. Sellevold, "Porosity, pore structure," in *Concrete Technology* (J. H. M. Stefan Jacobsen, ed.), ch. 8, pp. 1–14, Trondheim: NTNU, 2016. ISBN 82-7482-098-3.

[10] E. Fehling, M. Schmidt, J. Walraven, T. Leutbecher, and S. Fröhlich, *Ultra-high performance concrete UHPC: Fundamentals, design, examples*. John Wiley & Sons, 2014.

[11] B. A. beal, *Characterization of the behavior of ultra-high performance concrete*. PhD thesis, University of Maryland, Maryland, USA, 1 2005.

[12] R. C. Sverre Smeplass, "Frech concrete - proportioning," in *Concrete Technology* (S. Jacobsen, ed.), ch. 4, pp. 1–35, Trondheim: NTNU, 2016. ISBN 82-7482-098-3.

[13] C. Vogt, *Ultrafine particles in concrete - Influence of ultrafine particles on concrete properties and application to concrete mix design*. PhD thesis, Royal Institute of Technology, Stockholm, Sweden, 6 2010. doi: ISRN KTH/BKN/B—103—SE.

[14] B. Lagerblad and K. Kjellsen, "Normal and high strength concretes with conventional aggregates," *RILEM REPORT*, 1999.

[15] E. J. Sellevold, "Pozzolana," in *Concrete Technology* (S. Jacobsen, ed.), ch. 7, pp. 1–16, Trondheim: NTNU, 2016. ISBN 82-7482-098-3.

[16] R. Myrdal, "Admixtures," in *Concrete Technology* (S. Jacobsen, ed.), ch. 10, pp. 1–27, Trondheim: NTNU, 2016. ISBN 82-7482-098-3.

[17] J. Ma, M. Orgass, F. Dehn, D. Schmidt, and N. Tue, "Comparative investigations on ultrahigh performance concrete with and without coarse aggregates," 09 2004.

[18] H. Sobuz, "Manufacturing ultra-high performance concrete utilising conventional materials and production methods," 2016.

[19] I. F. for Structural Concrete (fib), *Structural Concrete Textbook on behaviour, design and performance, Second edition Volume 1: Design of concrete structures, conceptual design, materials*, vol. 1 of *10*. International Federation for Structural Concrete (fib), 2009.

[20] F. Jungmann, "Design relevant properties of hardened ultra high performance concrete," in *International Symposium on Ultra High Performance Concrete* (C. G. M. Schmidt, E. Fehling, ed.), ch. 8, pp. 327–338, Trondheim: University of Kassel, Germany, 2011.

[21] B. A. Graybeal, "Compressive behavior of ultra-high-performance fiber-reinforced concrete," *ACI materials journal*, vol. 104, no. 2, pp. 146–152, 2007.

[22] "Concrete technology - durability." https://www.cement.org/learn/concrete-technology/durability. Accessed: 2019-11-13.

[23] Øyvind Bjøntegaard, "Shrinkage, cracking," in *Concrete Technology* (S. Jacobsen, ed.), ch. 13, pp. 1–33, Trondheim: NTNU, 2016. ISBN 82-7482-098-3.

[24] F. Børsheim, "Ultrahøyfast betong med fokus på egenskapene støpelighet og trykkfasthet." University of Stavanger, 6 2017. Bachelor thesis.

[25] T. J. Rønnes, "Fuktforhold i kjellervegger av betong under grunnvannstand," Master's thesis, NTNU, Trondheim, 6 2015.

[26] D. P. Bentz, "Limestone and silica powder replacements for cement: Early-age performance," *PMC*, 2017.

Appendices

A: Mix designs in kg/batch with corrections due to moisture content in aggregates

Table A1: Mix design in kg/batch and moisture calculations (batches 1-9).

Batch number	1	2	3	4	5	6	7	8	9
Batch volume	55L	55L	55L	3.3L	3.3L	55L	55L	40L	50L
Batch date	28.08.19	28.08.19	28.08.19	18.09.19	18.09.19	10.09.19	10.09.19	29.08.19	29.08.19
CEM II/A-V 42,5 N (Anl-FA)	40.70	40.70	40.70	2.442	2.442	40.70	40.70	-	-
CEM III/A 52.5 R (Variodur 40)	-	-	-	-	-	-	-	31.12	38.95
CEM I 52,5 R (Industri)	-	-	-	-	-	-	-	-	-
Merit 5000 (slag)	-	-	-	-	-	-	-	-	-
Elkem microsilica 940U	8.03	8.03	8.03	0.482	0.482	8.03	8.03	6.15	7.69
Millisil W12	10.89	10.89	10.89	0.653	-	-	10.89	-	-
Betofill VK50	-	-	-	-	0.710	11.83	-	7.42	9.28
Danish quartz sand 0-1mm	-	-	51.22	-	-	-	-	-	-
German quartz H33	51.59	51.59	-	-	-	-	-	-	-
Gneiss-granite 0-4mm	-	-	-	3.109	3.109	36.25	36.25	16.08	20.05
Quartz-diorite 5-8mm	-	-	-	-	-	16.12	16.12	29.98	32.46
Weidacon 0.15/9mm	8.03	8.03	8.03	0.482	0.482	8.03	8.03	-	-
SAPs BASF	-	-	-	-	-	-	-	-	0.117
Mapei Dynamon SX-N	1.650	-	-	-	-	-	-	-	-
Sika Visco-Crete UHPC-2	-	0.55	0.55	0.033	0.033	0.55	0.55	0.34	0.467
Free water	11.55	11.55	11.55	0.693	0.693	11.55	11.55	7.46	12.47
Moisture (dry) in aggregate	0.50%	0.50%	1.63%	2.99%	2.99%	2.56%*	2.56%*	1.50%*	1.50%*
Moisture in kg	0.06	0.06	0.84	0.093	0.093	0.93	0.93	0.24	0.30
Corrected free water	11.49	11.49	10.71	0.600	0.600	10.62	10.62	7.22	12.17
Total weight	132.38	131.28	130.13	7.801	7.858	132.13	131.19	98.31	121.18

*Moisture content for quartz-diorite (5-8mm) was 0% for batches 6,7,8, and 9. The moisture percentage displayed in Table A.1 originates from the gneiss-granite (0-4mm).

Table A2: Mix design in kg/batch and moisture calculations (batches 10-18).

Batch number	10	11	12	13	14	15	16	17	18
Batch volume	55L	55L	3.3L	3.3L	3.3L	3.3L	3.3L	3.3L	3.3L
Batch date	10.09.19	10.09.19	18.09.19	18.09.19	30.09.19	30.09.19	30.09.19	06.10.19	06.10.19
CEM II/A-V 42,5 N (Anl-FA)	40.70	40.70	2.442	2.442	2.442	1.709	-	-	2.442
CEM III/A 52.5 R (Variodur 40)	-	-	-	-	-	-	-	-	-
CEM I 52,5 R (Industri)	-	-	-	-	-	-	2.528	2.528	-
Merit 5000 (slag)	-	-	-	-	-	0.710	-	-	-
Elkem microsilica 940U	8.03	8.03	0.482	0.482	0.482	0.482	0.482	0.482	0.482
Millisil W12	10.89	10.89	0.653	0.653	0.653	0.653	0.653	0.653	0.653
Betofill VK50	-	-	-	-	-	-	-	-	-
Danish quartz sand 0-1mm	-	-	-	-	-	-	-	-	-
German quartz H33	51.59	51.59	3.095	3.095	3.095	3.095	3.095	3.095	3.095
Gneiss-granite 0-4mm	-	-	-	-	-	-	-	-	-
Quartz-diorite 5-8mm	-	-	-	-	-	-	-	-	-
Weidacon 0.15/9mm	8.03	8.03	0.482	0.482	0.482	0.482	0.482	0.482	0.482
SAPs BASF	-	-	-	-	-	-	-	-	-
Mapei Dynamon SX-N	-	-	-	-	-	-	-	-	-
Sika Visco-Crete UHPC-2	0.698	0.698	0.0419	0.0495	0.0495	0.0495	0.0495	0.0578	0.0578
Free water	10.73	9.90	0.594	0.594	0.561	0.594	0.759	0.759	0.561
moisture (dry) in aggregate	0.50%	0.50%	0.50%	0.50%	0.40%	0.40%	0.40%	0.40%	0.40%
Moisture in kg	0.260	0.260	0.014	0.014	0.012	0.012	0.012	0.012	0.012
Corrected free water	10.47	9.64	0.580	0.580	0.549	0.582	0.747	0.747	0.549
Total weight	130.41	129.58	7.776	7.784	7.753	7.763	8.036	8.045	7.761

Table A3: Mix design in kg/batch and moisture calculations (batches 19-26).

Batch number	19	20	21	22	23	24	25	26
Batch volume	3.3L	3.3L	3.3L	3.3L	85L	85L	85L	85L
Batch date	06.10.19	21.10.19	21.10.19	21.10.19	05.11.19	05.11.19	05.11.19	05.11.19
CEM II/A-V 42,5 N (Anl-FA)	-	-	2.442	2.442	62.90	62.90	62.90	62.90
CEM III/A 52.5 R (Variodur 40)	2.442	2.442	-	-	-	-	-	-
CEM I 52,5 R (Industri)	-	-	-	-	-	-	-	-
Merit 5000 (slag)	-	-	-	-	-	-	-	-
Elkem microsilica 940U	0.482	0.482	0.482	0.482	12.41	12.41	12.41	12.41
Millisil W12	0.653	0.653	0.653	0.653	16.83	16.83	16.83	16.83
Betofill VK50	-	-	-	-	-	-	-	-
Danish quartz sand 0-1mm	-	-	-	-	-	-	-	-
German quartz H33	3.095	3.095	3.095	3.095	79.73	79.73	79.73	79.73
Gneiss-granite 0-4mm	-	-	-	-	-	-	-	-
Quartz-diorite 5-8mm	-	-	-	-	-	-	-	-
Weidacon 0.15/9mm	0.482	0.482	0.482	0.482	12.41	12.41	12.41	12.41
SAPs BASF	-	-	-	-	-	-	-	-
Mapei Dynamon SX-N	-	-	-	-	-	-	-	-
Sika Visco-Crete UHPC-2	0.0495	0.0419	0.033	0.0495	1.079	1.079	1.275	1.275
Free water	0.594	0.594	0.693	0.644	17.85	16.58	16.58	15.30
moisture (dry) in aggregate	0.40%	0.50%	0.50%	0.50%	0.50%	0.50%	0.50%	0.50%
Moisture in kg	0.012	0.014	0.014	0.014	0.399	0.399	0.399	0.399
Corrected free water	0.582	0.580	0.679	0.630	17.45	16.18	16.18	14.90
Total weight	7.790	7.776	7.866	7.834	202.8	201.5	201.7	200.5

B: Calculations of tensile strength

$$01A4A = \frac{2 \cdot 1104.0 \cdot 10^3 N}{\pi \cdot 150mm \cdot 300mm} = 15.6N/mm^2$$

$$01A4B = \frac{2 \cdot 529.7 \cdot 10^3 N}{\pi \cdot 150mm \cdot 300mm} = 7.5N/mm^2$$

$$02A4A = \frac{2 \cdot 632.0 \cdot 10^3 N}{\pi \cdot 150mm \cdot 300mm} = 8.9N/mm^2$$

$$02A4B = \frac{2 \cdot 631.5 \cdot 10^3 N}{\pi \cdot 150mm \cdot 300mm} = 8.9N/mm^2$$

$$03A4A = \frac{2 \cdot 436.7 \cdot 10^3 N}{\pi \cdot 150mm \cdot 300mm} = 6.2N/mm^2$$

$$03A4B = \frac{2 \cdot 676.5 \cdot 10^3 N}{\pi \cdot 150mm \cdot 300mm} = 9.6N/mm^2$$

$$06A4A = \frac{2 \cdot 450.0 \cdot 10^3 N}{\pi \cdot 150mm \cdot 300mm} = 6.4N/mm^2$$

$$06A4B = \frac{2 \cdot 684.9 \cdot 10^3 N}{\pi \cdot 150mm \cdot 300mm} = 9.7N/mm^2$$

$$07A4A = \frac{2 \cdot 716.9 \cdot 10^3 N}{\pi \cdot 150mm \cdot 300mm} = 10.1N/mm^2$$

$$07A4B = \frac{2 \cdot 758.1 \cdot 10^3 N}{\pi \cdot 150mm \cdot 300mm} = 10.7N/mm^2$$

$$10A4A = \frac{2 \cdot 964.5 \cdot 10^3 N}{\pi \cdot 150mm \cdot 300mm} = 13.6N/mm^2$$

$$10A4B = \frac{2 \cdot 677.0 \cdot 10^3 N}{\pi \cdot 150mm \cdot 300mm} = 9.6N/mm^2$$

$$11A4A = \frac{2 \cdot 1299.1 \cdot 10^3 N}{\pi \cdot 150mm \cdot 300mm} = 18.4N/mm^2$$

$$23A4A = \frac{2 \cdot 641.4 \cdot 10^3 N}{\pi \cdot 150mm \cdot 300mm} = 9.1N/mm^2$$

$$23A4B = \frac{2 \cdot 582.6 \cdot 10^3 N}{\pi \cdot 150mm \cdot 300mm} = 8.2N/mm^2$$

$$24A4A = \frac{2 \cdot 610.4 \cdot 10^3 N}{\pi \cdot 150mm \cdot 300mm} = 8.6N/mm^2$$

$$24A4B = \frac{2 \cdot 576.6 \cdot 10^3 N}{\pi \cdot 150mm \cdot 300mm} = 8.2N/mm^2$$

$$25A4A = \frac{2 \cdot 512.3 \cdot 10^3 N}{\pi \cdot 150mm \cdot 300mm} = 7.3N/mm^2$$

$$25A4B = \frac{2 \cdot 669.1 \cdot 10^3 N}{\pi \cdot 150mm \cdot 300mm} = 9.5N/mm^2$$

$$26A4A = \frac{2 \cdot 877.9 \cdot 10^3 N}{\pi \cdot 150mm \cdot 300mm} = 12.4N/mm^2$$

$$26A4B = \frac{2 \cdot 656.7 \cdot 10^3 N}{\pi \cdot 150mm \cdot 300mm} = 9.3N/mm^2$$

C: Calculations related to the modulus of elasticity

Table C1: Input values for testing modulus of elasticity (Method A).

Batch	$f_{ck.cube}$	f_{ck} $(0.86 \cdot f_{ck.cube})$	Upper stress $(\frac{f_{ck}}{3})$	Lower stress $(0.125 * f_{ck})$	Preload stress σ_p	Average Stabilized modulus of elasticity
1	132.2	113.7	37.9	14.2	2	44275
2	154.6	133.0	44.3	16.6	2	49322
3	151.2	130.0	43.3	16.3	2	49045
6	139.5	120.0	40.0	15.0	2	43644
7	147.7	127.0	42.4	15.9	2	42617
8	138.3	119.0	39.7	14.9	2	41871
9	124.4	107.0	35.7	13.4	2	35106
10	151.4	130.2	43.4	16.3	2	48838
11	155.5	133.7	44.6	16.7	2	49254
23	155.4	133.6	44.5	16.7	2	47737
24	141.6	121.8	40.6	15.2	2	45398
25	145.9	125.5	41.8	15.7	2	46796
26	153.2	131.8	43.9	16.5	2	46626

D: Calculations of flexural strength

$$23A5A = \frac{33.0 \cdot 10^3 N \cdot 460mm}{100mm \cdot (100mm)^2} = 15.2N/mm^2$$

$$23A5B = \frac{31.8 \cdot 10^3 N \cdot 460mm}{100mm \cdot (100mm)^2} = 14.6N/mm^2$$

$$23A5C = \frac{29.1 \cdot 10^3 N \cdot 460mm}{100mm \cdot (100mm)^2} = 13.4N/mm^2$$

$$24A5A = \frac{36.7 \cdot 10^3 N \cdot 460mm}{100mm \cdot (100mm)^2} = 16.9N/mm^2$$

$$24A5B = \frac{42.8 \cdot 10^3 N \cdot 460mm}{100mm \cdot (100mm)^2} = 19.7N/mm^2$$

$$24A5C = \frac{35.0 \cdot 10^3 N \cdot 460mm}{100mm \cdot (100mm)^2} = 16.1N/mm^2$$

$$25A5A = \frac{31.1 \cdot 10^3 N \cdot 460mm}{100mm \cdot (100mm)^2} = 14.3N/mm^2$$

$$25A5B = \frac{33.4 \cdot 10^3 N \cdot 460mm}{100mm \cdot (100mm)^2} = 15.4N/mm^2$$

$$25A5C = \frac{27.6 \cdot 10^3 N \cdot 460mm}{100mm \cdot (100mm)^2} = 12.7N/mm^2$$

$$26A5A = \frac{45.8 \cdot 10^3 N \cdot 460mm}{100mm \cdot (100mm)^2} = 21.1N/mm^2$$

$$26A5B = \frac{38.7 \cdot 10^3 N \cdot 460mm}{100mm \cdot (100mm)^2} = 17.8N/mm^2$$

E: Weights from PF-method

Table E1: PF-Method weights.

Spcm.	**Dried weight** (m_1)	**Capillary suction**											**Submerged 72h**		**Pressure (50atm) (24h)**
		10m	**30m**	**1h**	**2h**	**3h**	**4h**	**6h**	**24h**	**48h**	**72h**	**96h** (m_4)	**Weight air** (m_2)	**Volume** (cm^2)	**air weight** (m_3)
23B6A	468.6	469.3	469.6	469.9	470.2	470.5	470.7	471.0	471.9	472.5	472.9	473.2	476.9	199	478.5
23B6B	488.7	489.4	489.8	490.1	490.5	490.7	490.9	491.2	492.2	492.7	493.1	493.3	497.0	208	498.4
23B6C	492.8	493.6	493.9	494.2	494.7	494.9	495.2	495.6	496.6	497.1	497.5	497.8	501.2	210	-
23B6D	491.0	491.8	492.2	492.5	492.9	493.1	493.4	493.7	494.7	495.2	495.5	495.7	498.9	209	-
24B6A	488.2	489.0	489.2	489.6	489.9	490.1	490.3	490.6	491.5	491.9	492.2	492.5	495.1	209	496.3
24B6B	487.7	488.5	488.8	489.2	489.5	489.7	490.0	490.3	491.1	491.7	491.9	492.2	494.8	208	495.2
24B6C	464.5	465.2	465.5	465.7	465.9	466.1	466.4	466.6	467.4	467.8	468.1	468.5	471.1	198	-
24B6D	490.7	491.4	491.7	491.9	492.3	492.4	492.6	493.0	493.9	494.4	494.6	494.9	497.5	209	-
25B6A	501.7	502.5	502.9	503.2	503.6	503.8	504.0	504.3	505.4	505.8	506.2	506.5	508.9	214	509.5
25B6B	488.3	489.1	489.4	489.7	490.0	490.2	490.4	490.7	491.6	492.1	492.5	492.8	495.4	205	495.7
25B6C	472.9	473.7	473.9	474.3	474.7	474.8	475.0	475.2	476.1	476.6	476.9	477.2	479.2	201	-
25B6D	472.8	473.6	473.9	474.2	474.6	474.8	475.1	475.4	476.3	476.8	477.2	477.5	479.5	202	-
26B6A	491.2	492.0	492.2	492.4	492.7	492.9	493.0	493.2	494.1	494.6	495.0	495.3	497.4	206	499.1
26B6B	517.8	518.6	518.8	519.0	519.2	519.4	519.5	519.8	520.6	521.1	521.4	521.7	524.1	218	524.7
26B6C	503.2	503.9	504.2	504.5	504.9	505.0	505.2	505.4	506.3	506.8	507.1	507.4	509.8	213	-
26B6D	480.1	480.9	481.0	481.3	481.5	481.7	481.8	482.0	482.9	483.2	483.5	483.8	486.3	204	-

F: Capillary absorptions in tabular form for batch 23-26

Table F1: Capillary absorption (kg/m^2) for batch 23.

$\sqrt{time(s)}$	23B6A		23B6B		23B6C		23B6D		Average absorption (kg/m^2)
	Weight (g)	Absorbed (kg/m^2)	Weight (g)	Absorbed (kg/m^2)	Weight (g)	Absorbed (kg/m^2)	Weight (g)	Absorbed (kg/m^2)	
0	468.6	0	488.7	0	492.8	0	491.0	0	0
25	469.3	0.07	489.4	0.07	493.6	0.08	491.8	0.08	0.08
42	469.6	0.10	489.8	0.11	493.9	0.11	492.2	0.12	0.11
60	469.9	0.13	490.1	0.14	494.2	0.14	492.5	0.15	0.14
85	470.2	0.16	490.5	0.18	494.7	0.19	492.9	0.19	0.18
104	470.5	0.19	490.7	0.20	494.9	0.21	493.1	0.21	0.20
120	470.7	0.21	490.9	0.22	495.2	0.24	493.4	0.24	0.23
147	471.0	0.24	491.2	0.25	495.6	0.28	493.7	0.27	0.26
294	471.9	0.33	492.2	0.35	496.6	0.38	494.7	0.37	0.36
416	472.5	0.39	492.7	0.40	497.1	0.43	495.2	0.42	0.41
509	472.9	0.43	493.1	0.44	497.5	0.47	495.5	0.45	0.45
588	473.2	0.46	493.3	0.46	497.8	0.50	495.7	0.47	0.47

Table F2: Capillary absorption (kg/m^2) for batch 24.

$\sqrt{time(s)}$	24B6A		24B6B		24B6C		24B6D		Average absorption (kg/m^2)
	Weight (g)	Absorbed (kg/m^2)	Weight (g)	Absorbed (kg/m^2)	Weight (g)	Absorbed (kg/m^2)	Weight (g)	Absorbed (kg/m^2)	
0	488.2	0	487.7	0	464.5	0	490.7	0	0
25	489.0	0.08	488.5	0.08	465.2	0.07	491.4	0.07	0.08
42	489.2	0.10	488.8	0.11	465.5	0.10	491.7	0.10	0.10
60	489.6	0.14	489.2	0.15	465.7	0.12	491.9	0.12	0.13
85	489.9	0.17	489.5	0.18	465.9	0.14	492.3	0.16	0.16
104	490.1	0.19	489.7	0.20	466.1	0.16	492.4	0.17	0.18
120	490.3	0.21	490.0	0.23	466.4	0.19	492.6	0.19	0.21
147	490.6	0.24	490.3	0.26	466.6	0.21	493.0	0.23	0.24
294	491.5	0.33	491.1	0.34	467.4	0.29	493.9	0.32	0.32
416	491.9	0.37	491.7	0.40	467.8	0.33	494.4	0.37	0.37
509	492.2	0.40	491.9	0.42	468.1	0.36	494.6	0.39	0.39
588	492.5	0.43	492.2	0.45	468.5	0.40	494.9	0.42	0.43

Table F3: Capillary absorption (kg/m^2) for batch 25.

$\sqrt{time(s)}$	**25B6A**		**25B6B**		**25B6C**		**25B6D**		**Average**
	Weight (g)	**Absorbed** (kg/m^2)	**Weight** (g)	**Absorbed** (kg/m^2)	**Weight** (g)	**Absorbed** (kg/m^2)	**Weight** (g)	**Absorbed** (kg/m^2)	**absorption** (kg/m^2)
0	501.7	0	488.3	0	472.9	0	472.8	0	0
25	502.5	0.08	489.1	0.08	473.7	0.08	473.6	0.08	0.08
42	502.9	0.12	489.4	0.11	473.9	0.10	473.9	0.11	0.11
60	503.2	0.15	489.7	0.14	474.3	0.14	474.2	0.14	0.14
85	503.6	0.19	490.0	0.17	474.7	0.18	474.6	0.18	0.18
104	503.8	0.21	490.2	0.19	474.8	0.19	474.8	0.20	0.20
120	504.0	0.23	490.4	0.21	475.0	0.21	475.1	0.23	0.22
147	504.3	0.26	490.7	0.24	475.2	0.23	475.4	0.26	0.25
294	505.4	0.37	491.6	0.33	476.1	0.32	476.3	0.35	0.34
416	505.8	0.41	492.1	0.38	476.6	0.37	476.8	0.40	0.39
509	506.2	0.45	492.5	0.42	476.9	0.40	477.2	0.44	0.43
588	506.5	0.48	492.8	0.45	477.2	0.43	477.5	0.47	0.46

Table F4: Capillary absorption (kg/m^2) for batch 26.

$\sqrt{time(s)}$	**26B6A**		**26B6B**		**26B6C**		**26B6D**		**Average**
	Weight (g)	**Absorbed** (kg/m^2)	**Weight** (g)	**Absorbed** (kg/m^2)	**Weight** (g)	**Absorbed** (kg/m^2)	**Weight** (g)	**Absorbed** (kg/m^2)	**absorption** (kg/m^2)
0	491.2	0	517.8	0	503.2	0	480.1	0	0
25	492.0	0.08	518.6	0.08	503.9	0.07	480.9	0.08	0.08
42	492.2	0.10	518.8	0.10	504.2	0.10	481.0	0.09	0.10
60	492.4	0.12	519.0	0.12	504.5	0.13	481.3	0.12	0.12
85	492.7	0.15	519.2	0.14	504.9	0.17	481.5	0.14	0.15
104	492.9	0.17	519.4	0.16	505.0	0.18	481.7	0.16	0.17
120	493.0	0.18	519.5	0.17	505.2	0.20	481.8	0.17	0.18
147	493.2	0.20	519.8	0.20	505.4	0.22	482.0	0.19	0.20
294	494.1	0.29	520.6	0.28	506.3	0.31	482.9	0.28	0.29
416	494.6	0.34	521.1	0.33	506.8	0.36	483.2	0.31	0.34
509	495.0	0.38	521.4	0.36	507.1	0.39	483.5	0.34	0.37
588	495.3	0.41	521.7	0.39	507.4	0.42	483.8	0.37	0.40

G: Miniature slump flow images

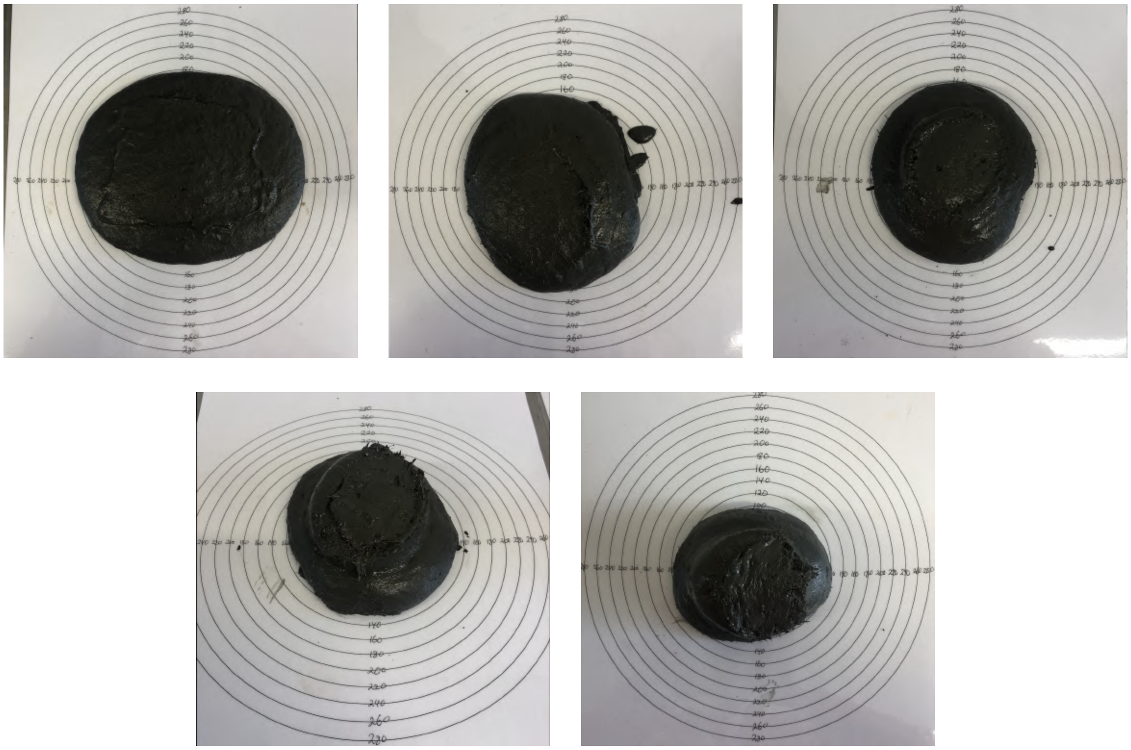

Figure G1: Miniature slump flow for batch 1 (0, 5, 10, 15, and 30 minutes from top left)

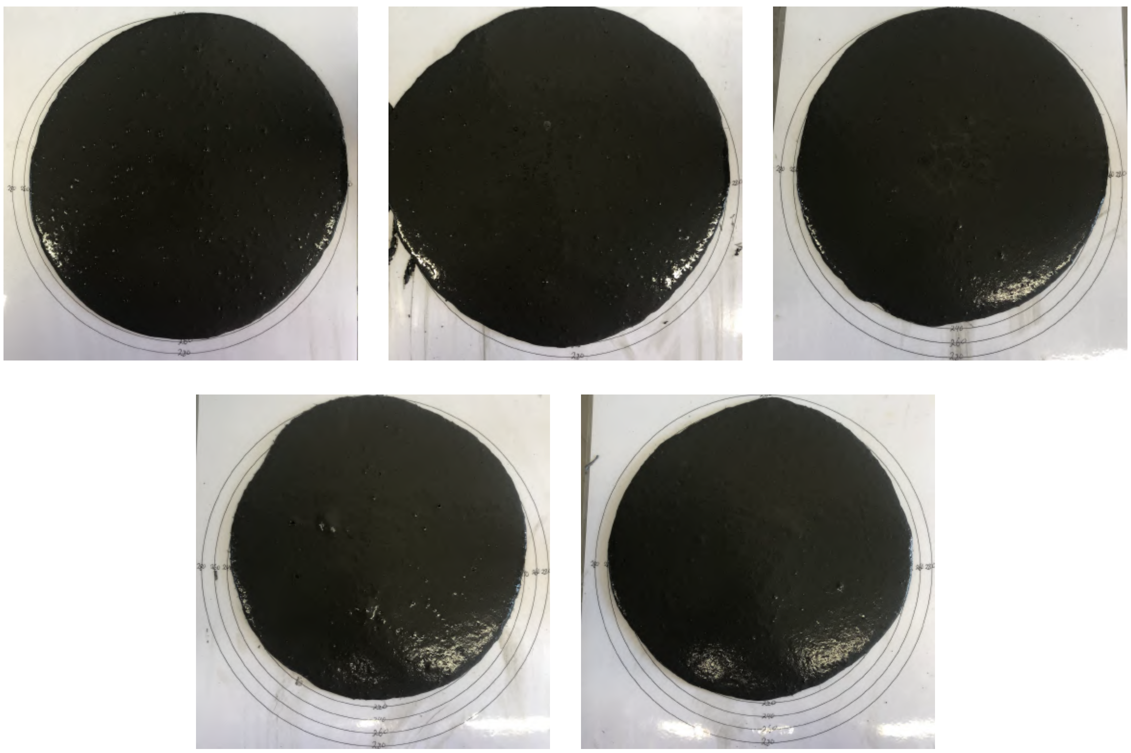

Figure G2: Miniature slump flow for batch 2 (0, 5, 10, 15, and 30 minutes from top left)

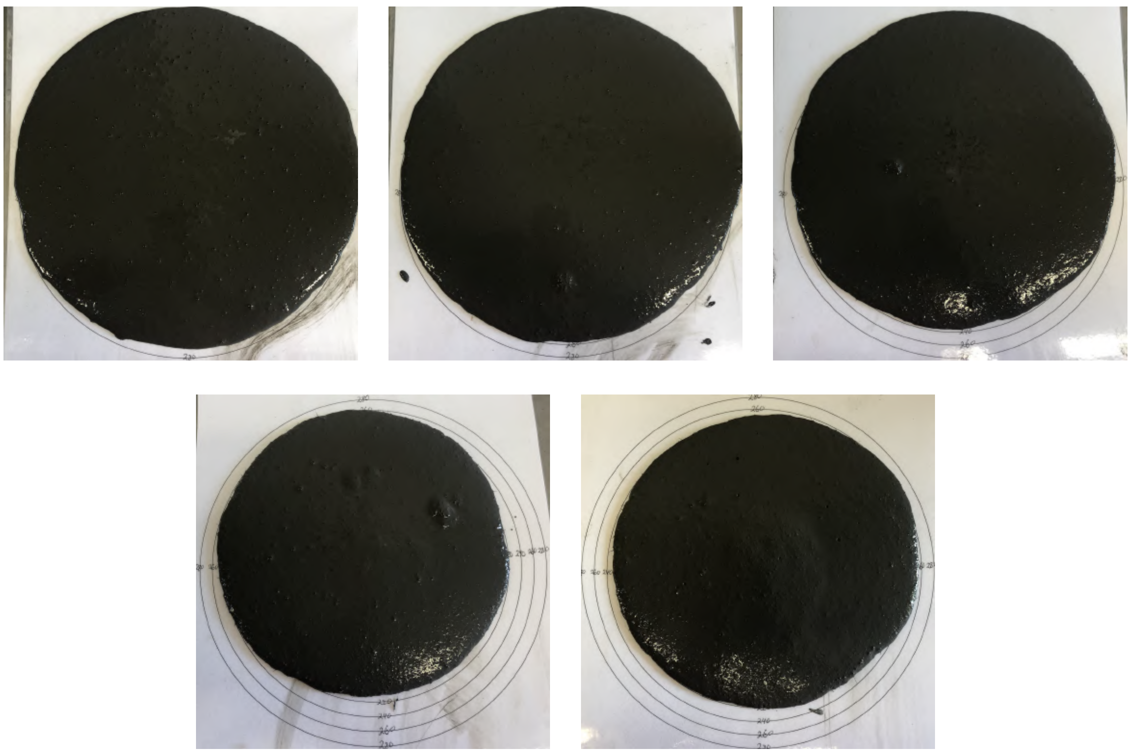

Figure G3: Miniature slump flow for batch 3 (0, 5, 10, 15, and 30 minutes from top left)

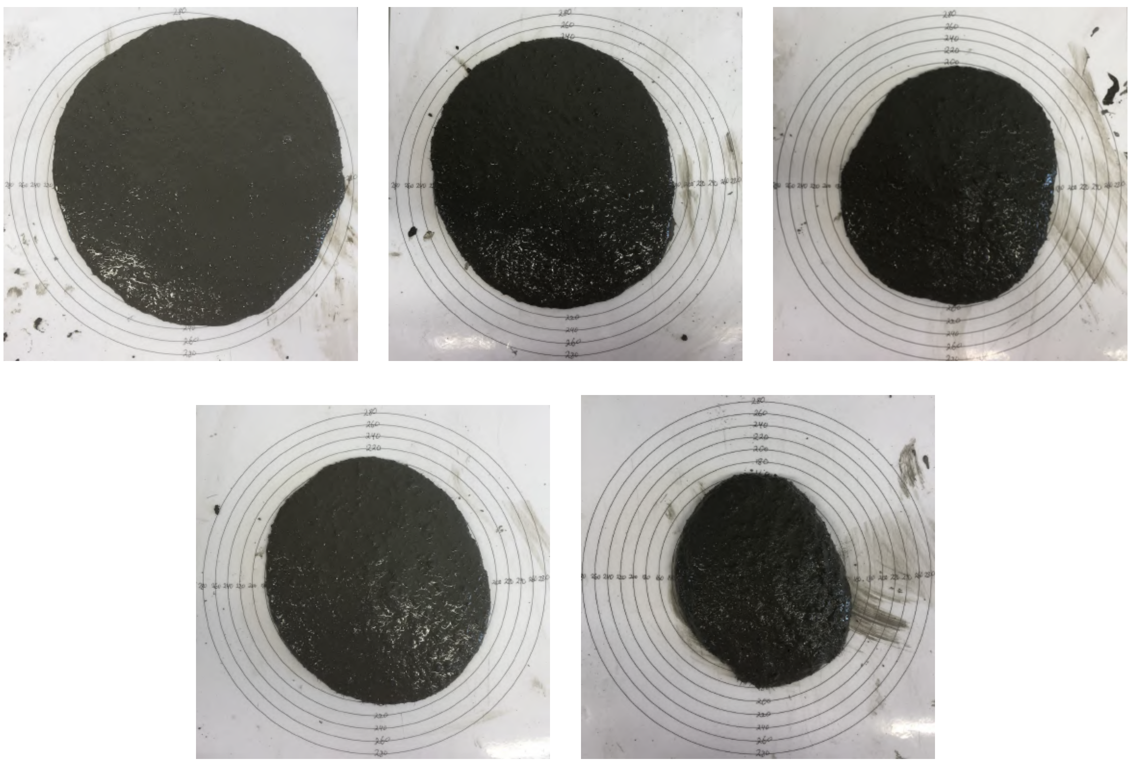

Figure G4: Miniature slump flow for batch 4 (0, 5, 10, 15, and 30 minutes from top left)

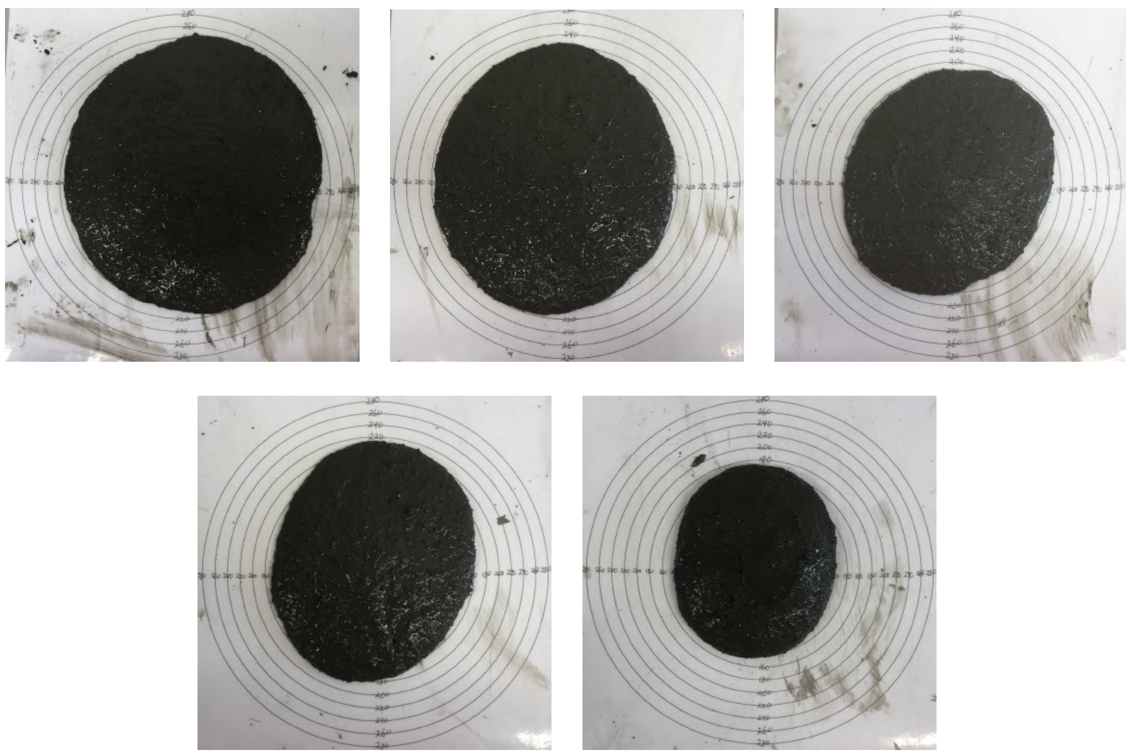

Figure G5: Miniature slump flow for batch 5 (0, 5, 10, 15, and 30 minutes from top left)

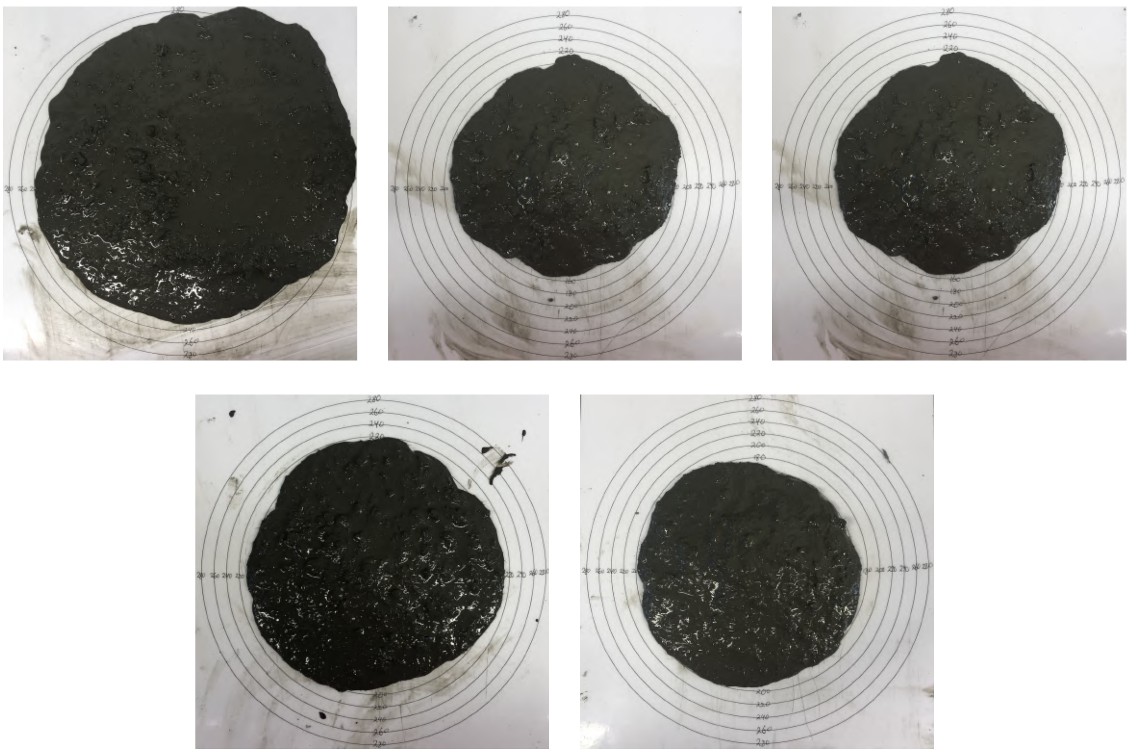

Figure G6: Miniature slump flow for batch 6 (0, 5, 10, 15, and 30 minutes from top left)

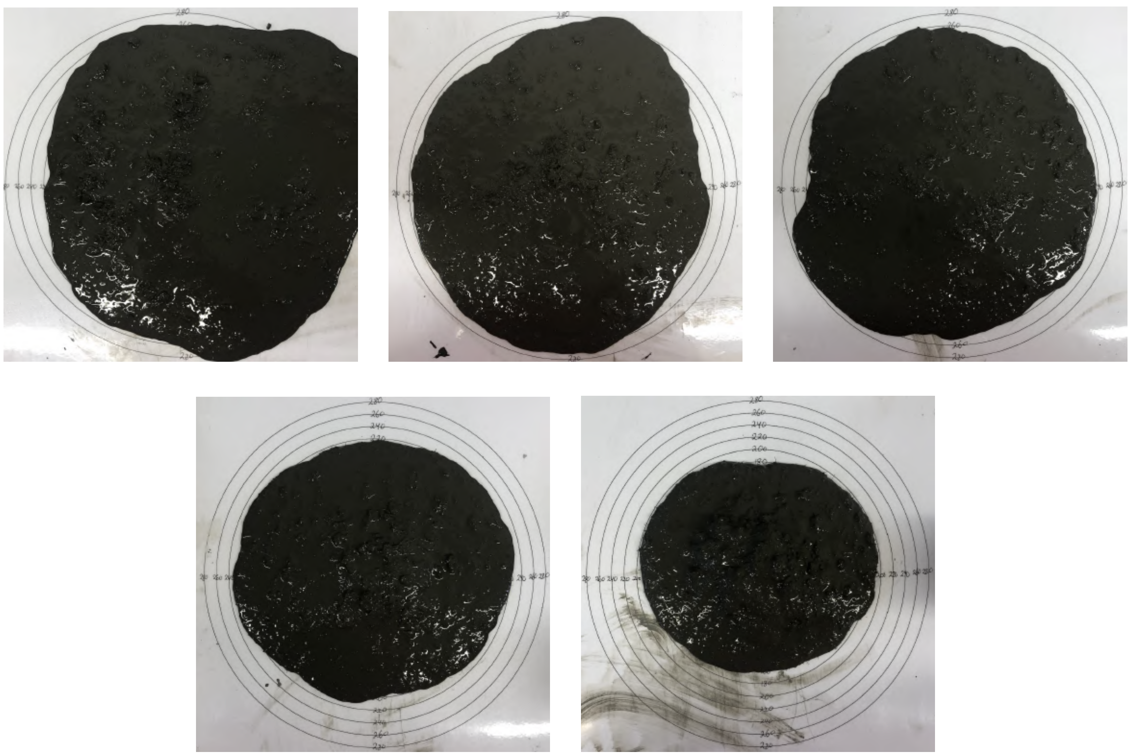

Figure G7: Miniature slump flow for batch 7 (0, 5, 10, 15, and 30 minutes from top left)

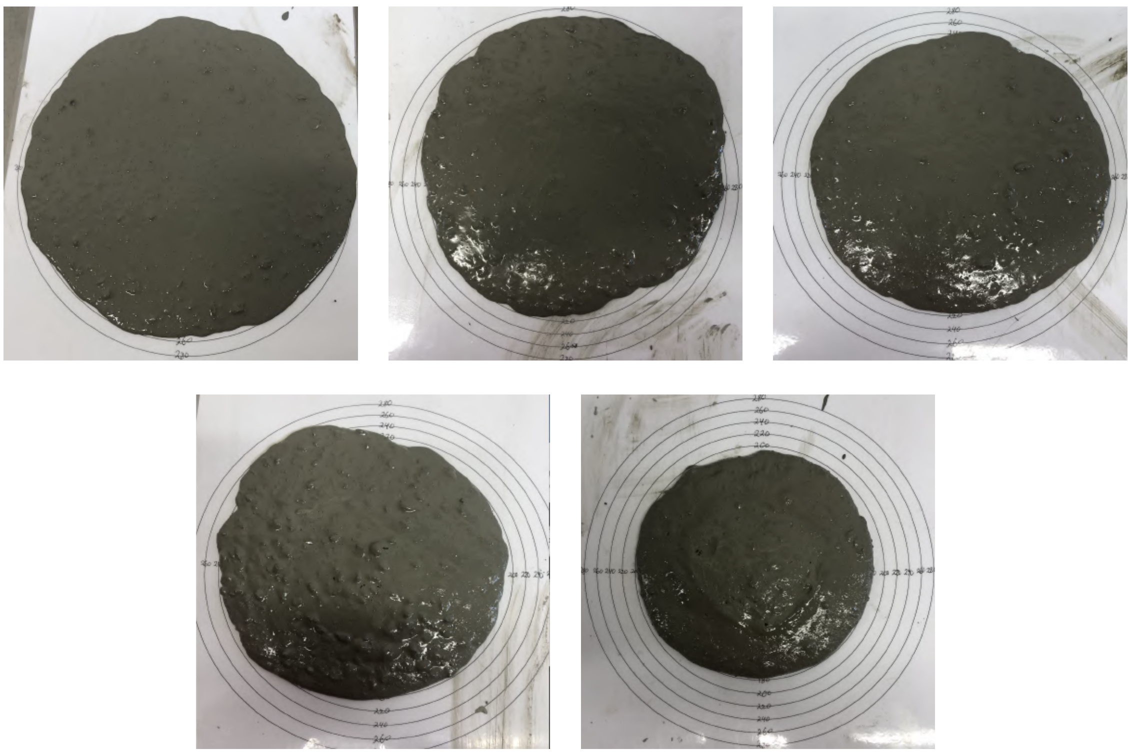

Figure G8: Miniature slump flow for batch 8 (0, 5, 10, 15, and 30 minutes from top left)

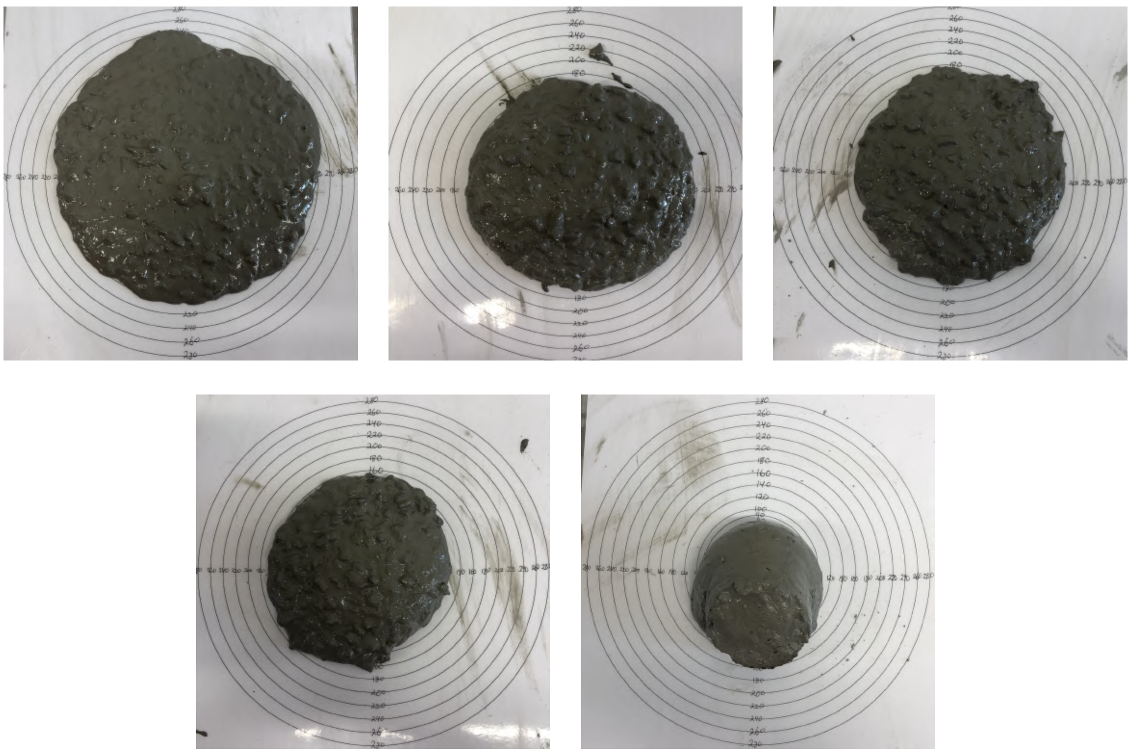

Figure G9: Miniature slump flow for batch 9 (0, 5, 10, 15, and 30 minutes from top left)

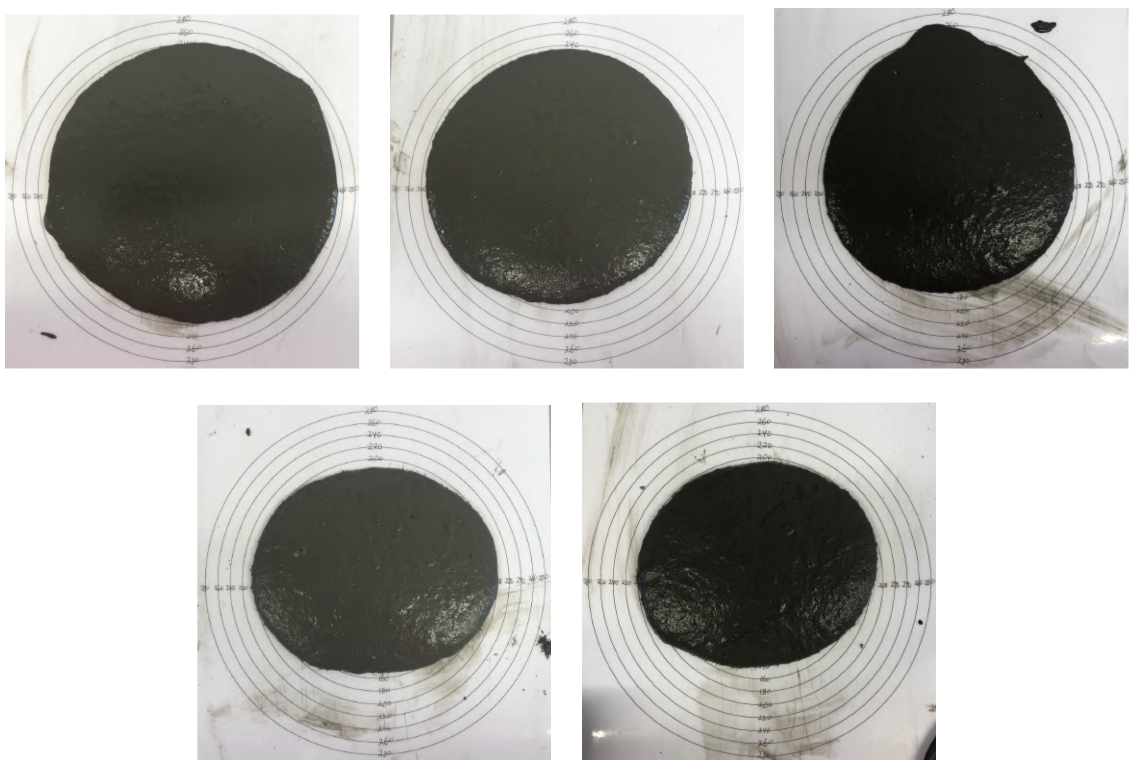

Figure G10: Miniature slump flow for batch 10 (0, 5, 10, 15, and 30 minutes from top left)

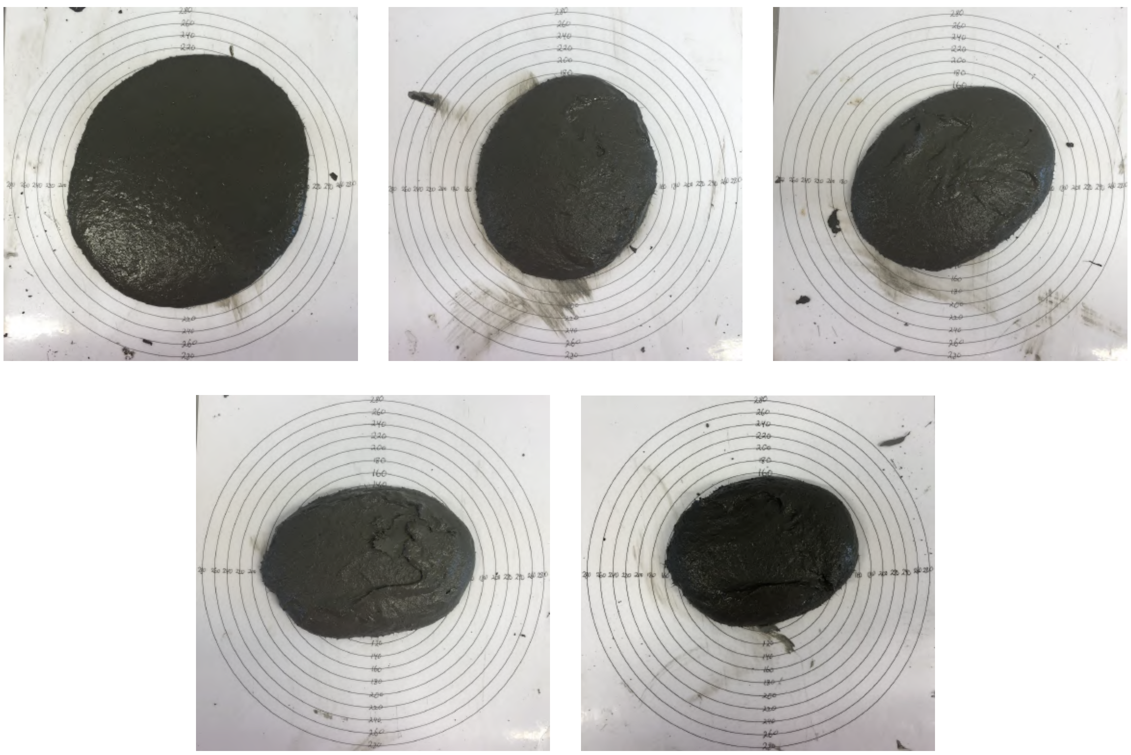

Figure G11: Miniature slump flow for batch 11 (0, 5, 10, 15, and 30 minutes from top left)

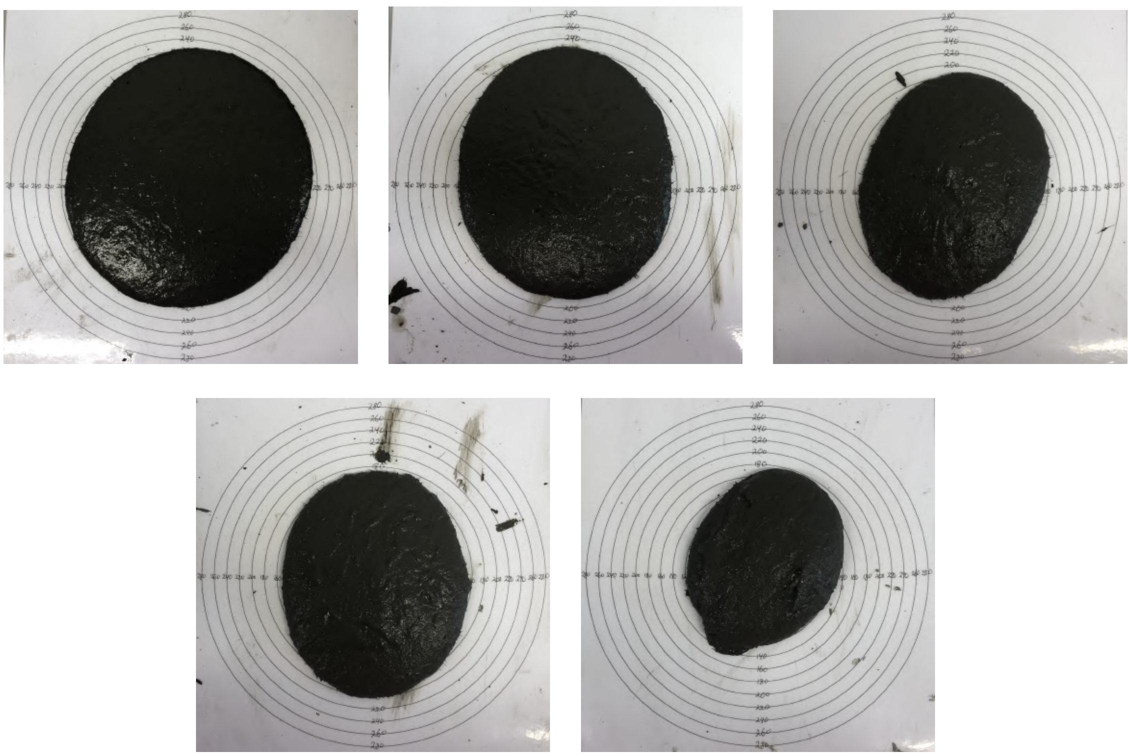

Figure G12: Miniature slump flow for batch 12 (0, 5, 10, 15, and 30 minutes from top left)

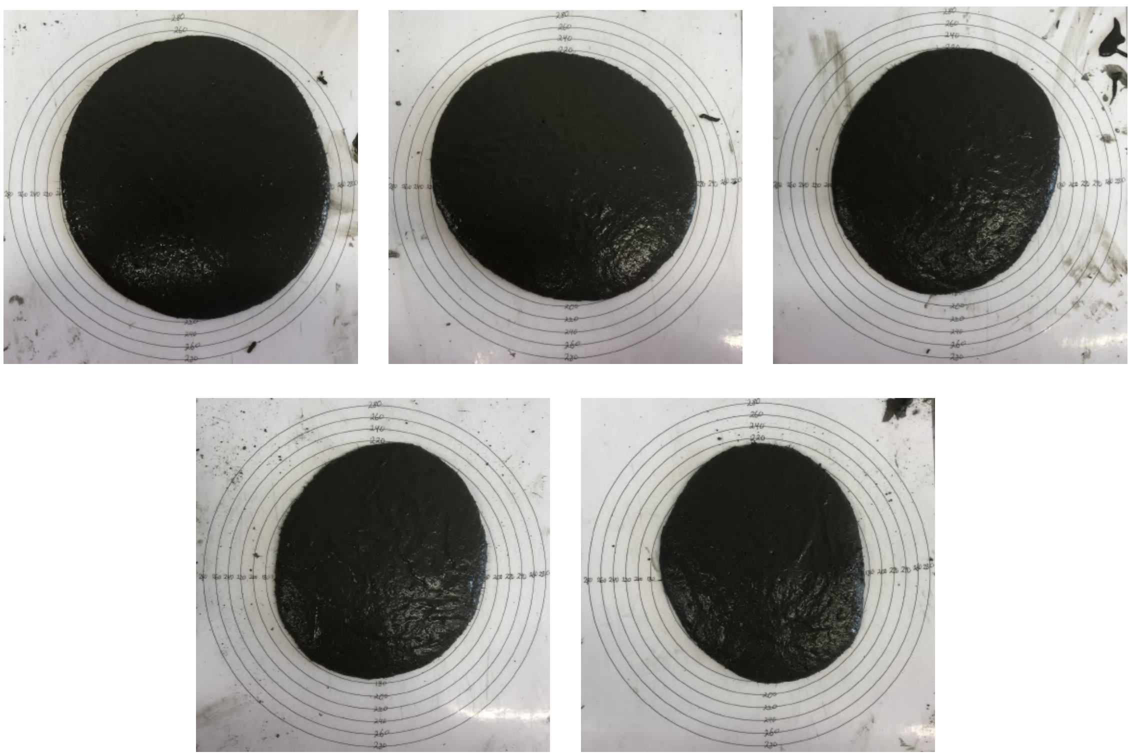

Figure G13: Miniature slump flow for batch 13 (0, 5, 10, 15, and 30 minutes from top left)

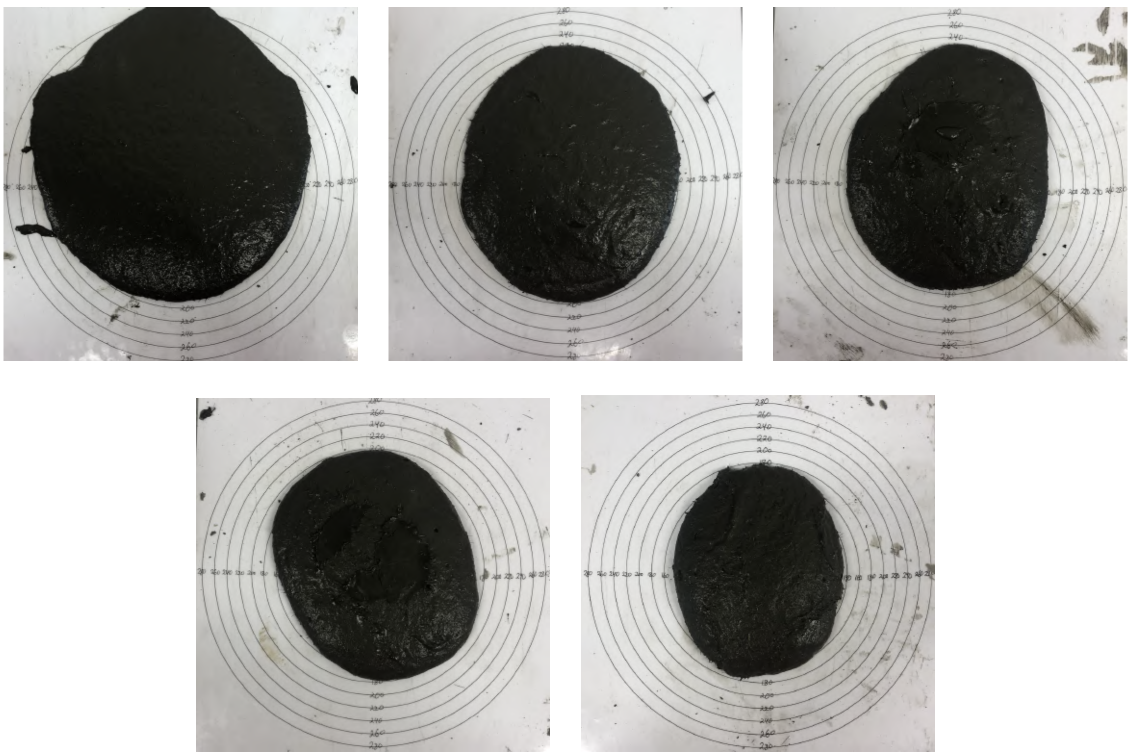

Figure G14: Miniature slump flow for batch 14 (0, 5, 10, 15, and 30 minutes from top left)

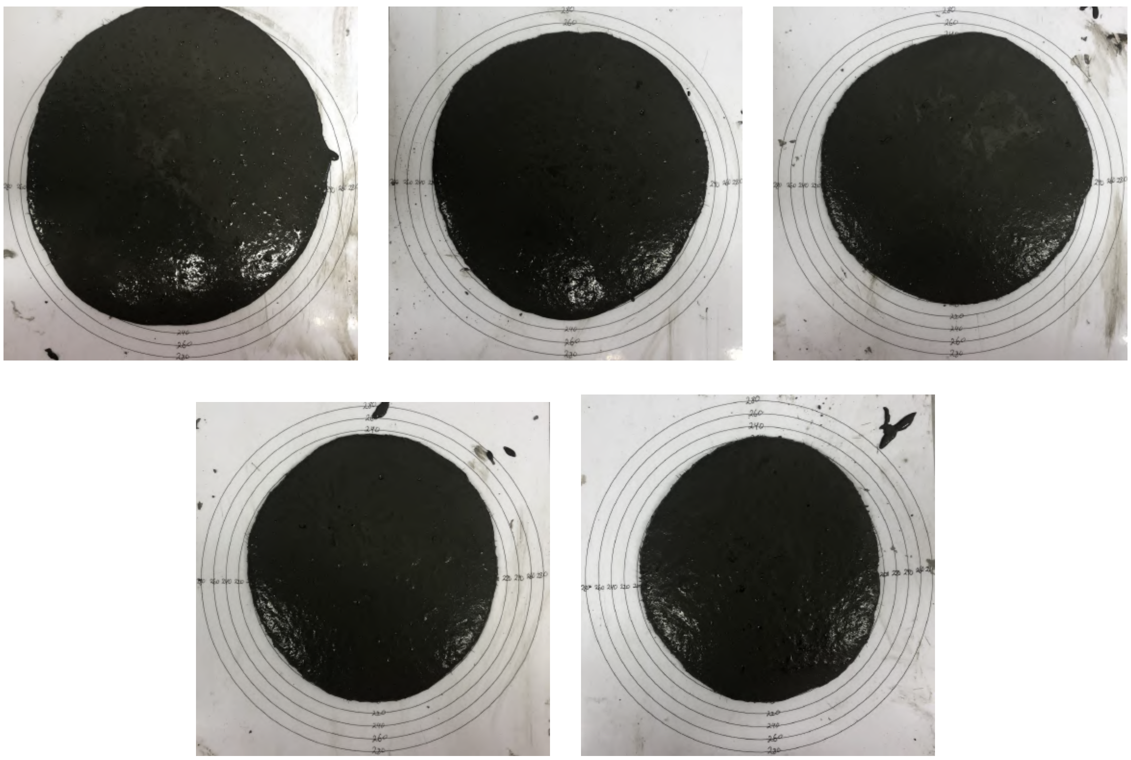

Figure G15: Miniature slump flow for batch 15 (0, 5, 10, 15, and 30 minutes from top left)

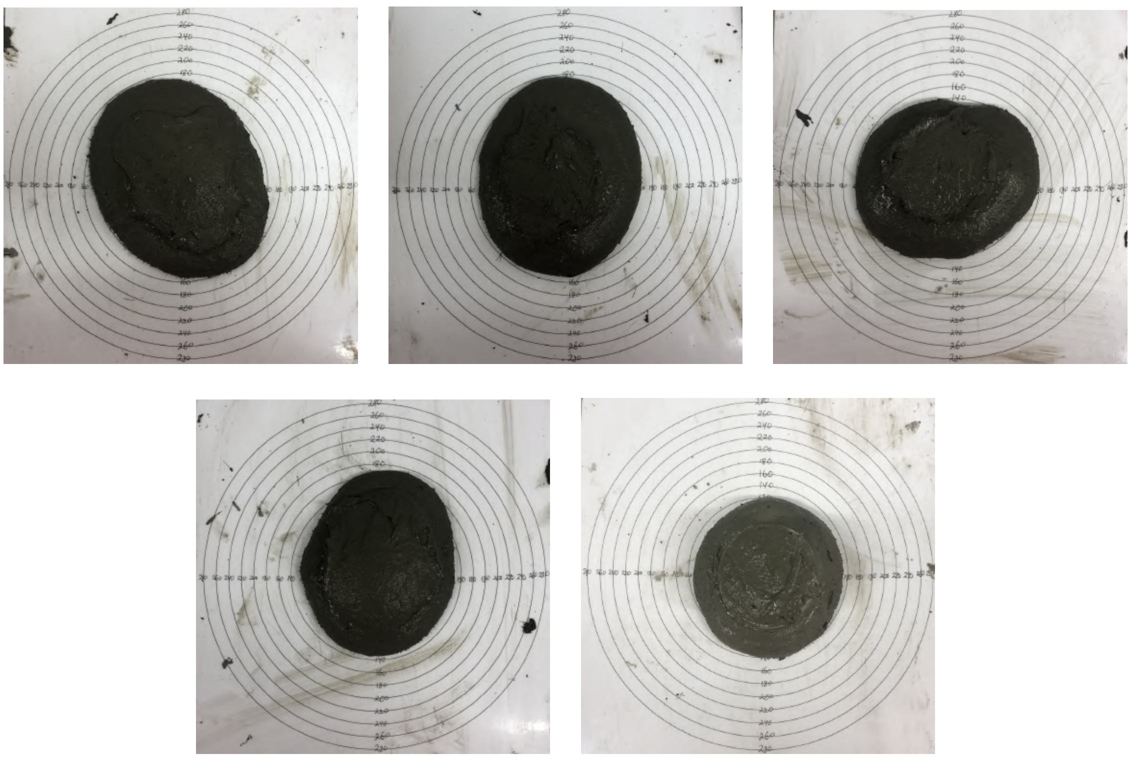

Figure G16: Miniature slump flow for batch 16 (0, 5, 10, 15, and 30 minutes from top left)

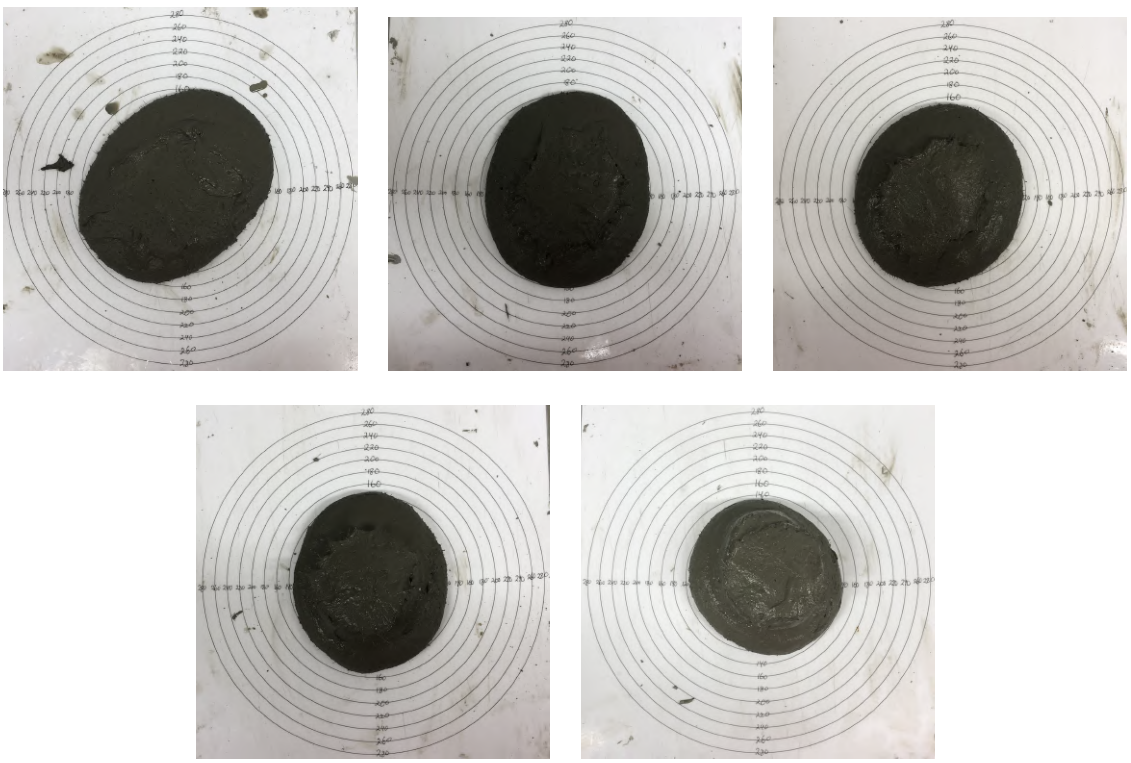

Figure G17: Miniature slump flow for batch 17 (0, 5, 10, 15, and 30 minutes from top left)

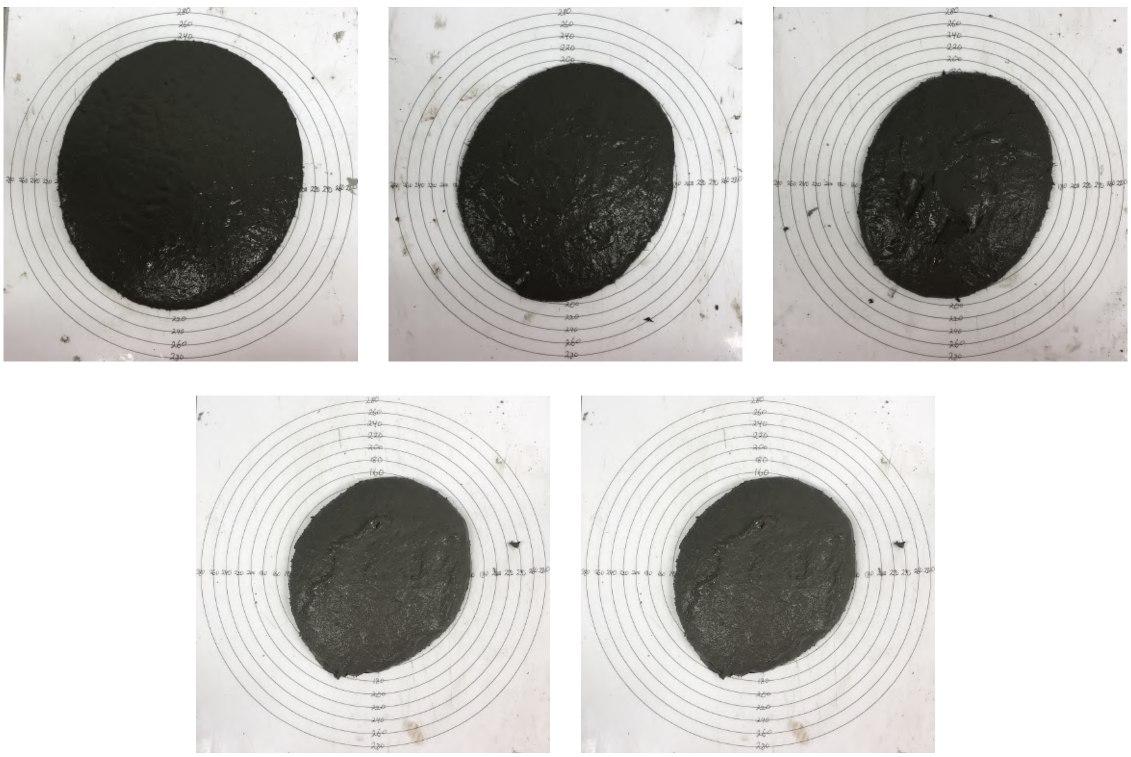

Figure G18: Miniature slump flow for batch 18 (0, 5, 10, 15, and 30 minutes from top left)

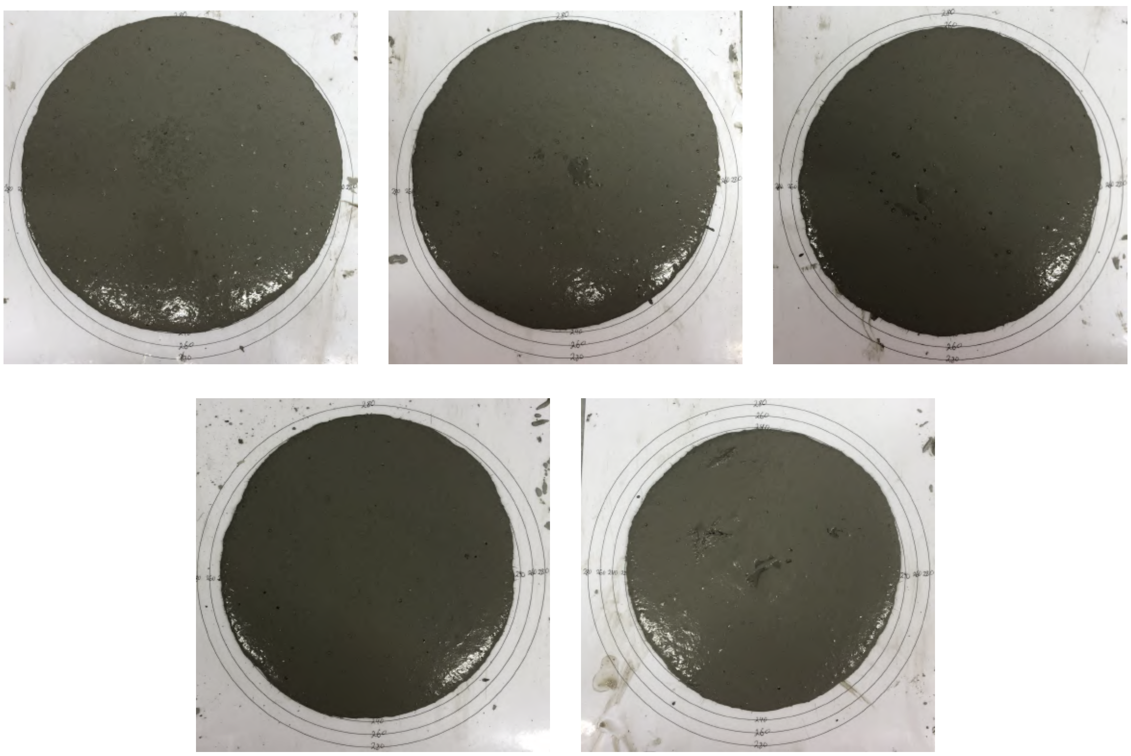

Figure G19: Miniature slump flow for batch 19 (0, 5, 10, 15, and 30 minutes from top left)

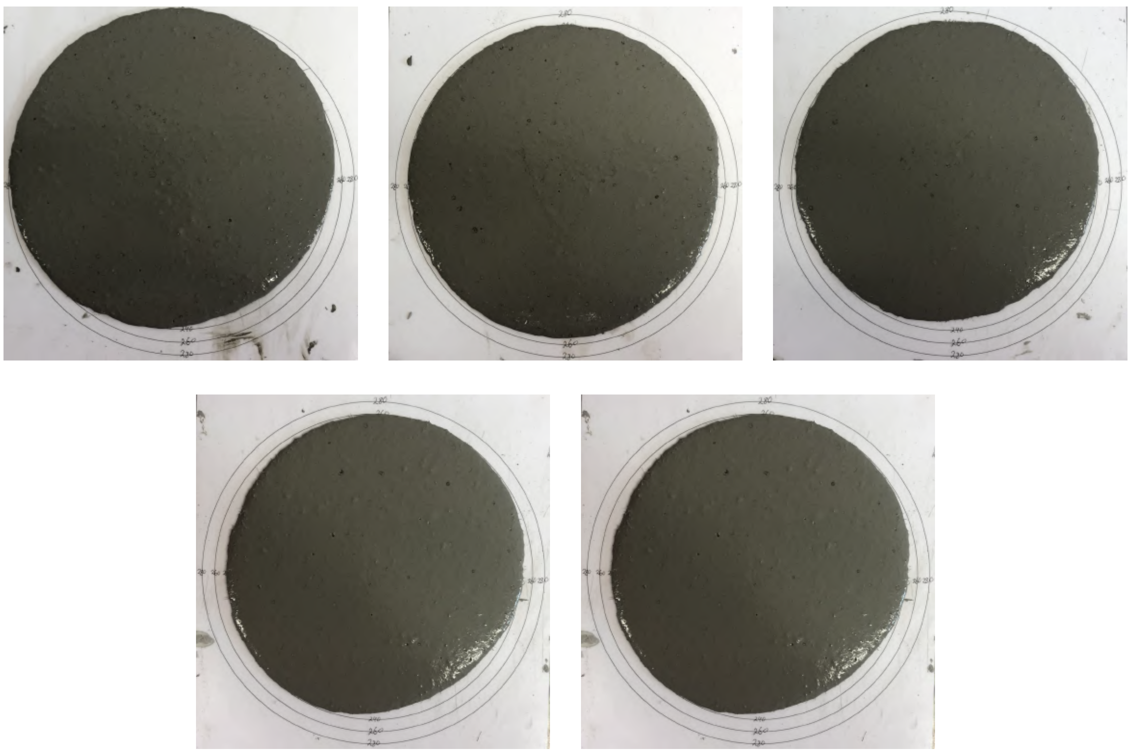

Figure G20: Miniature slump flow for batch 20 (0, 5, 10, 15, and 30 minutes from top left)

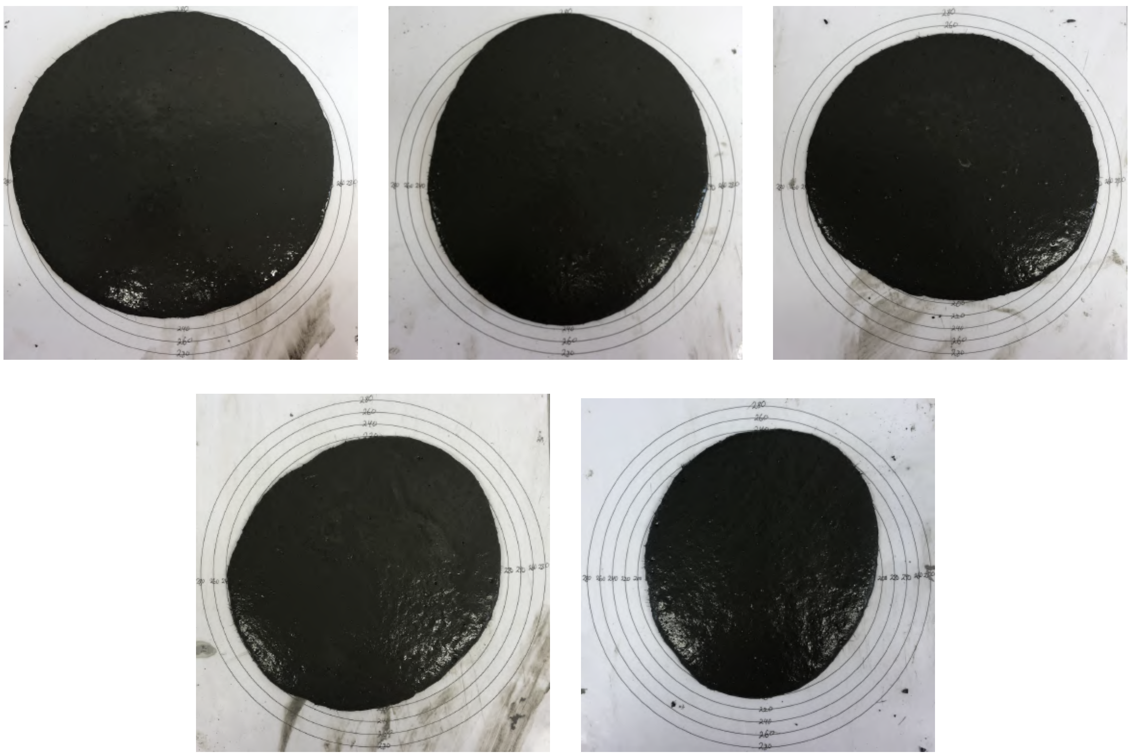

Figure G21: Miniature slump flow for batch 21 (0, 5, 10, 15, and 30 minutes from top left)

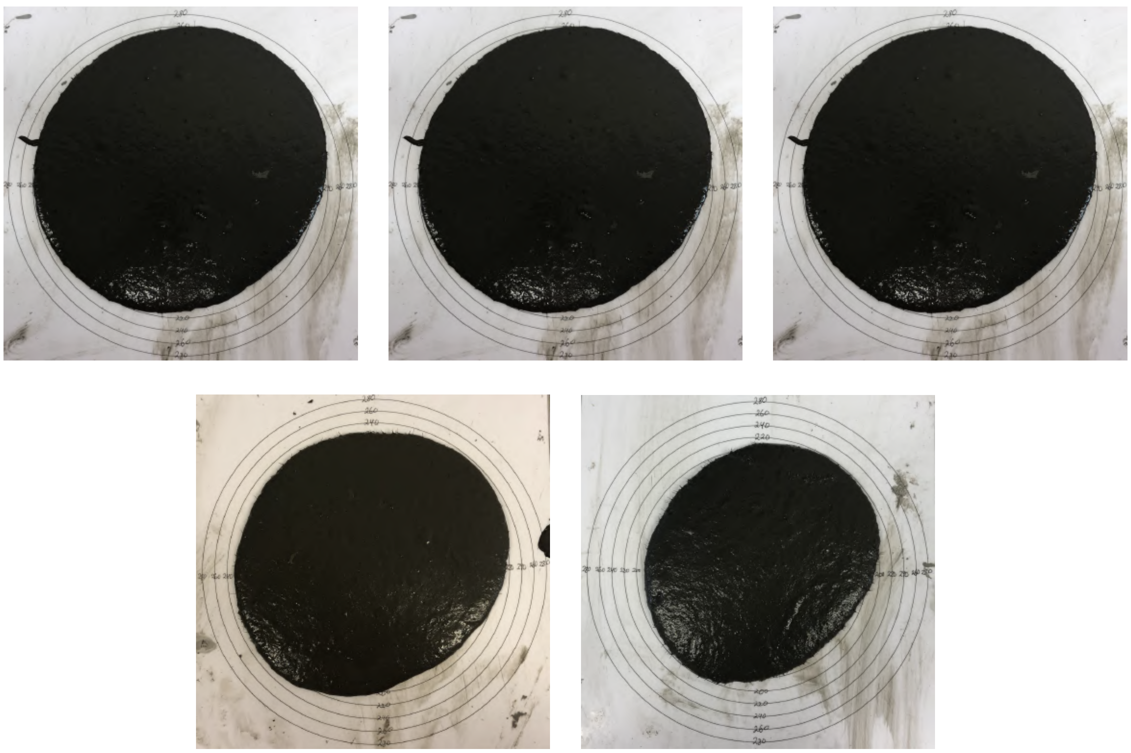

Figure G22: Miniature slump flow for batch 22 (0, 5, 10, 15, and 30 minutes from top left)

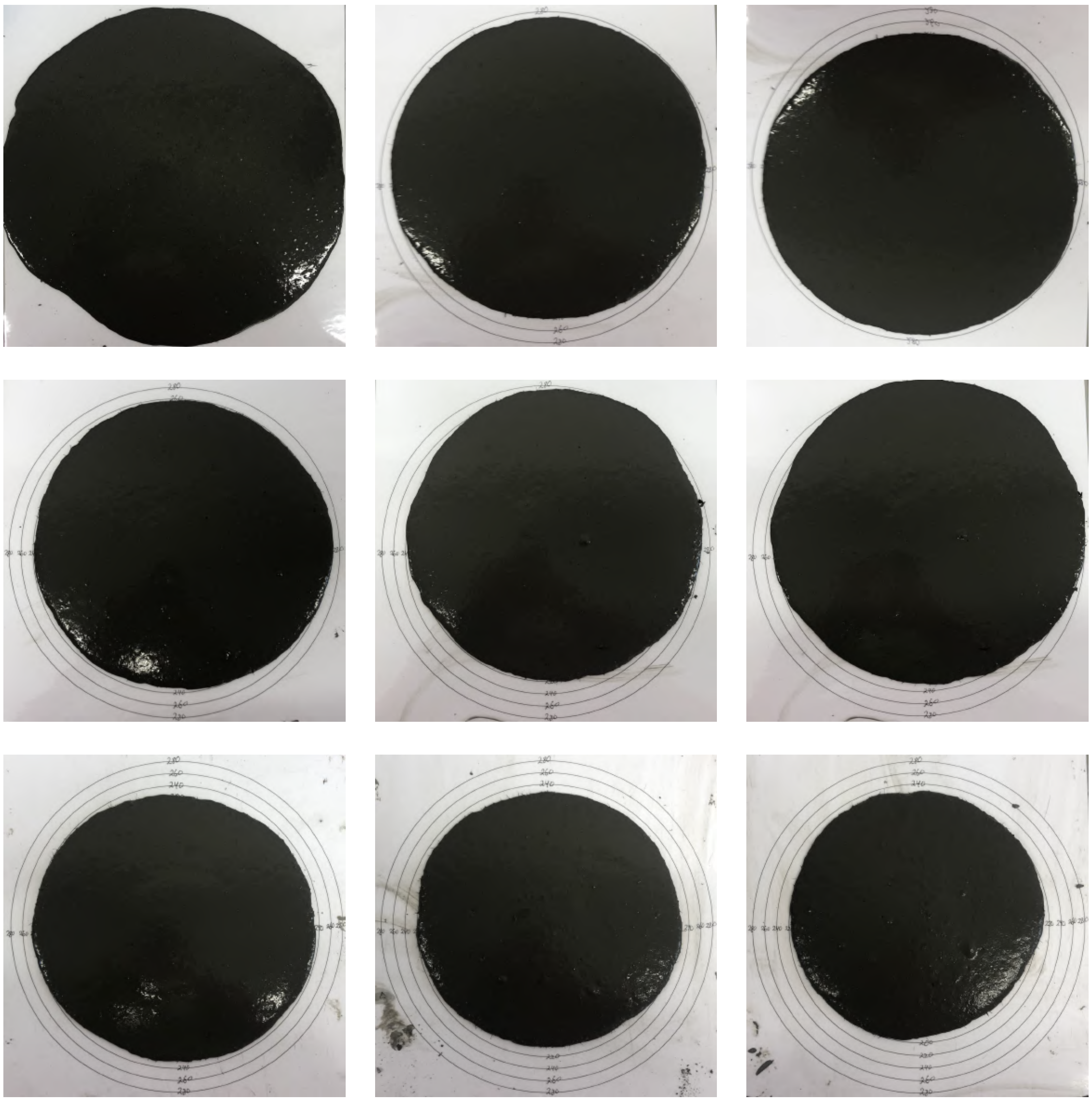

Figure G23: Miniature slump flow for batch 23 (0, 5, 10, 15, 20, 30, 40, 50, and 60 min from top left)

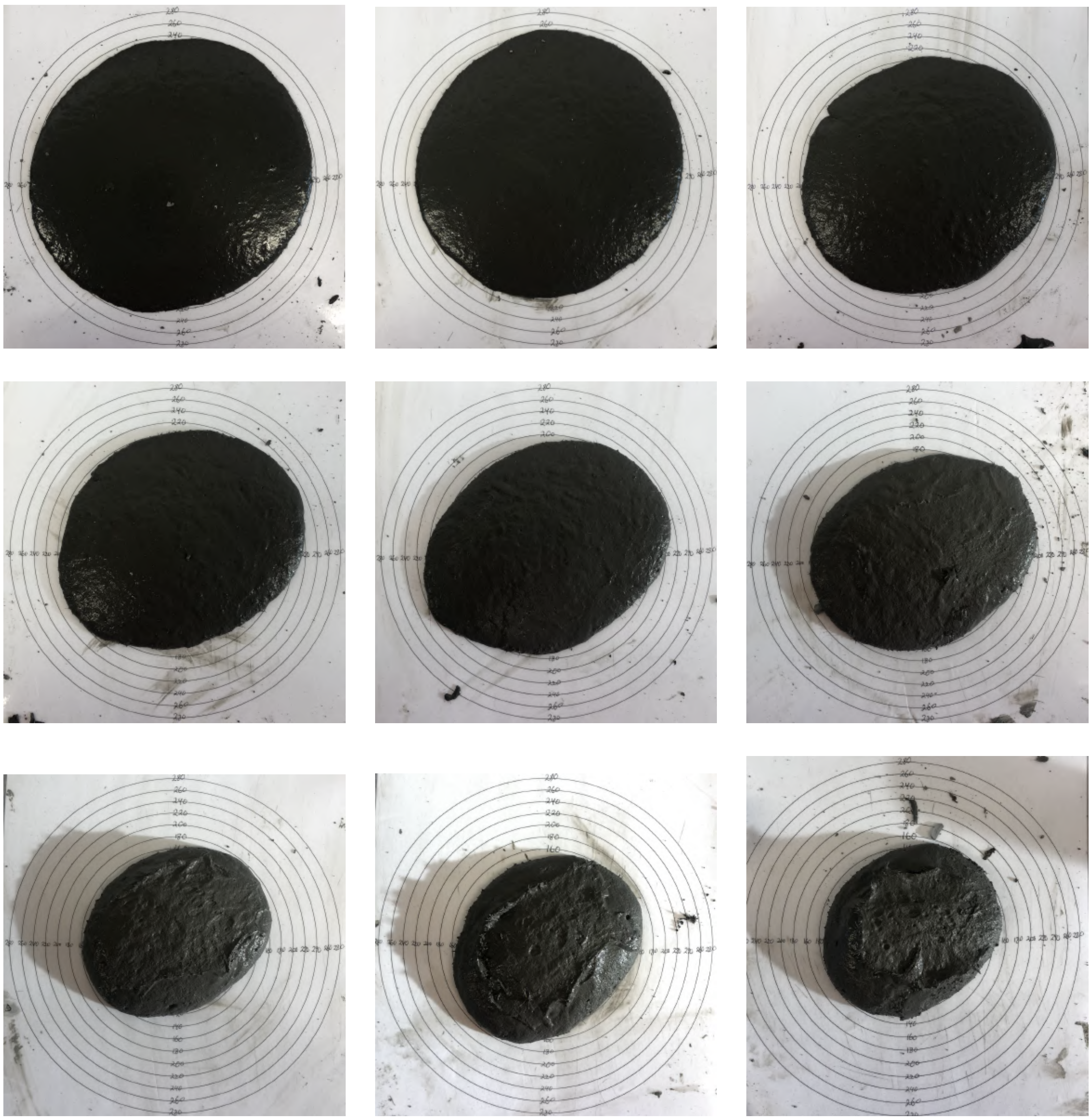

Figure G24: Miniature slump flow for batch 24 (0, 5, 10, 15, 20, 30, 40, 50, and 60 min from top left)

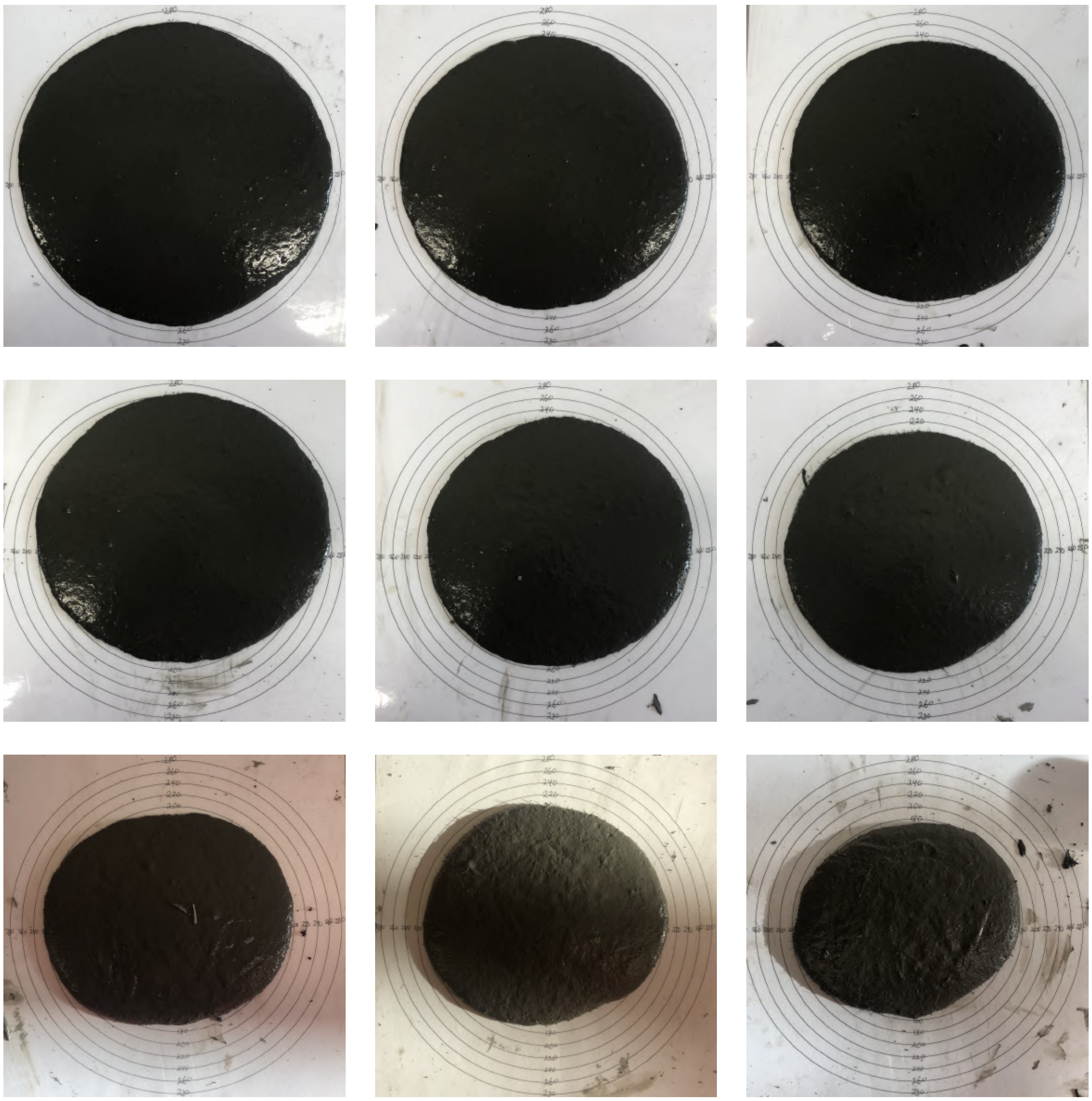

Figure G25: Miniature slump flow for batch 25 (0, 5, 10, 15, 20, 30, 40, 50, and 60 min from top left)

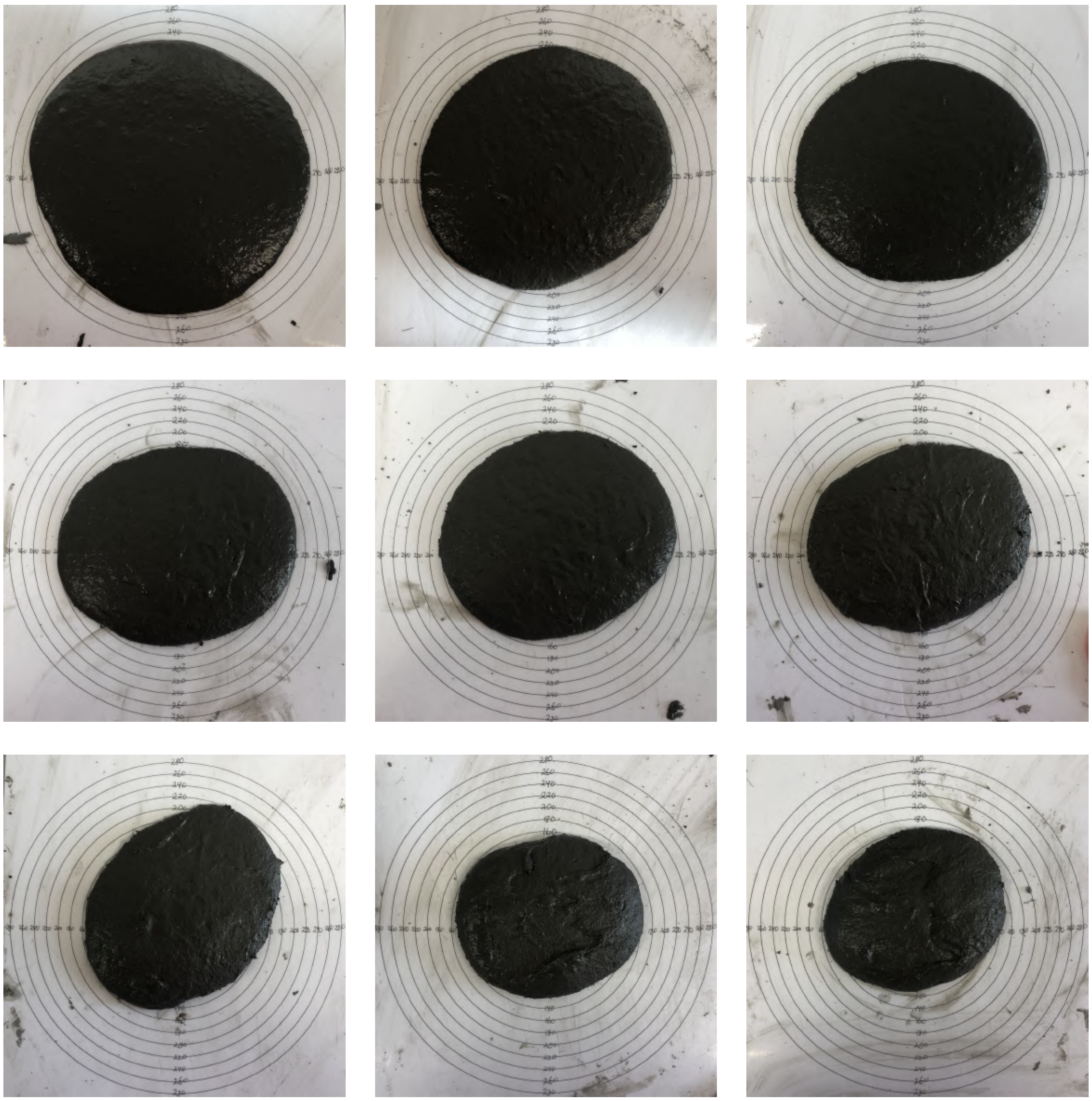

Figure G26: Miniature slump flow for batch 26 (0, 5, 10, 15, 20, 30, 40, 50, and 60 min from top left)

H: Particle size distribution curves

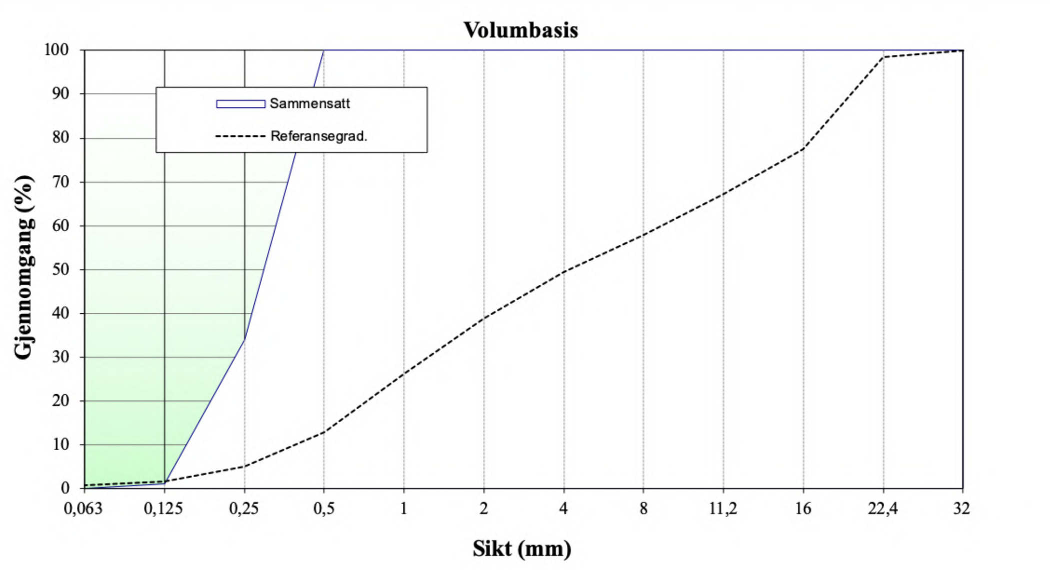

Figure H1: Particle-size distribution curve for batch 2 (German quartz H33)

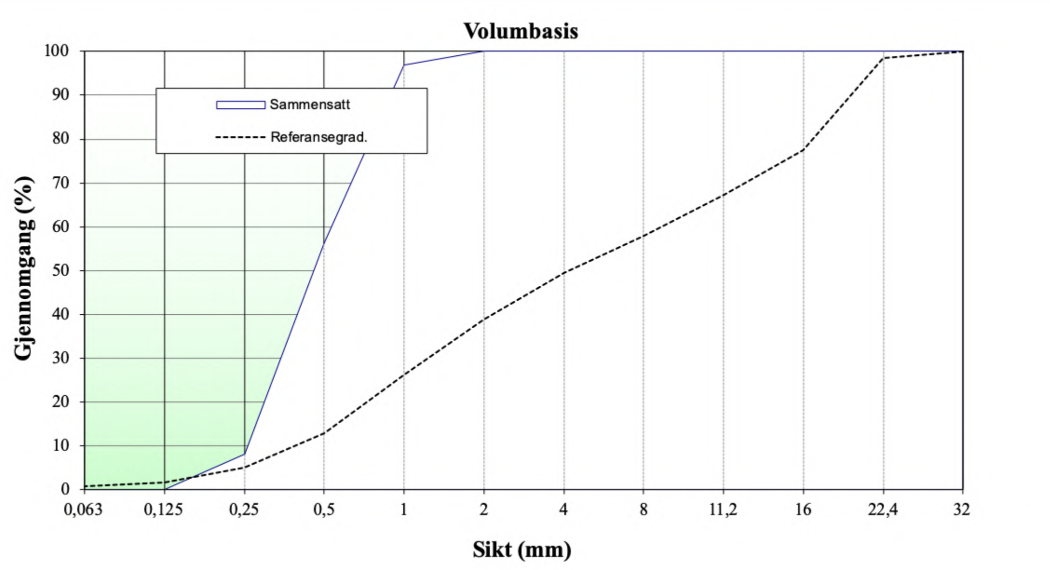

Figure H2: Particle-size distribution curve for batch 3 (Danish quartz sand)

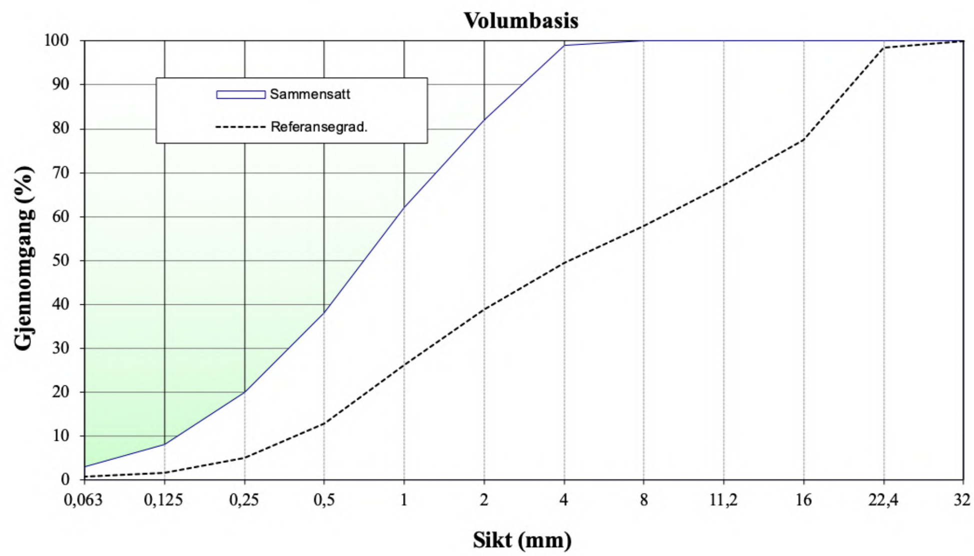

Figure H3: Particle-size distribution curve for batch 4 (gneiss-granite)

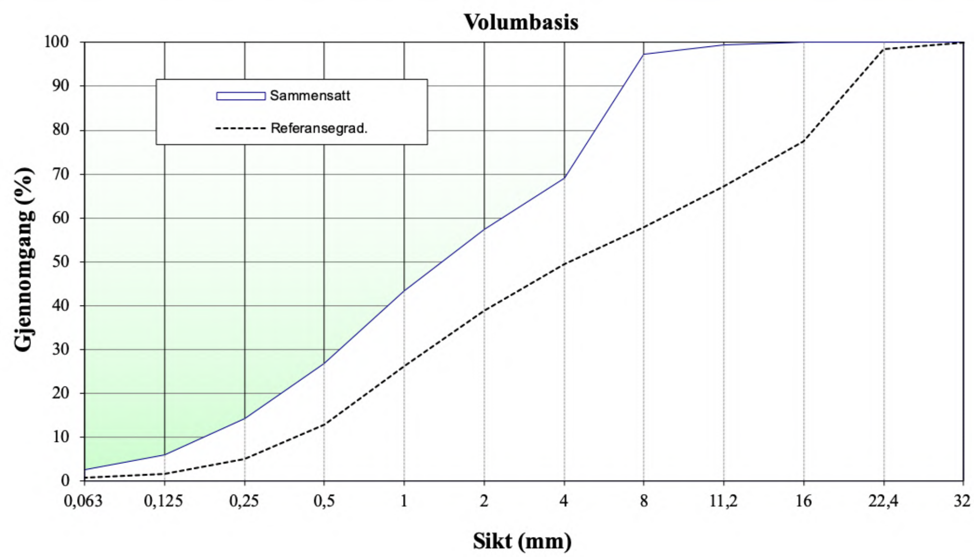

Figure H4: Particle-size distribution curve for batch 7 (70 vol-% gneiss-granite and 30 vol-% quartz-diorite)

I: Product data sheets

PRODUCT DATA SHEET

ANLEGGSEMENT FA

CEM II/A-V

LAST REVISION MARCH 2019

The cement satisfies the requirements according to NS-EN 197-1:2011 to Portland-fly ash cement CEM II/A-V 42.5 N.

Properties		Declared values	Requirements according to NS-EN 197-1:2011
Fineness (Blaine m^2/kg)		390	
Specific weight (kg/dm^3)		3.02	
Soundness (mm)		1	≤ 10
Initial setting time (min)		165	≥ 60
Compressive strength (MPa)	1 day	12	
	2 days	21	≥ 10
	7 days	37	
	28 days	53	≥ 42.5 ≤ 62.5
Sulfate (% SO_3)		≤ 3.5	≤ 3.5
Chloride (% Cl^-)		≤ 0.085	≤ 0.10
Water soluble chromium (ppm Cr^{6+})		≤ 2	≤ 2[1]
Alkalies (% Na_2O_{ekv})[2]		0.9	
Clinker (%)		81	80-94
Fly ash (%)		15	6 - 20
Limestone (minor additional constituents %)		4	< 5

1. According to EU regulation REACH Annex XVII point 47 Chromium VI compounds.
2. Total alkali content of the cement.

NORCEM
HEIDELBERGCEMENT Group

Norcem AS, P.O Box 142, Lilleaker, N-0216 Oslo
Tlf. 22 87 84 00 firmapost@norcem.no www.norcem.no

Figure I1: Product data sheet - Binder - CEM II/A-V 42.5 N - Norcem Anleggsement FA - Page 1/1

PRODUKTDATABLAD

INDUSTRISEMENT

CEM I 52,5 R

SIST REVIDERT JULI 2016

Sementen tilfredsstiller kravene i NS-EN 197-1:2011 til Portlandsement CEM I 52,5 R.

Egenskap		Deklarerte data	Krav ifølge NS-EN 197-1:2011
Finhet (Blaine m^2/kg)		550	
Spesifikk vekt (kg/dm^3)		3,13	
Volumbestandighet (mm)		1	≤ 10
Begynnendestørkning (min)		110	≥ 45
Trykkfasthet (MPa)	1 døgn	33	
	2 døgn	41	≥ 30
	7 døgn	50	
	28 døgn	59	≥ 52,5
Sulfat (% SO_3)		≤ 4,0	≤ 4,0
Klorid (% Cl^-)		≤ 0,085	≤ 0,10
Vannløselig krom (ppm Cr^{6+})		≤ 2	≤ 2 [1]
Alkalier (% Na_2O_{ekv})		1,3	
Klinker (%)		96	95-100
Sekundærebestanddeler (%)		4	0-5

1. I henhold til EU forordning REACH Vedlegg XVII punkt 47 krom VI forbindelser.

NORCEM
HEIDELBERGCEMENTGroup

Norcem AS, Postboks 142, Lilleaker, 0216 Oslo
Tlf. 22 87 84 00 firmapost@norcem.no www.norcem.no

Figure I2: Product data sheet - Binder - CEM I 52,5 R - Norcem Industrisement - Page 1/1

Dyckerhoff VARIODUR®
Premium cements with MIKRODUR® Technology

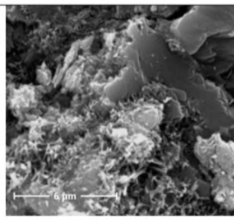

Standard concrete

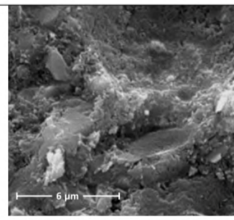

High-performance concrete with MIKRODUR Technology

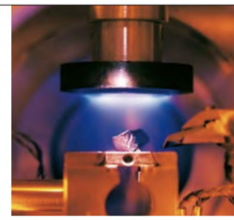

Scanning electron microscope

Evaluation of scanning electron microscope

Dyckerhoff VARIODUR premium cements enable concretes with exceptional properties without complex approval procedures, since as standard cements they are exclusively made from standardized cement constituents.

Dyckerhoff premium cements are high-performance binders for manufacturing concretes that must meet especially strict requirements. Constant uniform product quality is already ensured by the choice of raw materials in the cement plant by a special separation and mixing process, and by stringent quality control.

Dyckerhoff premium cements are granulometrically optimized by the unique MIKRODUR Technology. The interstitial filling of the cement matrix ensures an extremely dense structure in the concrete. Specifically graded proportions of finely ground granulated blast furnace slags ensure high consistency.

Exposure classes

Class	Description of the environment	Informative examples where exposure classes may occur
XA1	Slightly aggressive chemical environment according to EN 206-1: 2001-07, Table 2	Containers of wastewater treatment plants; slurry containers
XA2	Moderately aggressive chemical environment according to EN 206-1: 2001-07, Table 2 and marine structures	Concrete elements that come into contact with seawater; concrete constructions in soils aggressive to concrete
XA3	Highly aggressive chemical environment according to EN 206-1: 2001-07, Table 2	Industrial wastewater treatment plants with chemically aggressive wastewaters; silage silos and feed alleys; cooling towers with flue-gas discharge

Dyckerhoff VARIODUR CEM II/B-S 52.5 R, CEM III/A 52.5 R and CEM III/A 52.5 N-SR (na) are standard cements for the manufacture of high-strength and ultra-high-strength concretes with high resistance to aggressive media.

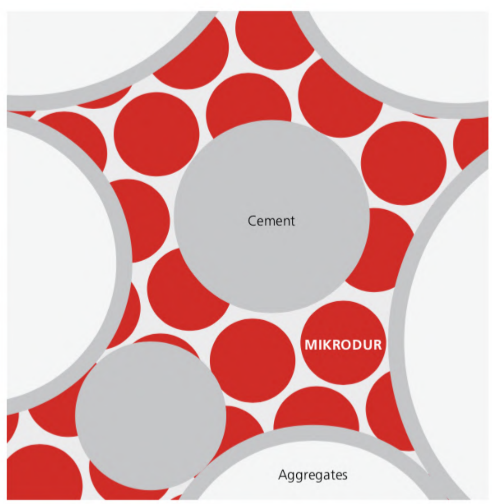

Figure I3: Product data sheet - Binder - CEM III/A 52,5 R - Dyckerhoff Variodur 40 - Page 1/5

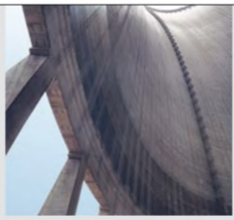
Natural draft cooling tower


Manufacture of concrete pipes


Industrial wastewater treatment plant


High-strength mass concrete

Concretes made with Dyckerhoff VARIODUR are recommended for all structural components exposed to aggressive environments. VARIODUR 50 has been tested for high sulfate resistance and is classified as SR cement (German General Building Authority Approval: DIBt No. Z-3.11-1938).

Dyckerhoff VARIODUR for construction of natural draft cooling towers

Cement formulations adjusted to process engineering combine durability with rapid development of early strength for high climbing performance of the formwork. High-performance concretes are moreover characterized by a uniform appearance in bright, attractive exposed concrete quality.

Dyckerhoff VARIODUR for use in wastewater components

The dense structure with good early and final strengths ensures great resistance when exposed to environments of changing aggressiveness. This is of equal significance for in-situ concrete components and concrete pipes manufactured in precast plants.

Development of hydration heat floor slab component A Kranhaus Süd structure, Cologne

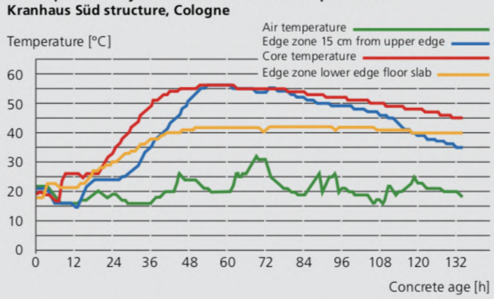

Dyckerhoff VARIODUR for high-strength mass concrete

Optimized consistent heat of hydration on a low level and, at the same time, great strength potential for meeting special requirements. Sulfate-resistant and high resistance to freeze-thaw with de-icing salt. In the massive 21 x 32 x 1.60 m thick foundation of the Kranhaus Süd structure in Cologne, Germany, C60/75 high-strength mass concrete with a consistency of F5 was used. At a maximum core temperature of 55 °C, the difference to the edge zone was less than 15 K.

Cement data

Dyckerhoff VARIODUR		VARIODUR 30 CEM II/B-S 52.5 R	VARIODUR 40 CEM III/A 52.5 R	VARIODUR 50 CEM III/A 52.5 N-SR (na)
Water demand	[%]	30	31	32
Initial setting time	[min]	175	180	220
Relative brightness	[Y]	50	53	55
Compressive strength 2d	[MPa]	38	34	28
Compressive strength 7d	[MPa]	63	60	56
Compressive strength 28d	[MPa]	72	73	74

Figure I4: Product data sheet - Binder - CEM III/A 52,5 R - Dyckerhoff Variodur 40 - Page 2/5

Renovation and extension of bridges
with special concretes based on Dyckerhoff VARIODUR

Example: renovation of…

…Hollandse Brug

Example: Bridge extension…

…in the SAAone projekt

Renovation of deck slabs (Almere)

Hollandse Brug is the name of the highway bridge along the A6 motorway that connects the Dutch capital of Amsterdam with the city of Almere, which was established on the Flevoland Polder as recently as in 1975. In 2010, the reinforced-concrete bridge of 350-m length was provided with a new deck slab of special concrete from Dyckerhoff Basal made with the Dyckerhoff premium cement VARIODUR 50 CEM III/A 52.5 N-SR (na). The Dyckerhoff Basal plant based in Almere delivered around 2,000 m³ of ready-mixed concrete for renovating the more than 10,000 m² of road surface.

The renovation was planned with a concrete slab 17 cm thick to be placed on the existing bridge construction and provided with 8-mm epoxy resin coating for additional surface protection. The requirements placed on the concrete after 48 hours, with a granular blast furnace slag content of at least 50 % in the cement, specified high adhesive tensile strength and rapid compressive strength of > 35 MPa, as well as < 2.5 % residual moisture for applying the epoxy resin coating. In addition, high resistance was required to freeze-thaw with de-icing salt (exposure class XF4), as well as low-shrinkage hardening and absence of cracks.

Concrete-technological data renovation Almere

Strength class	C60/75
Exposure class	XC4, XD3, XF4
Flow spread	F4: 490 – 550 mm
CEM III/A 52.5N-SR (na)	340 kg/m³
Fly ash	50 kg/m³
w/c ratio	0.45
Compressive strength 2d	40 MPa
Compressive strength 7d	65 MPa
Compressive strength 28d	80 MPa
Wheathering CDF test	348 g/m²

Extension project SAAone (Amsterdam-Almere)

The structure, built in in 2016, is an extension of the already existing bridge across Gooimeer and IJmeer between Amsterdam and Almere in the Netherlands that had become too narrow.

The bridge across the Amsterdam-Rhine Canal was designed to be self-supporting. The high-strength ready-mixed concrete of strength class C70/85 chosen for this project was also produced with Dyckerhoff VARIODUR 50 CEM III/A 52.5 N-SR (na) due to low heat of hydration and high resistance of the high-performance concrete to freeze-thaw with de-icing salt.

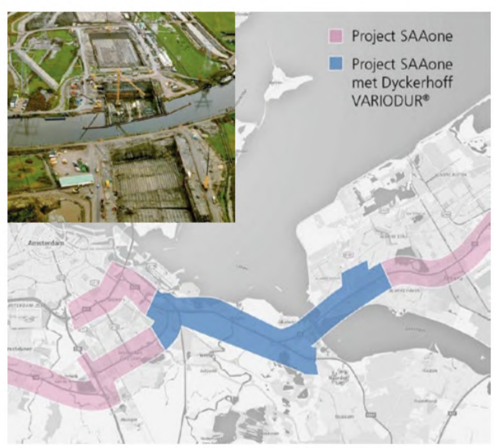

Figure I5: Product data sheet - Binder - CEM III/A 52,5 R - Dyckerhoff Variodur 40 - Page 3/5

Example: renovation of …

… Ewijk Bridge

Application of high-strength concrete …

… with a special finisher

Renovation with XPOSAL 105 based on Dyckerhoff VARIODUR 30

The old Waal Bridge (Ewijk Bridge) was built in 1976. It is one of the steel bridges in the Netherlands that, prior to renovation, was no longer able to support current traffic levels.

A method that has previously been applied many times in the Netherlands consists of strengthening the supporting slab by a deck cover of reinforced high-strength concrete (C90/105). This reduces the stress by up to 80 % in the supporting slab compared to an asphalt cover layer, thereby significantly increasing the service life of the bridge.

The composition of the high-strength concrete was developed by Dyckerhoff Basal in the Netherlands together with the Wilhelm Dyckerhoff Institut in Wiesbaden, Germany. The result: Dyckerhoff XPOSAL 105 stands for a robust high-strength concrete of compressive strength class C90/105 based on Dyckerhoff VARIODUR 30 CEM II/B-S 52.5 R. All the concrete was delivered by the Dyckerhoff Basal plant in Arnhem. In 20 working days in the period from June to December 2016, a total of approx. 2,400 m³ of Dyckerhoff XPOSAL 105 was delivered; on two occasions, concreting also took place at night.

The Dutch contractor consortium consisting of Strukton and Ballast Nedam had developed a special finisher that placed strict requirements on the uniformity of the concrete. The paving equipment used is capable of generating high compaction energy to ensure a very strong bond between concrete and steel over a width of 12 m. At a speed of 20 cm per minute, 100 m of bridge decks were placed in one day. On the steel surface, a bonding course of bauxite and epoxy resin was applied for optimal adhesion. Use was made of both conventional steel reinforcement as well as 75 kg/m³ of steel fibers, added by a new batching unit at the plant. The mixing trucks had been provided with special 'rain caps' to guard against rainwater to ensure optimal consistency of Dyckerhoff XPOSAL 105.

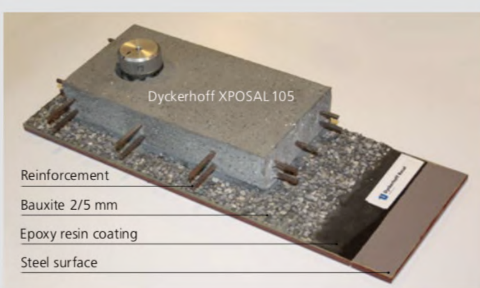

Concrete-technological data renovation Ewijk

Strength / exposure class	C90/105; XF4
Flow spread	F3 / F4: 450 – 500 mm
Processing time	≥ 2 hours
Air entrainment	≤ 2.0 %
Density	≤ 2,500 kg/m³ (± 5 %)
Flexural strength	10 MPa (± 25 %)
Young's modulus	50,000 MPa (± 10 %)
Autogenous shrinkage	≤ 3.0 ‰
Resistance to freeze-thaw with de-icing salt	≤ 100 g/m²
Chloride migration	≤ 2.0 * 10^{-12} m²/sec
Coarse aggregate 2/5 mm	ASR resistant
Steel fibers (L = 12.5 mm, D = 0.4 mm)	≥ 75 kg/m³ (evenly distributed)

Figure I6: Product data sheet - Binder - CEM III/A 52,5 R - Dyckerhoff Variodur 40 - Page 4/5

UHPC
Ultra High Performance Concrete

Columns (7 cm)

Staircases (3 cm)

Fish-farming basin (6 cm)…

…made of glued elements

Ultra High Performance Concretes are based on optimization of the packing density of the hardened cement paste. This is achieved, as generally known, by filling the cavities with special admixtures such as silica fume, which, moreover, due to the pozzolanic reaction of the structure of the cement paste, additionally increases its density.

However, high-performance concretes can more easily be obtained with modern cement technology, as the examples on pages 4 and 5 show. The DAfStb guideline on UHPC contains high-strength classes, which will later also be included in the new versions of the concrete standards: C130/145, C150/165 and 175/190.

While C175/190 will likely be available only with extremely high dosing of micro steel fibers, C150/165 is capable of achieving this class with moderate dosing of micro steel fibers and C130/145 entirely without any, using Dyckerhoff VARIODUR 40, together with suitable superplasticizers.

When performing strength tests, great care must be taken to use only absolutely faultless steel forms and that the surfaces of the cylinder specimen are ground plane-parallel prior to testing.

Special structural building components – e.g., columns with a diameter of 7 cm, a staircase exhibit example with steps of 3 cm thickness and a two-level basin for fish-farming filled with seawater with a wall thickness of 6 cm – are examples of possible applications of UHPC. (Application examples made with ULTRALITH by Benno Drössler GmbH & Co. Bauunternehmung KG, Siegen, Germany, based on Dyckerhoff NANODUR® Compound 5941)

However, in the area of structural engineering, only standard cements can currently be used. For verification of performance, a simple UHPC formulation with VARIODUR 40 CEM III/A 52.5 R was tested, without silica fume and without the often performed special granulometric grading of aggregate sizes.

Pit sand 0/2 mm and high-grade basalt chippings 2/5 mm were used here, as well as a special superplasticizer based on polycarboxylate ether (PCE) for adjustment to an easy-to-process consistency for low water/cement ratios.

UHPC formulation

VARIODUR 40 CEM III/A 52.5 R		700 kg/m³
Pit sand 0/2 mm		480 kg/m³
High-grade basalt chippings 2/5 mm		1,300 kg/m³
Superplasticizer on PCE base for low w/c ratios		16.8 kg/m³
Water (incl. water from PCE)		136 kg/m³
w/c ratio		< 0.20
Flow spread		430 mm
Compressive strength (10/10/10 cm cube)	7d	147 MPa
Compressive strength (15/30 cm cylinder)	7d	137 MPa
Young's modulus	7d	54,000 MPa
Compressive strength (10/10/10 cm cube)	28d	162 MPa
Compressive strength (15/30 cm cylinder)	28d	158 MPa
Young's modulus	28d	55,600 MPa

Figure I7: Product data sheet - Binder - CEM III/A 52,5 R - Dyckerhoff Variodur 40 - Page 5/5

Product specification

Merit 5000

Edition: 05
Issued: 2010-04-07

SP's certification no: **0402**

Cert.no:
0402-CPD-301802 08

EN 15167-1

SITAC
SP
Kontroll

Approval:
1112/87

Quality assurance

The chemical composition of the slag is continuously analysed and the slag accepted for granulation is sorted out. The specific surface of the material is analyzed during the grinding process. Physical and chemical properties of Merit 5000 are checked in an extensive program continuously. Merit 5000 is a qualified product by the Swedish Institute for Technical Approval in Construction (SITAC) and controlled by the Swedish National Testing and Research Institute (SP). Merox AB is certified according to ISO 9001:2000 and ISO 14001:1996.

Application field

Mineral additive type II in concrete. Part of selflevelling compound increasing bearing capacity in soils.

Origin & manufacturing

Merit 5000 is produced from blast furnace slag from SSAB Oxelösund, rapidly cooled with water. The material is thereafter dried before being grounded at the mill in Grängesberg.

Concrete properties

Concrete with Merit 5000 may result in a slower generation of heat and compressive strength development compared to standard concrete. This should be taken into consideration, especially in low temperatures so that the curing is fully satisfied before tearing possible mould. The final compressive strength of concrete with Merit 5000 is equivalent or higher to that of standard concrete.

Handling advice

Merit 5000 should be handled in the same way as standard cement. For further information contact the producer.

Health- and environmental effect

See the material safety data sheet.

Chemical Content [weight-%]

Compound	Mean	Max	Min
CaO	31	38	29
SiO_2	34	40	30
MgO	17	18	10
Al_2O_3	13	15	10
TiO_2	2,4		
Mn_2O_3	0,8		
FeO	0,4		
S^{2-}	1,3	1,6	
SO_3	0,25	1,0	
ekv Na_2O	0,9	1,4	

Physical Properties

Property	Mean	Max	Min
Specific surface [Blaine cm^2/g]	5000	5400	4600
Specific Weight [kg/m^3]	2920	2980	2850
Glass content [%]	99		92

MEROX
- A member of the SSAB group -

SSAB Merox AB
613 80 Oxelösund, Sweden
Phone: +46 155 25 44 00
Fax +46 155 25 52 21

Figure I8: Product data sheet - Binder - Merox Merit 5000 Slagg - Page 1/1

Elkem
A Bluestar Company

Elkem ASA
Drammensveien 169
Postboks 334, Skøyen
NO-0213 Oslo
Norway
Tel: +47 22 45 01 00
www.elkem.com

Product Data Sheet

Elkem Microsilica® Grade 940 for fibre cement

Elkem Microsilica® Grade 940 is a dry silica fume available in two main forms: Undensified (U) and Densified (D)

Description

Elkem Microsilica® Grade 940 is a dry silica fume available in two main forms: Undensified (U) and Densified (D). In use, it acts physically as a filler and chemically as a highly reactive pozzolan. A key ingredient in many construction materials, Elkem Microsilica® is used in fibre cement products as a process aid, to improve ingredient dispersion and to improve hardened properties and overall durability.

Packing

The product is available in:

- 25 kg paper bags
- Big bags in various designs & sizes
- Bulk road tanker

Please contact our representative for more details.

Storage & handling

Elkem Microsilica® Grade 940 should be stored in dry conditions and not exposed to moisture.

Quality assurance & quality control

Elkem Silicon Materials' Management System for development, processing and supply of Elkem Microsilica® is certified to ISO 9001. The chemical and physical properties of Elkem Microsilica® are regularly tested.

Figure I9: Product data sheet - Binder - Elkem Microsilika 940U - Page 1/2

Elkem
A Bluestar Company

Elkem ASA
Drammensveien 169
Postboks 334, Skøyen
NO-0213 Oslo
Norway
Tel: +47 22 45 01 00
www.elkem.com

Chemical and physical properties

Properties	Unit	Specification
SiO_2	%	> 90
Retention on 45µm sieve	%	< 1.5*
H_2O (when packed)	%	< 1.0
Bulk Density (U)	kg/m^3	200 – 350
Bulk Density (D)	kg/m^3	500 – 700

*Tested on Undensified.
Test methods are available on request.

Figure I10: Product data sheet - Binder - Elkem Microsilika 940U - Page 2/2

LEISTUNGSERKLÄRUNG

Kennnummer 13139-2013-1

gemäß Anhang III der Verordnung (EU) Nr. 305/2011
(Bauprodukte-Verordnung)
für die durch Aufbereitung natürlicher Materialien gewonnenen Gesteinskörnungen für Mörtel

1. Kenncodes der Produkttypen:

FH 31-13139-2013-1	F 32-13139-2013-1	F 34-13139-2013-1	F 36-13139-2013-1
F 38-13139-2013-1	W 3-13139-2013-1	W 6-13139-2013-1	W 8-13139-2013-1
W 10-13139-2013-1	W 12-13139-2013-1		

2. Sortennummern zur Identifikation des Bauprodukts gemäß Artikel 11 Absatz 4:
   Siehe Sortenverzeichnis 13139-2013-1

3. Gesteinskörnung für Mörtel nach EN 13139:2002

4. Name und Kontaktanschrift des Herstellers gemäß Artikel 11 Absatz 5:
   Quarzwerke GmbH
   Kaskadenweg 40
   50226 Frechen
   Herstellwerk: Frechen

5. *Gegebenenfalls Name und Kontaktanschrift des Bevollmächtigten, der mit den Aufgaben gemäß Artikel 12 Absatz 2 beauftragt ist:*
   Nicht relevant

6. System zur Bewertung und Überprüfung der Leistungsbeständigkeit des Bauprodukts gemäß Anhang V:
   System 2+

7. Die notifizierte Stelle Baustoffüberwachungsverein Nordrhein Westfalen e.V. (Kennnummer 0778) hat die Erstinspektion des Werkes und der werkseigenen Produktionskontrolle sowie die laufende Überwachung, Bewertung und Evaluierung der werkseigenen Produktionskontrolle nach dem System 2+ vorgenommen und Folgendes ausgestellt:
   Bescheinigung der Konformität der werkseigenen Produktionskontrolle
   Nr. 0778-CPR-8.601-1/3

8. nicht relevant

9. Erklärte Leistung
   Die Leistung zu dem jeweiligen wesentlichen Merkmal ist im Anhang Sortenverzeichnis 13139-2013-1 aufgeführt.

10. Die Leistung der Produkte gemäß den Nummern 1 und 2 entspricht der erklärten Leistung nach Nummer 9. Verantwortlich für die Erstellung dieser Leistungserklärung ist allein der Hersteller gemäß Nummer 4.

Unterzeichnet für den Hersteller und im Namen des Herstellers von:

Dietmar Linn Laborleiter Zentrallabor
(Name und Funktion)

Frechen, 19.07.2016
(Ort und Datum der Ausstellung) *(Unterschrift)*

Figure I11: Product data sheet - Filler - Millisil W12 - Page 1/2

Anhang zur Leistungserklärung 13139-2013-1

Wesentliche Merkmale	Leistung	Leistung	Leistung	Leistung			
Sortennummer	W 6	W 8	W 10	W 12			
Korngruppe	**Füller (Gesteinsmehl)**	**Füller (Gesteinsmehl)**	**Füller (Gesteinsmehl)**	**Füller (Gesteinsmehl)**			
Kornzusammensetzung	NPD	NPD	NPD	NPD			
Kornrohdichte Mg/m³	2,65	2,65	2,65	2,65			
Gehalt an Feinanteilen	f_{72}	F_{85}	F_{94}	F_{98}			
Muschelschalengehalt	NPD	NPD	NPD	NPD			
Chloride [M.-%]	< 0,02	< 0,02	< 0,02	< 0,02			
Säurelösliches Sulfat	AS 0,2	AS 0,2	AS 0,2	AS 0,2			
Gesamtschwefel [M.-%]	<1	< 1	< 1	< 1			
Bestandteile, die Erstarrungs- und Erhärtungsverhalten des Betons verändern	Bestanden	Bestanden	Bestanden	Bestanden			
Raumbeständigkeit	NPD	NPD	NPD	NPD			
Wasseraufnahme	NPD	NPD	NPD	NPD			
Frost-Tau-Wechselbeständigkeit	NPD	NPD	NPD	NPD			
Widerstand gegen Alkalikieselsäure-Reaktivität	E I	E I	E I	E I			
Leichtgewichtige organische Verunreinigungen	< 0,1	< 0,1	< 0,1	< 0,1			

Typische Korngrößenverteilung für feine Gesteinskörnungen

Sorte Nr.	Korngruppe	werktypische Kornzusammensetzung Durchgang durch das Sieb (mm) in M.-%					
		0,063	0,125	2			**Bemerkung**
W 6	Füller	72	96	100			
W 8	Füller	85	99	100			
W 10	Füller	94	100				
W 12	Füller	98	100				

Figure I12: Product data sheet - Filler - Millisil W12 - Page 2/2

VERDALSKALK

YTELSESERKLÆRING NR. 1111 CPR-0108 003-VK-BEf-18-01

1. Entydig identifikasjonskode for produkttypen	**Kalksteinfiller for betong**
2. Type-, parti- eller serienummer eller en annen form for angivelse som muliggjør identifisering av byggevaren i samsvar med artikkel 11 nr. 4	**Betofill VK 50**
3. Produsentens tilsiktede bruksområder for byggevaren, i samsvar med den relevante harmoniserte tekniske spesifikasjonen	**Tilslag for Betong**
4. Navn, registrert varemerke og kontaktadresse til produsenten i henhold til artikkel 11 nr. 5	**Verdalskalk AS, avdeling Havna, Kalkveien 40, 7670 Inderøy**
5. Navn og kontaktadresse til godkjent representant hvis mandat omfatter oppgavene angitt i artikkel 12 nr. 2 (om relevant)	**Ikke relevant**
6. Det eller de systemer for vurdering og kontroll av byggevarens konstante ytelse, som fastsatt i vedlegg V	**System 2+**
7. Dersom ytelseserklæringen gjelder en byggevare som omfattes av en harmonisert standard	**NS-EN 12620:2002 + A1:2008+NA:2016** **Sertifiseringsorganet Kontrollrådet (1111) har utstedt sertifikat for produksjonskontrollen i samsvar med system 2+ basert på første-gangsrevisjon av produksjonsanlegget og produksjonskontrollen.**
8. Angitt ytelse	**Se neste side**

9. Ytelsen for varen som angitt i nr. 1 og 2, er i samsvar med ytelsen angitt i nr. 8

Denne ytelseserklæringen er utstedt på eget ansvar av produsenten, som angitt i punkt nr. 4.

Undertegnet for og på vegne av produsenten av:

Geir Olav Jensen, Daglig leder

(navn og stilling)

Inderøy, 01. april 2019

Sted og utstedelsesdato

Underskrift

Side 1

Figure I13: Product data sheet - Filler - Betofill VK 50 - Page 1/2

Harmonisert teknisk spesifikasjon: **NS-EN 12620:2002 +A1:2008+NA:2016**

Vesentlige egenskaper	Ytelse
Filler størrelse	**0/0,1**
Gradering: 2 mm 0,125 mm 0,063 mm	**100 %** **100 %** **98 %**
Korndensitet	**2,72 Mg/m³**
Sammensetning/innhold Klorider Syreløselige sulfater Totalt innhold av svovel	 **<0,005 %** **$AS_{0,2}$** **0,01 %**
Renhet	**MB_FIK**
Bestanddeler som endrer størknings- og herdingstiden av betong	**Ikke innhold av slike elementer**
Alkali silika reaktivitet Sammenligningsverdi	**0 %** **3,0**
Angivelse av andre farlige stoffer	**Ingen kjente**

Side 2

Figure I14: Product data sheet - Filler - Betofill VK 50 - Page 2/2

LEISTUNGSERKLÄRUNG
Kennnummer 13139-2013-1
gemäß Anhang III der Verordnung (EU) Nr. 305/2011
(Bauprodukte-Verordnung)
für die durch Aufbereitung natürlicher Materialien gewonnenen Gesteinskörnungen für Mörtel

1. Kenncodes der Produkttypen:

H 31-13139-2013-1	H 32-13139-2013-1	H 33-13139-2013-1	H 35-13139-2013-1
W 3-13139-2013-1	W 4-13139-2013-1	W 6-13139-2013-1	W 8-13139-2013-1
W 11-13139-2013-1			

2. Sortennummern zur Identifikation des Bauprodukts gemäß Artikel 11 Absatz 4:
siehe Sortenverzeichnis 13139-2013-1

3. Gesteinskörnung für Mörtel nach EN 13139:2002

4. Name und Kontaktanschrift des Herstellers gemäß Artikel 11 Absatz 5:
Quarzwerke GmbH
Kaskadenweg 40
50226 Frechen
Herstellwerk: Haltern

5. *Gegebenenfalls Name und Kontaktanschrift des Bevollmächtigten, der mit den Aufgaben gemäß Artikel 12 Absatz 2 beauftragt ist:*
Nicht relevant

6. System zur Bewertung und Überprüfung der Leistungsbeständigkeit des Bauprodukts gemäß Anhang V:
System 2+

7. Die notifizierte Stelle Baustoffüberwachungsverein Nordrhein Westfalen e.V. (Kennnummer 0778) hat die Erstinspektion des Werkes und der werkseigenen Produktionskontrolle sowie die laufende Überwachung, Bewertung und Evaluierung der werkseigenen Produktionskontrolle nach dem System 2+ vorgenommen und Folgendes ausgestellt:
Bescheinigung der Konformität der werkseigenen Produktionskontrolle
Nr. 0778-CPR-8.601-1/2

8. nicht relevant

9. Erklärte Leistung
Die Leistung zu dem jeweiligen wesentlichen Merkmal ist im Anhang Sortenverzeichnis 13139-2013-1 aufgeführt.

10. Die Leistung der Produkte gemäß den Nummern 1 und 2 entspricht der erklärten Leistung nach Nummer 9. Verantwortlich für die Erstellung dieser Leistungserklärung ist allein der Hersteller gemäß Nummer 4.

Unterzeichnet für den Hersteller und im Namen des Herstellers von:

Dietmar Linn Laborleiter Zentrallabor
(Name und Funktion)

Quarzwerke GmbH
Zentrallaboratorium
Kaskadenweg 70-82, 50226 Frechen
Telefon: (0 22 34) 101-0
Telefax: (0 22 34) 101-600

Frechen, 19.07.2016
(Ort und Datum der Ausstellung) *(Unterschrift)*

Figure I15: Product data sheet - Aggregate - German Quartz H33 - Page 1/2

Anhang zur Leistungserklärung 13139-2013-1

SORTENVERZEICHNIS
13139-2013-1

Erklärte Leistung zu den wesentlichen Merkmalen nach der harmonisierten technischen Spezifikation EN 13139:2002

Wesentliche Merkmale	Leistung	Leistung	Leistung	Leistung	Leistung	Leistung	
Sortennummer	H 31	H 32	H 33	H 35	W 3	W 4	
Korngruppe	**0/1**	**0/0,5**	**0/0,5**	**0/0,25**	**0/0,25**	**0/0,25**	
Kornzusammensetzung	NPD	NPD	NPD	NPD	NPD	NPD	
Kornrohdichte Mg/m³	2,65	2,65	2,65	2,65	2,65	2,65	
Gehalt an Feinanteilen	f_3	f_3	f_3	f_3	f_{38}	f_{49}	
Muschelschalengehalt	NPD	NPD	NPD	NPD	NPD	NPD	
Chloride [M.-%]	< 0,02	< 0,02	< 0,02	< 0,02	< 0,02	< 0,02	
Säurelösliches Sulfat	AS 0,2	AS 0,2	AS 0,2	AS 0,2	AS 0,2	AS 0,2	
Gesamtschwefel [M.-%]	<1	< 1	< 1	< 1	< 1	< 1	
Bestandteile, die Erstarrungs- und Erhärtungsverhalten des Betons verändern	Bestanden	Bestanden	Bestanden	Bestanden	Bestanden	Bestanden	
Raumbeständigkeit	NPD	NPD	NPD	NPD	NPD	NPD	
Wasseraufnahme	NPD	NPD	NPD	NPD	NPD	NPD	
Frost-Tau-Wechselbeständigkeit	NPD	NPD	NPD	NPD	NPD	NPD	
Widerstand gegen Alkalikieselsäure-Reaktivität	E I	E I	E I	E I	E I	E I	
Leichtgewichtige organische Verunreinigungen	< 0,1	< 0,1	< 0,1	< 0,1	< 0,1	< 0,1	

Typische Korngrößenverteilung für feine Gesteinskörnungen

Sorte Nr.	Korngruppe	werktypische Kornzusammensetzung Durchgang durch das Sieb (mm) in M.-%					
		0,063	0,125	0,25	0,5	1	**Bemerkung**
H 31	0/1	0	0	8	90	100	
H 32	0/0,5	0	0	16	98	100	
H 33	0/0,5	0	1	44	100		
H 35	0/0,25	1	7	90	100		
W 3	0/0,25	38	68	100			
W 4	0/0,25	49	78	100			

Figure I16: Product data sheet - Aggregate - German Quartz H33 - Page 2/2

CE

Hostrup Sand A/S
Hostrupvej 42B 6710 Esbjerg V
Denmark

Marking affixed to: 14 **Valid from:** 15-01-2014 **Replaces:** New

DoP - Declaration of Performance

DoP nr.: 15012014-106

1: Product type: Fine aggregate - quaternary outwash deposited materiels - quartz sand

2: Item Identification: Bakkesand 0-1 Kl.: E from gravel pit, Hostrupvej 42B, 6710 Esbjerg V Denmark

3: Intended use: EN 13242 Fine aggregate - Aggregate for hydraulically bound and unbound materiels for civil engineering work and road construction

4: Manufacturer: Office Hostrup Sand A/S
Sdr. Egknudvej 1
6870 Ølgod

Office Tlf. +45 75 24 61 34
Gravel pit Tlf. +45 20 72 21 28
CVR nr. 32940633

5: Authorised representative Not relevant

6: Assesment and Verification of Constancy of performance (AVCP): 4

7: The notified body's task: Not relevant

8: Declared performance: Essential Propeties refers to points in EN 13242:2002+A1:2007

Test method	Property	Essential Propeties	Category		Declared value		
EN 933-1	Grading	E.P. 4.2	d/D: 0/2		Passing %		
		E.P. 4.3	G_F:85	Sieve	Typical	Min.	Max.
				8mm	100	100	100
				5,6mm	100	100	100
				4mm	100	100	100
				2mm	100	100	100
				1mm	97	91	99
				0,5mm	56	46	66
				0,25mm	8	0	15
				0,125mm	0	0	6
EN 933-1	Fines content	E.P. 4.6	f_3	0,063mm	0,1	0	2
EN 933-9	Fines Quality	E.P. 4.7	NPD		Fines content <3%		
EN 1097-6	Density & Absorption				Typisk	Min.	Max.
	Particle densitty ssd	E.P. 5.4		Mg/m3	2,64	2,60	2,68
	Water absorption	E.P. 5.5		%WA	0,3	0	0,5
EN 13242-7.3.2	Water absorption-freeze-thaw	E.P. 7.3.2	$WA_{24}1$				
EN 1744-1	Chlorid content				Typical		Max.
	Chlorid			% C	<0,001		<0,001
	Water solube alkali			% Na_2Oækv	<0,0009		<0,0009
EN 1744-1	Organic material, humus	E.P. 6.4.1			Brighter than standard color		
EN 932-3	Petrographic description				Quartz sand		
	Acid soluble sulphate	E.P. 6.2	NPD				
	Total sulphur	E.P. 6.3	NPD				
	Emission of radioactivity		NPD				
	Release of other dangerous substances		NPD				

9: The performance of the product identified in points 1 and 2 is in conformity with the declared performance in point 8.
This performance declaration issued at the sole responsibility of the manufacturer identified in point 4.

Ølgod, date 15-01-2014

Jan Lillegaard, Director

Figure I17: Product data sheet - Aggregate - Danish Quartz sand - Page 1/1

CE

1111

NorStone Årdal, 4137 Årdal, Norge

17

NS-EN 12620:2002+A1:2008+NA:2016

Tilslag for betong

Ytelseserklæring nr / Entydig identifikasjonskode

101715-102 003 100 Knust-Natur 0/4mm (B) Gneis-Granitt

Standarder		Kategorier
	Kornstørrelse	0/4
NS EN 933-1	Gradering	G_F85
	Toleransekategori	-
	Kornform	
NS EN 933-3	Flisighetsindeks	
NS EN 1097-6	**Korndensitet**	2,64 Mg/m³ - 2,68 Mg/m³
NS EN 1097-6	**Vannabsorbsjon**	$WA_{24}1$
NS-EN12620 F.2.3	**Motstand mot frysing og tining**	-
	Renhet	
NS EN 933-1	Finstoffinnhold	f_{10}
NS EN 933-7	Skjellinnhold	SC_{10}
NS EN 933-5	**Prosentandel knuste korn**	C_{IK}
	Sammensetning / innhold	
NS EN 1744-1§ 7	Klorider	$Cl_{0,02}$
NS EN 1744-1§ 11	Totalt innhold av svovel	<0.1%
NS EN 1744-1§ 12	Syreløselige sulfater	$AS_{0,2}$
NS-EN 1744-1§ 15	Bestanddeler som endrer stųrknings- og herdingstiden av betong	Lysere
NB 21	**Alkalireaktivitet (sammeligningsverdi)**	0,9%
ASTM C1260-14	**Accelereret mørtelprismeekspansion**	<0.10%
NS EN 932-3	Petrografisk beskrivelse	Sand med knuste korn fra løssmasseforekomst. Hovedsakelig sammensatt av kubisk rundede/skarpkantede korn av granitt,gneis,feltspatiske bergarter og mørke bergarter.Løst belegg på kornoverflater, enkelte forvitrede korn og enkelte meget svake korn.

Figure I18: Product data sheet - Aggregate - Gneiss-Granite - Page 1/3

NORSTONE
HEIDELBERGCEMENTGroup

Side - 2 -

Material	Vare nr	Dato	Avdeling
0/4	101715-102	07.11.2017	NorStone Årdal

	Gjennomgang(%)																
	0,063	0,125	0,25	0,5	1	2	4	5,6	8	11,2	16	22,4	31,5	45	56	63	90
Typisk gradering	3,0	8,0	20,0	38,0	62,0	82,0	99,0	100,0									
Min.	2,0		17,0		57,0		98,0	100,0									
Max.	4,0		22,0		67,0		100,0										

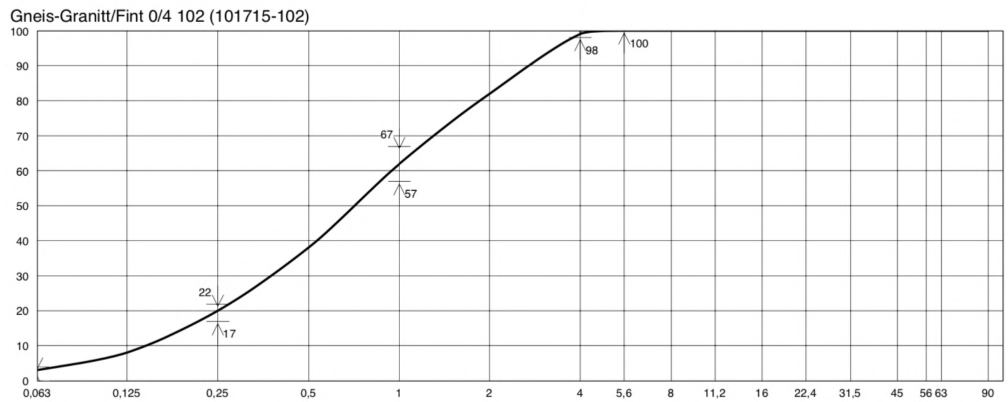

07.11.2017
Dato

A. Cernauskiene
Prepared by

Figure I19: Product data sheet - Aggregate - Gneiss-Granite - Page 2/3

Ytelseserklæring

I henhold til forordning (EU) nr. 305/2011 (byggevarer), vedlegg III

Side -3-

Ytelseserklæring nr: **101715-102 003**		NORSTONE HEIDELBERGCEMENT Group
100 Knust-Natur 0/4mm (B) Gneis-Granitt	Vare nr: **101715-102**	
Bruksområder for byggevaren(e):	**Tilslag for betong**	
Det eller de systemer for vurdering og kontroll av byggevarens konstante ytelse	**System 2+**	NorStone Årdal
Dersom ytelseserklæringen gjelder en byggevare som omfattes av en harmonisert Standard	**NS-EN 12620:2002+A1:2008+NA:2016**	NorStone Årdal, 4137 Årdal, Norge
Sertifiseringsorganet:	**Kontrollrådet-1111**	www.norstone.no
har utstedt sertifikat for produksjonskontrollen i samsvar med	**System 2+**	Tlf:0047-51754200
basert på førstegangsrevisjon av produksjons-anlegget og produksjonskontrollen:	**1111-CPD-0007**	Tlf:0047-51754201
Ytelseserklæring arkiveres i ti år.		

Harmonisert teknisk spesifikasjon	**Standarder**	**Vesentlige egenskaper**	**Ytelse**
NS EN 12620:2002+A1:2008+NA:2016			**Kategorier**
		Kornstørrelse	0/4
	NS EN 933-1	Gradering	G_F85
		Toleransekategori	-
		Kornform	
	NS EN 933-3	Flisighetsindeks	
	NS EN 933-4	Shape indeks	NPD
	NS EN 1097-6	**Korndensitet**	2,64 Mg/m³ - 2,68 Mg/m³
	NS EN 1097-6 §8	**Vannabsorbsjon**	$WA_{24}1$
	NSEN 12620 F.2.3	**Motstand mot frysing og tining**	-
		Renhet	
	NS EN 933-1	Finstoffinnhold	f_{10}
	NS EN 933-7	Skjellinnhold	SC_{10}
		Motstand mot knusing	
	NS EN 1097-2 §5	Los Angeles-prøving	LA_{30}
	NS EN 1097-2 §6	Slagprøving	NPD
		Motstand mot polering/slitasje	
	NS EN 1097-8	Poleringsverdi	NPD
	NS EN 1097-1	Motstand mot slitasje for grovt tilslag	NPD
	NS EN 1097-9	Motstand mot piggdekkslitasje	NPD
		Sammensetning / innhold	
	NS EN 1744-1§ 7	Klorider	$Cl_{0,02}$
	NS EN 1744-1§ 11	Totalt innhold av svovel	<0.1%
	NS EN 1744-1§ 12	Syreløselige sulfater	$AS_{0,2}$
	NS EN 1744-1§ 15	Bestanddeler som endrer stųrknings- og herdingstiden av betong	Lysere
	NB21	**Alkalireaktivitet (sammeligningsverdi)**	0,9%
	ASTM C1260-14	**Accelereret mørtelprismeekspansion**	<0.10%
	NS-EN 932-3	**Innhold av kalkstein**	0,0%
	NS EN 932-3	**Petrografisk beskrivelse**	Sand med knuste korn fra løssmasseforekomst. Hovedsakelig sammensatt av kubisk rundede/skarpkantede korn av granitt,gneis,feltspatiske bergarter og mørke bergarter.Løst belegg på kornoverflater, enkelte forvitrede korn og enkelte meget svake korn.

Ytelsen for denne varen som angitt ovenfor, er i samsvar med spesifikasjonene for produktet angitt i tabellen. Denne ytelseserkl¿ringen er utstedt på eget ansvar av produsenten, NorStone Årdal. Undertegnet for og på vegne av produsenten av:

Årdal 07.11.2017 — Svein Johan Mæland, Driftsleder (navn og stilling)

(Sted og utstedelsesdato) (Underskrift)

Figure I20: Product data sheet - Aggregate - Gneiss-Granite - Page 3/3

CE

1111

Norstone Tau, 4120 Tau, Norway

04

NS-EN 13043:2002 + NA:2008

Tilslag til bituminøse masser og overflatebehandlinger for veger, flyplasser og andre trafikkarealer

Ytelseserklæring nr / Entydig identifikasjonskode

101658 004 100 % Knust 5/8mm (A) Kvartsdiorit

Standarder		Kategorier
	Kornstørrelse	5/8
NS EN 933-1	Gradering	$G_C85/20$
	Toleransekategori	-
	Kornform	
NS EN 933-3	Flisighetsindeks	FI_{20}
NS EN 1097-6	**Korndensitet**	2,75 Mg/m³ - 2,79 Mg/m³
NS EN 1097-6	**Vannabsorbsjon**	$WA_{24}1$
	Renhet	
NS EN 933-1	Finstoffinnhold	f_2
NS EN 933-9	Finstoffkvalitet	MB_F10
NS EN 933-5	**Prosentandel knuste korn**	$C_{100/0}$
	Motstand mot knusing	
NS EN 1097-2 §5	Los Angeles-prøving	LA_{15}
	Motstand mot polering/slitasje	
NS EN 1097-8	Poleringsverdi	PSV_{50}
NS EN 1097-1	Motstand mot slitasje for grovt tilslag	$M_{DE}10$
NS EN 1097-9	Motstand mot piggdekkslitasje	A_N7
NS EN 13043 4.2.9.1	**Motstand mot frysing og tining**	F_1
NS EN 932-3	**Petrografisk beskrivelse**	Kvartsdiorit

Figure I21: Product data sheet - Aggregate - Quartz diorite 1 - Page 1/3

NORSTONE
HEIDELBERGCEMENT Group

Material	Vare nr	Dato	Avdeling
5/8	101658	01.06.2016	NorStone Tau

	Gjennomgang(%)																
	0,063	0,125	0,25	0,5	1	2	4	5,6	8	11,2	16	22,4	31,5	45	56	63	90
Typisk gradering	1,4	1,4	1,4	1,4	1,4	2,0	2,0	15,0	91,0	100,0							
Min.									85,0	98,0	100,0						
Max.	2,0					5,0		20,0	99,0	100,0							

Kvartsdiorit/Grovt 5/8 (101658)

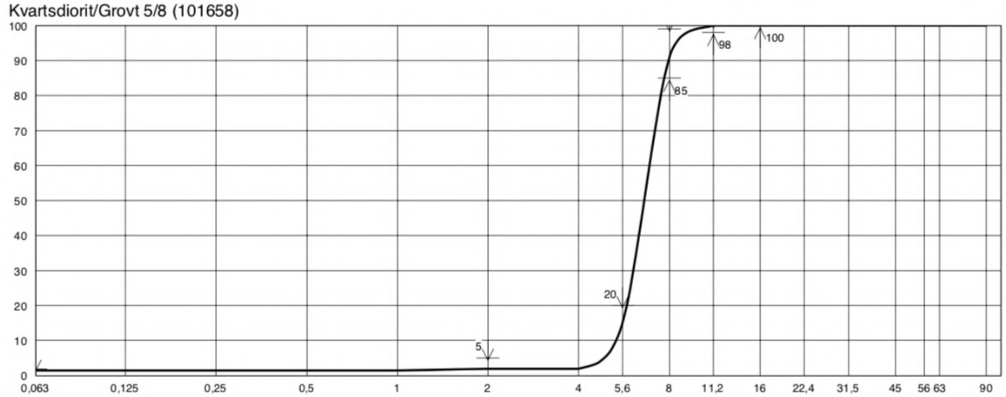

01.06.2016
Dato

A. Cernauskiene
Prepared by

Figure I22: Product data sheet - Aggregate - Quartz diorite 1 - Page 2/3

Ytelseserklæring

I henhold til forordning (EU) nr. 305/2011 (byggevarer), vedlegg III

Ytelseserklæring nr:	101658 004	
100 % Knust 5/8mm (A) Kvartsdiorit	Vare nr: 101658	NORSTONE HEIDELBERGCEMENT Group
Bruksområder for byggevaren(e):	**Tilslag til bituminøse masser og overflatebehandlinger for veger, flyplasser og andre trafikkarealer**	
Det eller de systemer for vurdering og kontroll av byggevarens konstante ytelse :	**System 2+**	Norstone Tau
Dersom ytelseserklæringen gjelder en byggevare som omfattes av en harmonisert Standard	**NS-EN 13043:2002 + NA:2008**	Norstone Tau, 4120 Tau, Norway
Sertifiseringsorganet	**Kontrollrådet-1111**	www.norstone.no
har utstedt sertifikat for produksjonskontrollen i samsvar med	**System 2+**	Tlf:0047-51740700
basert på f¸rstegangsrevisjon av produksjons-anlegget og produksjonskontrollen:	**1111-CPR-0229**	Fax:0047-51740699

Harmonisert teknisk spesifikasjon	Standarder	Vesentlige egenskaper	Ytelse
NS-EN 13043:2002 + NA:2008			**Kategorier**
		Kornstørrelse	5/8
	NS EN 933-1	Gradering	$G_C85/20$
		Toleransekategori	-
		Kornform	
	NS EN 933-3	Flisighetsindeks	FI_{20}
	NS EN 933-4	Shape indeks	SI_{NR}
	NS EN 1097-6	**Korndensitet**	2,75 Mg/m³ - 2,79 Mg/m³
		Renhet	
	NS EN 933-9	Finstoffkvalitet	MB_F10
	NS EN 933-1	Finstoffinnhold	f_2
	NS EN 933-5	**Prosentandel knuste korn**	$C_{100/0}$
		Motstand mot knusing	
	NS EN 1097-2 §5	Los Angeles-prøving	LA_{15}
	NS EN 1097-2 §6	Slagprøving	SZ_{18}
		Motstand mot polering/slitasje	
	NS EN 1097-8	Poleringsverdi	PSV_{50}
	NS EN 1097-1	Motstand mot slitasje for grovt tilslag	$M_{DE}10$
	NS EN 1097-9	Motstand mot piggdekkslitasje	A_N7
	NS EN 13043 4.2.9.1	**Motstand mot frysing og tining**	F_1
	NS EN 1367-5	**Bestandighet mot varmesjokk**	NPD
	prEN 12697-11	**Vedhefting til bituminøse bindemidler**	NPD
	NS EN 1367-3	**Motstand mot forvitring**	NPD
	NS EN 1744-1	**Volumstabilitet**	NPD
		Farlige stoffer	Ikke påvist
	NS EN 932-3	**Petrografisk beskrivelse**	Kvartsdiorit

Ytelsen for denne varen som angitt ovenfor, er i samsvar med spesifikasjonene for produktet angitt i tabellen.

Denne ytelseserklæringen er utstedt på eget ansvar av produsenten, NorStone Tau

Undertegnet for og på vegne av produsenten av:

Marie Reumont, Driftsleder

(navn og stilling)

Tau 01.06.2016

(Sted og utstedelsesdato) (Underskrift)

Figure I23: Product data sheet - Aggregate - Quartz diorite 1 - Page 3/3

I.

WEIDACON

Stahldrahtfaser
aus patentiertem Kohlenstoffdraht,
nass, messing gezogen

STRATEC

MPA NRW

CE

Technische Daten

Fasertyp: Weidacon FM 0,15/9

Fasereigenschaften:

Material:	Stahldraht Werkstoffnummer nach DIN EN 10016-2	
Farbe:	metallisch messing	
Form:	Querschnitt: rund / Länge: gerade	
Abmessungen:	d= 0,15mm, l= 9mm oder nach Wahl	
Toleranzen: (gemäß DIN EN 14889-1)	Länge:	+/- 0,9mm vom Einzelwert und +/- 1,5mm vom Mittelwert
	Durchmesser:	+/- 0,015mm vom Einzelwert und +/- 0,015mm vom Mittelwert
Dichte:	7,85 kg/dm³	
Zugfestigkeit:	2800 N/mm² im Mittel	
E-Modul:	200.000MPa	

Chemische Analyse[Gew.%]:

	min.	max.
C	0,05	0,95
Mn	-	0,80
Si	-	0,30
P	-	0,035
S	-	0,035
Cr	0,15	0,20
Ni	0,20	0,25
Cu	0,25	0,35
Mo	0,05	0,08

Grafische Darstellung

Abbildung 1: Fasertyp Weidacon FM

Betoneigenschaften: Diese Stahldrahtfasern sind nach der gültigen DIN EN 14889-1 System 3 zertifiziert und überwacht.

Verpackungseigenschaften:

Losgröße: Kartons oder Säcke á 20 oder 25 kg auf Einwegpalette zu je 1.000 Kg in Folie eingeschweißt, spritzwassergeschützt

Technisches Datenblatt STRATEC Strahl- und Fasertechnik GmbH

70

Figure I24: Product data sheet - Steel fiber - Weidacon - Page 1/1

MAPEI

Dynamon SX-N

Superplastiserende tilsetningsstoff

BESKRIVELSE
Dynamon SX-N er et svært effektivt superplastiserende tilsetningsstoff basert på modifiserte akrylpolymerer. Produktet tilhører **Dynamon-systemet** basert på den Mapei-utviklede DPP-teknologien (DPP = Designed Performance Polymers), der tilsetningsstoffenes egenskaper skreddersys til ulike betongformål. **Dynamon-systemet** er utviklet på basis av Mapeis egen sammenstilling og produksjon av monomerer.

BRUKSOMRÅDER
Dynamon SX-N er et tilnærmet allround-produkt som er anvendelig i all betong for å øke støpeligheten og/eller redusere tilsatt vannmengde.

Noen spesielle bruksområder er:

- Vanntett betong med krav til høy eller svært høy fasthet og med strenge krav til bestandighet i aggressive miljøer.
- Betong med særlige krav til høy støpelighet; i konsistensklasser S4 og S5 etter NS-EN 206.
- Selvkomprimerende betong med ønske om lengre åpentid. Om nødvendig kan SKB stabiliseres med en viskositetsøker - **Viscofluid** eller **Viscostar**.
- Til produksjon av frostbestandig betong - da i kombinasjon med luftinnførende tilsetningsstoffer - **Mapeair**. Valg av type luftinnførende stoff gjøres ut fra egenskapene til de andre delmaterialer som er tilgjengelige.
- Til golvstøp for å oppnå en smidig betong med bedret støpelighet. Store doseringer og lave temperaturer kan retardere betongen noe.

EGENSKAPER
Dynamon SX-N er en vannløsning av aktive akrylpolymerer som effektivt dispergerer (løser opp) sementklaser.

Denne effekten kan prinsipielt utnyttes på tre måter:

1. For å redusere mengden tilsatt vann, men samtidig beholde betongens støpelighet. Lavere v/c-forhold gir høyere fasthet, tetthet og bestandighet i betongen.
2. For å forbedre støpeligheten sammenlignet med betonger med samme v/c-forhold. Fastheten forblir dermed den samme, men muliggjør forenklet utstøping.
3. For å redusere både vann og sementmengde uten å forandre betongens mekaniske styrke. Gjennom denne metoden kan en blant annet redusere kostnadene (mindre sement), redusere betongens svinnpotensial (mindre vann) og redusere faren for temperaturgradienter på grunn av lavere hydratasjonsvarme.
   Spesielt er denne siste effekten viktig ved betonger med større sementmengder.

Figure I25: Product data sheet - Superplasticizer - Mapei Dynamon SX-N - Page 1/2

Dynamon SX-N

KOMPATIBILITET MED ANDRE PRODUKTER

Dynamon SX-N lar seg kombinere med andre Mapei tilsetningsstoffer, som f.eks størkningsakselererende stoffer som **Mapefast** og størkningsretarderende stoffer som **Mapetard**.
Produktet lar seg også kombinere med luftinnførende tilsetningsstoffer, **Mapeair**, for produksjon av frostbestandig betong.

Valg av type luftinnførende stoff gjøres ut fra egenskapene til de andre delmaterialer som er tilgjengelige.

DOSERING

Dynamon SX-N tilsettes for å oppnå ønsket resultat (styrke, bestandighet, støpelighet, sementreduksjon) ved å variere doseringen mellom 0,4 og 2,0 % av sement + flyveaske + mikrosilika. Ved økt dosering økes også betongens åpentid, dvs. tiden betongen lar seg bearbeide. Større doseringsmengder og lave betongtemperaturer gir en retardert betong. Vi anbefaler alltid prøvestøper med aktuelle parametere.

Til forskjell fra konvensjonelle melamineller naftalenbaserte superplastiserende tilsetningsstoffer, utvikler **Dynamon SX-N** maksimal effekt uavhengig av tilsettingstidspunkt, men tilsetningstidspunktet kan påvirke nødvendig blandetid.

Dersom **Dynamon SX-N** tilsettes etter at minst 80 % av blandevannet er inne vil blandetiden generelt være kortest. Det er likevel viktig med utprøvinger tilpasset eget blandeutstyr.

Dynamon SX-N kan også tilsettes direkte i automikser på bygg- eller anleggsplass. Betongen bør da blandes med maksimal hastighet på trommelen i ett minutt pr. m^3 betong i lasset, men minimum 5 minutter.

EMBALLASJE

Dynamon SX-N leveres i 25 liters kanner, 200 liters fat, 1000 liter IBC-tanker og i tank.

LAGRING

Produktet må oppbevares ved temperaturer mellom +8°C og +35°C. I lukket emballasje bevarer produktet sine egenskaper i minst 12 måneder. Hvis produktet utsettes for direkte sollys, kan det føre til variasjoner i fargetonen uten at dette påvirker egenskapene til produktet.

SIKKERHETSINSTRUKSJONER FOR KLARGJØRING OG BRUK

For instruksjon vedrørende sikker håndtering av våre produkter, vennligst se siste utgave av sikkerhetsdatablad på vår nettside www.mapei.no

PRODUKT FOR PROFESJONELL BRUK.

MERK

De tekniske anbefalinger og detaljer som fremkommer i denne produktbeskrivelse representerer vår nåværende kunnskap og erfaring om produktene. All overstående informasjon må likevel betraktes som retningsgivende og gjenstand for vurdering. Enhver som benytter produktet må på forhånd forsikre seg om at produktet er egnet for tilsiktet anvendelse. Brukeren står selv ansvarlig dersom produktet blir benyttet til andre formål enn anbefalt eller ved feilaktig utførelse.

Vennligst referer til siste oppdaterte versjon av teknisk datablad som finnes tilgjengelig på vår webside www.mapei.no

JURIDISK MERKNAD

Innholdet i dette tekniske databladet kan kopieres til andre prosjektrelaterte dokumenter, men det endelige dokumentet må ikke suppleres eller erstatte betingelsene i det tekniske datablad, som er gjeldende, når MAPEI-produktet benyttes. Det seneste oppdaterte datablad er tilgjengelig på vår hjemmeside www.mapei.no
ENHVER ENDRING AV ORDLYDEN ELLER BETINGELSER, SOM ER GITT ELLER AVLEDET FRA DETTE TEKNISKE DATABLADET, MEDFØRER AT MAPEI SITT ANSVAR OPPHØRER.

Alle relevante referanser for produktet er tilgjengelige på forespørsel og fra www.mapei.no

Figure I26: Product data sheet - Superplasticizer - Mapei Dynamon SX-N - Page 2/2

J: Output file from compression testing

Toni Technik

Simple standard protocol **03.12.2019**

Parameter table:

Test protocol	: UHPC	Type strain extensometer	:
Tester	: Fredrik Knutsen	Machine data	: Controller TT1412
Customer	:		PistonStroke
Test standard	:		LoadCell 3 MN
Strength grade	:		Extensometer
Other	:		Extensometer2

Toni Technik

Simple standard protocol **03.12.2019**

Results:

Nr	Date	ID	a mm	b mm	Gauge length mm	F_m kN	Clock time	σ_m N/mm²
67	04.09.2019	1A2A	100,0	100,0	50	932,80	09:08:30a.m.	93,28
68	04.09.2019	1A2B	100,0	100,0	50	904,65	09:16:07a.m.	90,46
69	04.09.2019	1A2C	100,0	100,0	50	937,76	09:21:01a.m.	93,78
70	04.09.2019	1B2A	100,0	100,0	50	1683,18	09:26:33a.m.	168,32
71	04.09.2019	1B2B	100,0	100,0	50	1696,62	09:32:22a.m.	169,66
72	04.09.2019	1B2C	100,0	100,0	50	1638,51	09:41:39a.m.	163,85
73	04.09.2019	2A2A	100,0	100,0	50	1129,79	09:46:50a.m.	112,98
74	04.09.2019	2A2B	100,0	100,0	50	1120,29	09:50:40a.m.	112,03
75	04.09.2019	2A2C	100,0	100,0	50	1133,46	09:55:01a.m.	113,35
76	04.09.2019	2B2A	100,0	100,0	50	1820,45	10:00:25a.m.	182,04
77	04.09.2019	2B2B	100,0	100,0	50	1862,49	10:05:53a.m.	186,25
78	04.09.2019	2B2C	100,0	100,0	50	1833,96	10:11:28a.m.	183,40
79	04.09.2019	3A2A	100,0	100,0	50	1049,65	10:15:54a.m.	104,96
80	04.09.2019	3A2B	100,0	100,0	50	1063,91	10:19:44a.m.	106,39
81	04.09.2019	3A2C	100,0	100,0	50	1060,50	10:23:20a.m.	106,05
82	04.09.2019	3B2A	100,0	100,0	50	1771,09	10:28:44a.m.	177,11
83	04.09.2019	3B2B	100,0	100,0	50	1773,00	10:34:04a.m.	177,30
84	04.09.2019	3B2C	100,0	100,0	50	1750,70	10:39:17a.m.	175,07
85	05.09.2019	8A2A	100,0	100,0	50	1255,12	07:14:21a.m.	125,51
86	05.09.2019	8A2B	100,0	100,0	50	1237,10	07:19:26a.m.	123,71
87	05.09.2019	8A2C	100,0	100,0	50	1216,68	07:23:30a.m.	121,67
88	05.09.2019	8B2A	100,0	100,0	50	1585,66	07:30:14a.m.	158,57
89	05.09.2019	8B2B	100,0	100,0	50	1541,51	07:34:58a.m.	154,15
90	05.09.2019	8B2C	100,0	100,0	50	1588,29	07:41:35a.m.	158,83
91	05.09.2019	9B2A	100,0	100,0	50	1315,99	07:47:53a.m.	131,60
92	17.09.2019	6A2A	100,0	100,0	50	1035,49	10:26:11a.m.	103,55
93	17.09.2019	6A2B	100,0	100,0	50	1037,29	10:30:19a.m.	103,73
94	17.09.2019	6A2C	100,0	100,0	50	1020,99	10:33:49a.m.	102,10
95	17.09.2019	7A2A	100,0	100,0	50	1068,84	10:38:11a.m.	106,88
96	17.09.2019	7A2B	100,0	100,0	50	1093,94	10:41:33a.m.	109,39
97	17.09.2019	7A2C	100,0	100,0	50	1075,60	10:45:51a.m.	107,56
98	17.09.2019	6B2A	100,0	100,0	50	1614,42	10:50:45a.m.	161,44
99	17.09.2019	6B2B	100,0	100,0	50	1552,36	10:55:21a.m.	155,24
100	17.09.2019	6B2C	100,0	100,0	50	1602,18	10:59:57a.m.	160,22
101	17.09.2019	7B2A	100,0	100,0	50	1717,39	11:04:55a.m.	171,74
102	17.09.2019	7B2B	100,0	100,0	50	1683,89	11:09:33a.m.	168,39
103	17.09.2019	7B2C	100,0	100,0	50	1729,20	11:14:19a.m.	172,92
104	17.09.2019	10A2A	100,0	100,0	50	1134,81	11:18:15a.m.	113,48
105	17.09.2019	10A2B	100,0	100,0	50	1147,01	11:22:21a.m.	114,70
106	17.09.2019	10A2C	100,0	100,0	50	1154,71	11:26:09a.m.	115,47
107	17.09.2019	11A2A	100,0	100,0	50	1147,03	11:29:51a.m.	114,70
108	17.09.2019	11A2B	100,0	100,0	50	1182,48	11:33:51a.m.	118,25
109	17.09.2019	11A2C	100,0	100,0	50	1149,63	11:37:27a.m.	114,96
110	17.09.2019	10B2A	100,0	100,0	50	1824,65	11:42:43a.m.	182,46
111	17.09.2019	10B2B	100,0	100,0	50	1945,17	11:47:54a.m.	194,52
112	17.09.2019	10B2C	100,0	100,0	50	1883,80	11:53:09a.m.	188,38
113	17.09.2019	11B2A	100,0	100,0	50	1928,97	11:58:19a.m.	192,90
114	17.09.2019	11B2B	100,0	100,0	50	1972,26	12:03:33p.m.	197,23
115	17.09.2019	11B2C	100,0	100,0	50	1896,54	12:08:36p.m.	189,65
116	25.09.2019	4B2A	100,0	100,0	50	1667,70	07:55:34a.m.	166,77
117	25.09.2019	4B2B	100,0	100,0	50	1640,03	08:00:09a.m.	164,00
118	25.09.2019	4B2C	100,0	100,0	50	1585,72	08:07:25a.m.	158,57
119	25.09.2019	5B2A	100,0	100,0	50	1559,15	08:12:01a.m.	155,92
120	25.09.2019	5B2B	100,0	100,0	50	1520,64	08:16:32a.m.	152,06
121	25.09.2019	5B2C	100,0	100,0	50	1554,37	08:21:29a.m.	155,44
122	25.09.2019	12B2A	100,0	100,0	50	1949,01	08:28:43a.m.	194,90
123	25.09.2019	12B2B	100,0	100,0	50	1948,15	08:34:51a.m.	194,82
124	25.09.2019	12B2C	100,0	100,0	50	1945,26	08:40:16a.m.	194,53
125	25.09.2019	13B2A	100,0	100,0	50	1903,04	08:45:32a.m.	190,30

Nr	Date	ID	a mm	b mm	Gauge length mm	F_m kN	Clock time	σ_m N/mm²
126	25.09.2019	13B2B	100,0	100,0	50	1832,37	08:50:37a.m.	183,24
127	25.09.2019	13B2C	100,0	100,0	50	1892,61	09:00:20a.m.	189,26
128	25.09.2019	1A1A	100,0	100,0	50	1342,29	09:04:38a.m.	134,23
129	25.09.2019	1A1B	100,0	100,0	50	1308,10	09:08:45a.m.	130,81
130	25.09.2019	1A1C	100,0	100,0	50	1315,21	09:12:46a.m.	131,52
131	25.09.2019	2A1A	100,0	100,0	50	1523,02	09:17:15a.m.	152,30
132	25.09.2019	2A1B	100,0	100,0	50	1541,85	09:21:48a.m.	154,19
133	25.09.2019	2A1C	100,0	100,0	50	1573,06	09:26:25a.m.	157,31
134	25.09.2019	3A1A	100,0	100,0	50	1518,68	09:31:11a.m.	151,87
135	25.09.2019	3A1B	100,0	100,0	50	1500,35	09:35:36a.m.	150,03
136	25.09.2019	3A1C	100,0	100,0	50	1516,30	09:40:25a.m.	151,63
137	26.09.2019	8A1A	100,0	100,0	50	1358,19	06:29:40a.m.	135,82
138	26.09.2019	8A1B	100,0	100,0	50	1355,26	06:35:33a.m.	135,53
139	26.09.2019	8A1C	100,0	100,0	50	1436,85	06:39:46a.m.	143,68
140	26.09.2019	9A1B	100,0	100,0	50	1257,89	06:44:27a.m.	125,79
141	26.09.2019	9A1A	100,0	100,0	50	1175,80	06:49:01a.m.	117,58
142	26.09.2019	9A1C	100,0	100,0	50	1298,26	06:52:49a.m.	129,83
143	07.10.2019	14B2A	100,0	100,0	50	1905,97	16:35:29p.m.	190,60
144	07.10.2019	14B2B	100,0	100,0	50	1927,42	16:41:18p.m.	192,74
145	07.10.2019	14B2C	100,0	100,0	50	1916,69	16:46:53p.m.	191,67
146	07.10.2019	15B2A	100,0	100,0	50	1810,29	16:52:16p.m.	181,03
147	07.10.2019	15B2B	100,0	100,0	50	1755,18	16:57:27p.m.	175,52
148	07.10.2019	15B2C	100,0	100,0	50	1772,16	17:02:23p.m.	177,22
149	07.10.2019	16B2A	100,0	100,0	50	1666,50	17:07:29p.m.	166,65
150	07.10.2019	16B2B	100,0	100,0	50	1470,04	17:11:54p.m.	147,00
151	07.10.2019	16B2C	100,0	100,0	50	1470,21	17:16:10p.m.	147,02
152	08.10.2019	6A1A	100,0	100,0	50	1373,97	06:43:26a.m.	137,40
153	08.10.2019	6A1B	100,0	100,0	50	1378,73	06:47:36a.m.	137,87
154	08.10.2019	6A1C	100,0	100,0	50	1431,12	06:52:00a.m.	143,11
155	08.10.2019	7A1A	100,0	100,0	50	1504,17	06:56:57a.m.	150,42
156	08.10.2019	7A1B	100,0	100,0	50	1499,21	07:01:30a.m.	149,92
157	08.10.2019	7A1C	100,0	100,0	50	1428,38	07:06:09a.m.	142,84
158	08.10.2019	10A1A	100,0	100,0	50	1486,61	07:15:18a.m.	148,66
159	08.10.2019	10A1B	100,0	100,0	50	1495,05	07:20:10a.m.	149,51
160	08.10.2019	10A1C	100,0	100,0	50	1560,20	07:27:51a.m.	156,02
161	08.10.2019	11A1A	100,0	100,0	50	1568,70	07:32:18a.m.	156,87
162	08.10.2019	11A1B	100,0	100,0	50	1590,08	07:37:05a.m.	159,01
163	08.10.2019	11A1C	100,0	100,0	50	1505,84	07:41:19a.m.	150,58
164	13.10.2019	17B2A	100,0	100,0	50	1636,85	10:01:33a.m.	163,69
165	13.10.2019	17B2B	100,0	100,0	50	1658,01	10:06:18a.m.	165,80
166	13.10.2019	17B2C	100,0	100,0	50	1545,27	10:11:00a.m.	154,53
167	13.10.2019	18B2A	100,0	100,0	50	1889,52	10:16:21a.m.	188,95
168	13.10.2019	18B2B	100,0	100,0	50	1784,78	10:21:31a.m.	178,48
169	13.10.2019	18B2C	100,0	100,0	50	1823,01	10:26:30a.m.	182,30
170	13.10.2019	19B2A	100,0	100,0	50	2083,31	10:32:06a.m.	208,33
171	13.10.2019	19B2B	100,0	100,0	50	1976,84	10:37:21a.m.	197,68
172	13.10.2019	19B2C	100,0	100,0	50	2032,58	10:43:02a.m.	203,26
173	28.10.2019	20B2A	100,0	100,0	50	2052,12	07:38:46a.m.	205,21
174	28.10.2019	20B2B	100,0	100,0	50	2007,79	07:44:56a.m.	200,78
175	28.10.2019	20B2C	100,0	100,0	50	2101,45	07:50:34a.m.	210,14
176	28.10.2019	21B2A	100,0	100,0	50	1713,13	07:55:27a.m.	171,31
177	28.10.2019	21B2B	100,0	100,0	50	1737,98	08:00:20a.m.	173,80
178	28.10.2019	21B2C	100,0	100,0	50	1692,27	08:05:13a.m.	169,23
179	28.10.2019	22B2A	100,0	100,0	50	1762,50	08:19:28a.m.	176,25
180	28.10.2019	22B2B	100,0	100,0	50	1762,62	08:24:34a.m.	176,26
181	28.10.2019	22B2C	100,0	100,0	50	1773,24	08:29:25a.m.	177,32
182	12.11.2019	23A2A	100,0	100,0	50	1095,47	10:02:36a.m.	109,55
183	12.11.2019	23A2B	100,0	100,0	50	1047,90	10:06:07a.m.	104,79
184	12.11.2019	23A2C	100,0	100,0	50	1044,04	10:09:21a.m.	104,40
185	12.11.2019	23B2A	100,0	100,0	50	1856,64	10:14:28a.m.	185,66
186	12.11.2019	23B2B	100,0	100,0	50	1875,97	10:20:02a.m.	187,60

Nr	Date	ID	a mm	b mm	Gauge length mm	F_m kN	Clock time	σ_m N/mm²
187	12.11.2019	23B2C	100,0	100,0	50	1863,09	10:25:39a.m.	186,31
188	12.11.2019	24A2A	100,0	100,0	50	875,72	10:29:47a.m.	87,57
190	12.11.2019	24A2B	100,0	100,0	50	1041,95	10:36:44a.m.	104,20
191	12.11.2019	24A2C	100,0	100,0	50	1063,86	10:40:12a.m.	106,39
192	12.11.2019	24B2A	100,0	100,0	50	1793,59	10:45:09a.m.	179,36
193	12.11.2019	24B2B	100,0	100,0	50	1843,69	10:50:14a.m.	184,37
195	12.11.2019	24B2C	100,0	100,0	50	1831,17	10:55:55a.m.	183,12
196	12.11.2019	25A2A	100,0	100,0	50	1104,46	10:59:53a.m.	110,45
197	12.11.2019	25A2B	100,0	100,0	50	1076,85	11:03:34a.m.	107,69
198	12.11.2019	25A2C	100,0	100,0	50	1093,59	11:07:06a.m.	109,36
199	12.11.2019	25B2A	100,0	100,0	50	1920,33	11:12:31a.m.	192,03
200	12.11.2019	25B2B	100,0	100,0	50	1899,86	11:17:46a.m.	189,99
201	12.11.2019	25B2C	100,0	100,0	50	1833,71	11:22:48a.m.	183,37
203	12.11.2019	26A2A	100,0	100,0	50	1135,31	11:27:15a.m.	113,53
204	12.11.2019	26A2B	100,0	100,0	50	1084,31	11:30:43a.m.	108,43
205	12.11.2019	26A2C	100,0	100,0	50	1109,63	11:34:16a.m.	110,96
206	12.11.2019	26B2A	100,0	100,0	50	1836,30	11:39:24a.m.	183,63
207	12.11.2019	26B2B	100,0	100,0	50	1838,96	11:44:28a.m.	183,90
208	12.11.2019	26B2C	100,0	100,0	50	1805,68	11:49:24a.m.	180,57
209	03.12.2019	23A1A	100,0	100,0	50	1591,61	08:40:47a.m.	159,16
210	03.12.2019	23A1B	100,0	100,0	50	1511,14	08:46:42a.m.	151,11
211	03.12.2019	23A1C	100,0	100,0	50	1559,76	08:51:37a.m.	155,98
212	03.12.2019	24A1A	100,0	100,0	50	1429,15	08:55:55a.m.	142,91
213	03.12.2019	24A1B	100,0	100,0	50	1456,42	09:02:35a.m.	145,64
214	03.12.2019	24A1C	100,0	100,0	50	1361,58	09:06:59a.m.	136,16
215	03.12.2019	25A1A	100,0	100,0	50	1427,33	09:12:19a.m.	142,73
216	03.12.2019	25A1B	100,0	100,0	50	1525,82	09:16:57a.m.	152,58
217	03.12.2019	26A1C	100,0	100,0	50	1585,02	09:21:28a.m.	158,50
218	03.12.2019	26A1A	100,0	100,0	50	1460,59	09:26:23a.m.	146,06
219	03.12.2019	26A1B	100,0	100,0	50	1550,00	09:31:26a.m.	155,00
220	03.12.2019	25A1C	100,0	100,0	50	1424,86	09:35:32a.m.	142,49

Series graphics:

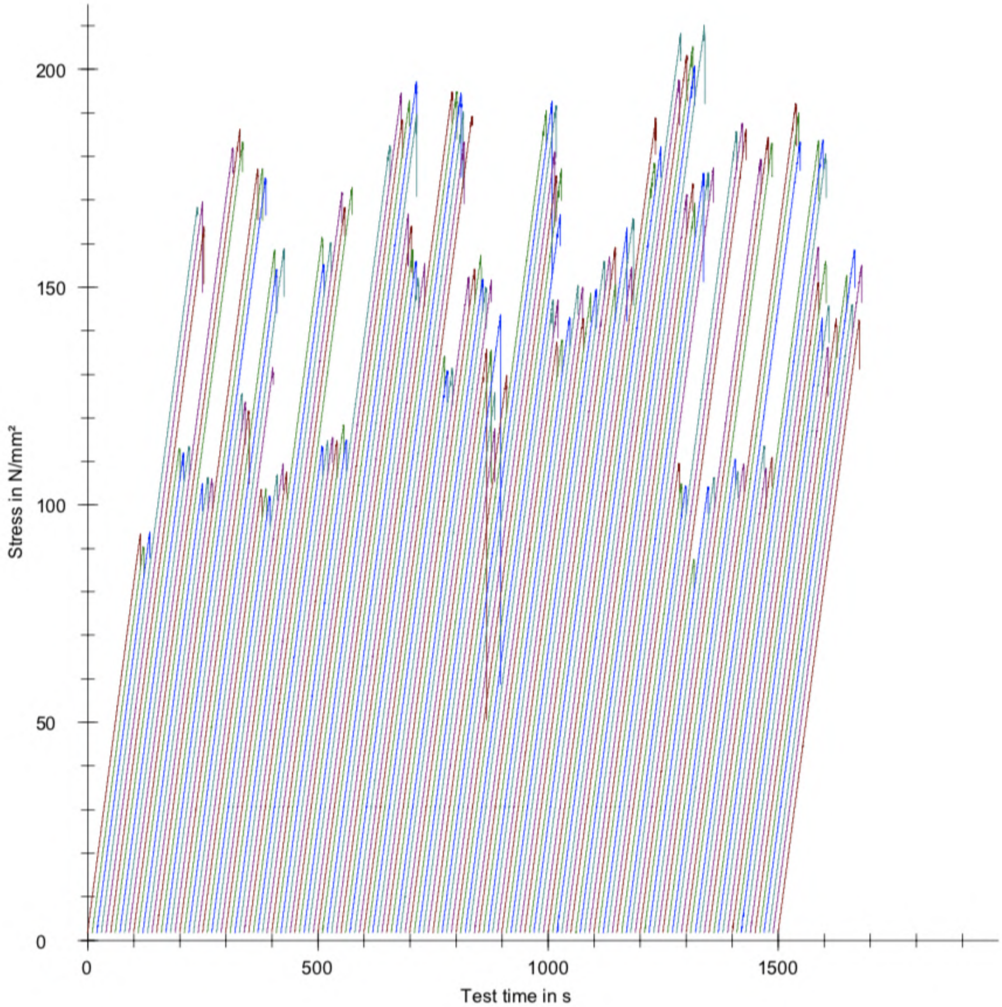

Statistics:

Series n = 151	a mm	b mm	Gauge length mm	F_m kN	σ_m N/mm²
n	151	151	151	151	151
$\bar{x}$	100,0	100,0	50	1529,31	152,93
s	0,0	0,0	0,000	311,22	31,12
max.	100,0	100,0	50	2101,45	210,14
min	100,0	100,0	50	875,72	87,57
med	100,0	100,0	50	1554,37	155,44
ν	0,00	0,00	0,00	20,35	20,35

K: Output file from modulus of elasticity testing

Toni Technik

Simple standard protocol **03.12.2019**

Parameter table:

Test protocol :
Tester :
Customer :
Test standard : EN12390-13 method A
Strength grade :
Creation date :
Age : 0 T
Other :

Type strain extensometer :
Machine data : Controller TT0322
PistonStroke
LoadCell 3 MN
Extensometer
Extensometer2

Results:

Nr	$\varepsilon_{b2,E1}$ mm	$\varepsilon_{b2,E2}$ mm	$\varepsilon_{b3,E1}$ mm	$\varepsilon_{b3,E2}$ mm	$\Delta\varepsilon_{b23,E}$ %	$\Delta\varepsilon_{b23,E}$ %	$\Delta\varepsilon_{b3,E1}$ %	$\sigma_{m\,a,1}$ N/mm	$\sigma_{m\,b,0}$ N/mm	$\varepsilon_{a,1}$ mm	$\varepsilon_{b,0}$ mm	$E_{C,0}$ N/mm	$\sigma_{m\,a,3}$ N/mm	$\sigma_{m\,b,2}$ N/mm	$\varepsilon_{a,3}$ mm	$\varepsilon_{b,2}$ mm	$E_{C,S}$ N/mm
max.					10,00	10,00	20,00										
min					-10,00	-10,00	-20,00										
1	0,057	0,062	0,056	0,061	0,21	0,06	2,27	37,92	14,24	0,174	0,061	42103	37,91	14,20	0,175	0,065	43325
2	0,056	0,054	0,057	0,053	0,25	0,32	1,64	37,93	14,24	0,165	0,052	42167	37,91	14,18	0,166	0,061	45224
3	0,066	0,052	0,067	0,052	0,03	0,10	6,33	44,35	16,64	0,172	0,051	45944	44,33	16,60	0,173	0,057	47815
4	0,067	0,054	0,067	0,054	0,01	0,09	5,28	44,36	16,66	0,165	0,054	49918	44,34	16,59	0,166	0,057	50828
6	0,059	0,055	0,059	0,055	0,05	0,03	2,06	43,34	16,28	0,172	0,055	45957	43,36	16,22	0,174	0,058	46784
7	0,064	0,058	0,064	0,058	0,00	0,03	2,75	43,35	16,27	0,174	0,058	46510	43,35	16,23	0,175	0,069	51305
8	0,049	0,070	0,050	0,070	0,36	0,01	8,34	39,69	14,89	0,198	0,070	38662	39,67	14,84	0,200	0,081	41871
10	0,053	0,064	0,053	0,064	0,07	0,05	4,83	35,69	13,40	0,202	0,065	32469	35,67	13,33	0,203	0,076	35106
11	0,062	0,061	0,063	0,060	0,23	0,37	1,20	40,01	15,00	0,185	0,059	39556	39,99	14,96	0,187	0,069	42666
12	0,045	0,064	0,045	0,064	0,06	0,05	8,96	40,00	15,01	0,188	0,064	40317	40,01	14,97	0,190	0,078	44621
13	0,043	0,078	0,045	0,077	0,79	0,28	13,45	42,36	15,90	0,216	0,076	38004	42,37	15,85	0,218	0,094	42837
14	0,052	0,080	0,052	0,080	0,10	0,09	10,55	42,38	15,91	0,216	0,080	39154	42,37	15,85	0,218	0,093	42396
15	0,041	0,075	0,041	0,074	0,45	0,11	14,28	43,42	16,30	0,200	0,074	43077	43,41	16,25	0,201	0,084	46376
16	0,055	0,052	0,055	0,052	0,05	0,10	1,40	43,42	16,29	0,169	0,052	46379	43,41	16,24	0,170	0,065	51299
17	0,051	0,071	0,052	0,070	0,24	0,17	7,55	44,59	16,73	0,187	0,069	47186	44,60	16,69	0,189	0,078	50157
18	0,064	0,048	0,063	0,048	0,17	0,31	6,76	44,58	16,74	0,166	0,049	47617	44,59	16,68	0,167	0,051	48351
19	0,067	0,061	0,066	0,060	0,26	0,07	2,37	44,53	16,72	0,182	0,060	45836	44,52	16,69	0,182	0,067	48265
20	0,065	0,064	0,065	0,064	0,08	0,06	0,36	44,51	16,73	0,189	0,064	44271	44,53	16,67	0,191	0,073	47208
21	0,060	0,064	0,060	0,063	0,15	0,10	1,37	40,62	15,22	0,181	0,063	43145	40,62	15,17	0,181	0,067	44610
22	0,047	0,062	0,048	0,062	0,48	0,29	6,36	40,62	15,23	0,177	0,061	43875	40,62	15,18	0,178	0,068	46186
23	0,058	0,061	0,058	0,061	0,14	0,08	1,31	41,84	15,72	0,177	0,061	44899	41,83	15,69	0,179	0,067	46729
24	0,053	0,061	0,053	0,060	0,23	0,13	3,07	41,81	15,72	0,175	0,060	45193	41,83	15,69	0,176	0,065	46862
25	0,066	0,066	0,066	0,066	0,04	0,00	0,24	43,93	16,52	0,193	0,066	43287	43,92	16,47	0,195	0,076	46156
26	0,052	0,062	0,052	0,062	0,19	0,13	4,18	43,91	16,53	0,181	0,061	45880	43,93	16,47	0,182	0,065	47096

Series graphics:

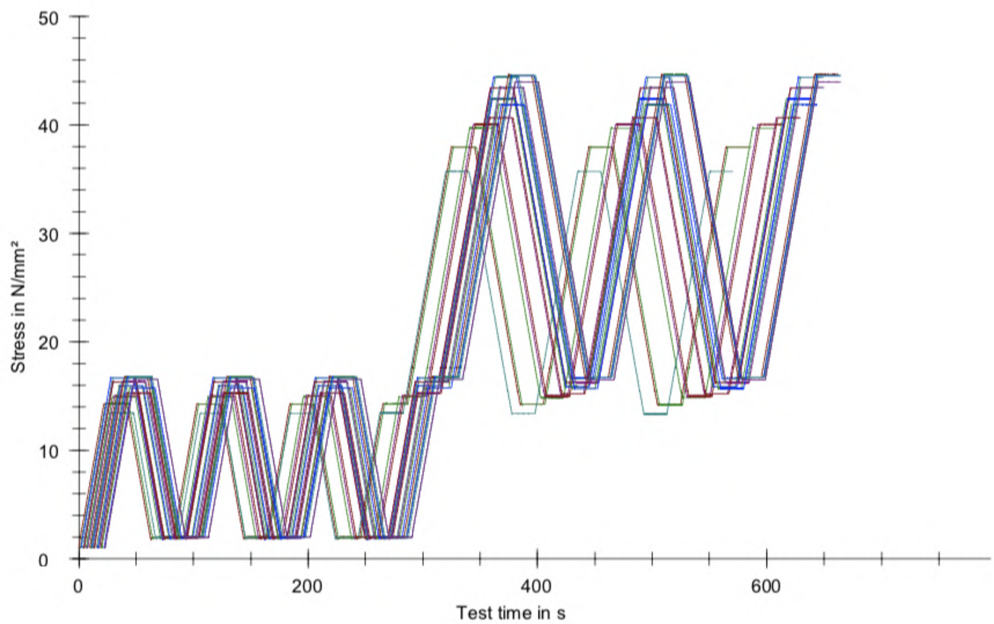

Statistics:

Series n = 24	σ_m N/mm²	$E_{C,0}$ N/mm²	$E_{C,S}$ N/mm²
$\bar{x}$	42,10	43392,46	46003,61
s	2,49	3852,86	3593,15
ν	5,92	8,88	7,81

L: Output file from splitting tensile testing

Toni Technik

Simple standard protocol **03.12.2019**

Parameter table:

Tester : Spaltestrekktest
Creation date: 02.05.2019
Age : 672 h
Other :

Type strain extensometer:
Machine data : Controller TT1412
PistonStroke
LoadCell 3 MN
Extensometer
Extensometer2

Results:

Nr	Date	ID	d mm	h mm	F_m kN	σ_m N/mm²
1	25.09.2019	23A4A	150,0	300,0	1103,99	62,47
2	25.09.2019	1A4B	150,0	300,0	529,65	29,97
3	25.09.2019	2A4A	150,0	300,0	632,04	35,77
4	25.09.2019	2A4B	150,0	300,0	631,52	35,74
5	25.09.2019	3A4A	150,0	300,0	436,73	24,71
6	25.09.2019	3A4B	150,0	300,0	676,75	38,30
7	08.10.2019	6A4A	150,0	300,0	449,97	25,46
8	08.10.2019	6A4B	150,0	300,0	684,91	38,76
9	08.10.2019	7A4A	150,0	300,0	716,85	40,57
10	08.10.2019	7A4B	150,0	300,0	758,13	42,90
11	08.10.2019	10A4A	150,0	300,0	964,47	54,58
12	08.10.2019	10A4B	150,0	300,0	676,95	38,31
13	08.10.2019	11A4A	150,0	300,0	694,13	39,28
14	08.10.2019	11A4B	150,0	300,0	1299,14	73,52
16	03.12.2019	23A4A	150,0	300,0	641,36	36,29
17	03.12.2019	23A4B	150,0	300,0	582,62	32,97
18	03.12.2019	24A4A	150,0	300,0	610,35	34,54
19	03.12.2019	24A4B	150,0	300,0	576,60	32,63
20	03.12.2019	25A4A	150,0	300,0	512,34	28,99
21	03.12.2019	25A4B	150,0	300,0	669,05	37,86
22	03.12.2019	26A4A	150,0	300,0	877,09	49,63
23	03.12.2019	26A4B	150,0	300,0	656,71	37,16

Toni Technik

Simple standard protocol **03.12.2019**

Series graphics:

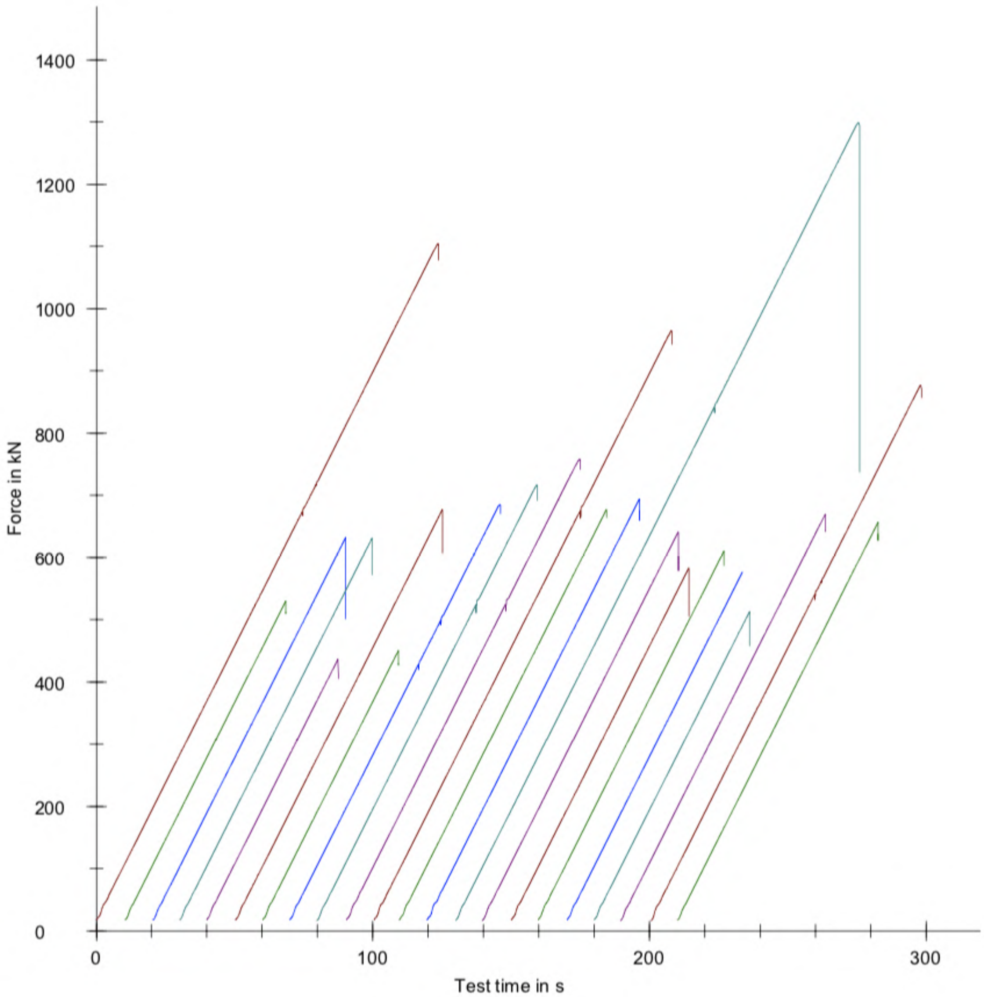

Statistics:

Series n = 22	d mm	h mm	F_m kN	σ_m N/mm²
n	22	22	22	22
$\bar{x}$	150,0	300,0	699,15	39,56
s	0,0	0,0	204,37	11,57
max.	150,0	300,0	1299,14	73,52
min	150,0	300,0	436,73	24,71
med	150,0	300,0	662,88	37,51
ν	0,00	0,00	29,23	29,23

M: Output file from flexural testing

Toni Technik

Simple standard protocol

03.12.2019

Parameter table:

Test protocol :
Tester :
Customer :
Test standard :
Strength grade :
Creation date :
Age : 0 T
Other :

Type strain extensometer :
Machine data : Controller TT1412
PistonStroke
LoadCell 250 kN

Results:

Nr	Date	ID	a mm	b mm	A mm^2	h mm	F_m kN
29	03.12.2019	23A5A	100,0	500,0	50000,0	100,0	32,99
30	03.12.2019	23A5B	100,0	500,0	50000,0	100,0	31,80
31	03.12.2019	23A5C	100,0	500,0	50000,0	100,0	29,14
32	03.12.2019	24A5A	100,0	500,0	50000,0	100,0	36,68
34	03.12.2019	24A5B	100,0	500,0	50000,0	100,0	42,75
35	03.12.2019	24A5C	100,0	500,0	50000,0	100,0	34,99
36	03.12.2019	25A5A	100,0	500,0	50000,0	100,0	31,11
37	03.12.2019	25A5B	100,0	500,0	50000,0	100,0	33,42
38	03.12.2019	25A5C	100,0	500,0	50000,0	100,0	27,62
39	03.12.2019	26A5A	100,0	500,0	50000,0	100,0	45,82
40	03.12.2019	26A5B	100,0	500,0	50000,0	100,0	38,73

Series graphics: